

EXPERIMENTAL AND THEORETICAL INVESTIGATION OF
COMPLEX FLOWS BY ULTRASOUND DOPPLER VELOCIMETRY

A THESIS SUBMITTED TO
THE GRADUATE SCHOOL OF NATURAL AND APPLIED SCIENCES
OF
MIDDLE EAST TECHNICAL UNIVERSITY

BY

VOLKAN KÖSELI

IN PARTIAL FULFILLMENT OF THE REQUIREMENTS
FOR
THE DEGREE OF DOCTOR OF PHILOSOPHY
IN
CHEMICAL ENGINEERING

JULY 2009

Approval of the thesis:

**EXPERIMENTAL AND THEORETICAL INVESTIGATION OF
COMPLEX FLOWS BY ULTRASOUND DOPPLER VELOCIMETRY**

submitted by **VOLKAN KÖSELİ** in partial fulfillment of the requirements for the degree of **Doctor of Philosophy in Chemical Engineering Department, Middle East Technical University** by,

Prof. Dr. Canan Özgen
Dean, Graduate School of **Natural and Applied Sciences**

Prof. Dr. Gürkan Karakaş
Head of Department, **Chemical Engineering**

Assoc. Prof. Dr. Yusuf Uludağ
Supervisor, **Chemical Engineering Dept., METU**

Examining Committee Members:

Prof. Dr. Erdoğan Alper
Chemical Engineering Dept., Hacettepe University

Assoc. Prof. Dr. Yusuf Uludağ
Chemical Engineering Dept., METU

Assoc. Prof. Dr. Serkan Özgen
Aerospace Engineering Dept., METU

Assoc. Prof. Dr. Halil Kalıpçılar
Chemical Engineering Dept., METU

Assoc. Prof. Dr. Göknur Bayram
Chemical Engineering Dept., METU

Date:

03.07.2009

I hereby declare that all information in this document has been obtained and presented in accordance with academic rules and ethical conduct. I also declare that, as required by these rules and conduct, I have fully cited and referenced all material and results that are not original to this work.

Name, Last name : Volkan Köseli

Signature :

ABSTRACT

EXPERIMENTAL AND THEORETICAL INVESTIGATION OF COMPLEX FLOWS BY ULTRASOUND DOPPLER VELOCIMETRY

Köseli, Volkan

Ph.D., Department of Chemical Engineering

Supervisor: Assoc. Prof. Dr. Yusuf Uludağ

July 2009, 128 pages

Non-invasive and fast flow measurement techniques have had increasing importance for the last decades. Scientists are looking for such quick techniques to be able to monitor real velocities without disturbing flow itself. Ultrasound Doppler velocimetry (UDV) being one of such techniques promising with advantages of getting simultaneous velocity measurements from several points and of applicability for opaque liquids as well. UDV is a technique which is still being developed for new applications and analysis of complex flows.

In this study effect of sinusoidal oscillating, turbulent (random) and viscoelastic fluid motions on UDV signals were investigated theoretically and experimentally. Obtained mathematical relations for random and viscoelastic motions were utilized to get statistics of flow and distribution of relaxation spectrum, respectively.

Analytical analysis and numerical simulation of sinusoidal oscillating flow depicted that there is a critical value for the ratio of oscillation amplitude to oscillation frequency for a specified set of measurement parameters of UDV. Above this critical value UDV is not successful to determine mean flow velocity. Mathematical relations between velocity probability density function (PDF) – velocity auto correlation function (ACF) and UDV signal spectrum were obtained in the analysis

of flow with random velocity. Comparison of velocity ACFs from direct velocity measurements and from raw in-phase (I) and quadrature (Q) signals through derived relation, revealed that time resolution of UDV technique is not enough for getting a good velocity ACF and thus turbulence spectrum. Using I and Q signals rather than measured velocities to get velocity ACF, increased the time resolution in the order of number of pulses used for getting one velocity value (N_{pm}).

Velocity PDF obtained from UDV spectrum was compared with the one obtained from measured velocities with the assumption of Gaussian PDF. Both velocity PDFs were consistent. Also some parameters of pipe turbulence from literature were compared with the presented findings from velocity ACF obtained from I and Q signals through derived relation. Results showed good compatibility.

In the last part of the study, complex viscosity of a linear viscoelastic fluid mathematically related to spectrum of UDV for a pipe flow with small-amplitude oscillating pressure field. Generalized Maxwell model was employed to express complex viscosity terms. Zero frequency (mean flow) component of UDV spectrum was used to obtain an equation for relaxation viscosities of generalized Maxwell model. Results have revealed that UDV technique can also be used to probe some of viscoelastic material functions.

In conclusion, UDV is relatively new but a promising technique for the measurement and analysis of complex flows in a non-invasive manner.

Keywords: Complex Flows, Linear Viscoelasticity, Non-invasive Flow Measurement, Pipe Turbulence, Random Signals, Ultrasonic Signal Processing, Ultrasound Doppler Velocimeter (UDV)

ÖZ

KOMPLEKS AKIŞLARIN ULTRASONİK DOPPLER HIZ ÖLÇÜM TEKNİĞİYLE DENEYSEL VE TEORİK OLARAK İNCELENMESİ

Köseli, Volkan

Doktora, Kimya Mühendisliği Bölümü

Tez Yöneticisi: Doç. Dr. Yusuf Uludağ

Temmuz 2009, 128 sayfa

Bir kaç on yıldan bu yana akışı rahatsız etmeyen ve hızlı ölçüm teknikleri artan öneme sahiptir. Bilim adamlarının, akış ortamındaki gerçek hızları akışı rahatsız etmeden ölçen bu tip hızlı tekniklere ihtiyacı vardır. Ultrasonik Doppler hız ölçümü (UDHÖ), eş zamanlı birçok noktada ölçüm yapabilme ve ışık geçirgenliği olmayan sıvılarla kullanılabilme gibi özellikleri sayesinde öne çıkan bir tekniktir. UDHÖ yeni uygulamalar ve karmaşık akışların analizi için hala geliştirilen bir tekniktir.

Bu çalışmada sinüsel salımlı, türbülent (rasgele) ve viskoelastik akışkan hareketlerinin, UDHÖ sinyalleri üzerine etkisi teorik ve deneysel olarak incelenmiştir. Rasgele ve viskoelastik akışlar için elde edilen matematiksel ilişkilerden, sırasıyla akış istatistiğini ve gevşeme spektrumunun dağılımını elde etmek için yararlanılmıştır.

Sinüsel salımlı akışın analitik analizi ve sayısal simülasyonu, belirli UDHÖ parametreleri için, akış salınım genliğinin akış salınım frekansına oranının bir sınır değerine sahip olduğunu göstermiştir. Bu kritik değer üzerinde UDHÖ ortalama akış hızını belirlemede başarılı değildir. Hızın olasılık yoğunluk fonksiyonu (PDF) ve oto ilişki fonksiyonu (ACF) ile UDHÖ sinyal spektrumu arasındaki matematiksel ilişkiler, rasgele hızda akış analizi kısmında elde edilmiştir. Direkt hız ölçümlerinden

ve türetilen eşitlik sayesinde fazda (I) – dik fazda (Q) sinyallerinden elde edilen ACF lerin karşılaştırılması, UDHÖ tekniğinin hız ölçümlerindeki zaman çözünürlüğünün iyi bir hız ACF si dolayısıyla türbülans spektrumu elde etmede yeterli olmadığını göstermiştir. Hız ACF si elde etmek için ölçülen hızlardan ziyade I-Q sinyallerini kullanmak zaman çözünürlüğünü, bir hız ölçümü yapmak için kullanılan sinyal sayısı (N_{pm}) oranında artırmıştır.

UDHÖ spektrumundan elde edilen hız PDF si, Gaussian PDF varsayımıyla ölçülen hızlardan elde edilenle karşılaştırıldı. Her iki PDF ninde uyum içinde olduğu görüldü. Ayrıca türetilen eşitlikle, ölçülen I-Q sinyallerini kullanarak elde edilen ACF den hesaplanan bazı boru türbülansı parametreleri, literatür değerleriyle karşılaştırıldı. Sonuçlar iyi derecede uyum gösterdi.

Çalışmanın son aşamasında, küçük genlikli salınımlı basınç alanına sahip boru akışı için doğrusal viskoelastik bir akışkanın kompleks viskozitesi, UDHÖ spektrumuyla matematiksel olarak ilişkilendirilmiştir. Kompleks viskozite terimleri genelleştirilmiş Maxwell modeliyle ifade edilmiştir. UDHÖ spektrumunun sıfır frekans (ortalama akış) bileşeni, genelleştirilmiş Maxwell modelindeki gevşeme viskoziteleri için eşitlik elde etmek amacıyla kullanılmıştır. Sonuçlar UDHÖ tekniğinin bazı viskoelastik materyal özelliklerinin belirlenmesinde kullanılabileceğini ortaya çıkartmıştır.

Sonuç olarak, UDHÖ görece yeni fakat karmaşık akışların rahatsız etmeden ölçümü ve analizi için gelecek vaad eden bir tekniktir.

Anahtar Kelimeler: Kompleks Akışlar, Doğrusal Viskoelastiklik, Rahatsız Etmeden Akış Ölçme, Boru Türbülansı, Rastgele Sinyaller, Ultrasonik Sinyal İşleme, Ultrasonik Doppler Hız Ölçümü (UDHÖ)

To My Dear Wife and My Dear Father

ACKNOWLEDGMENTS

I am very grateful to my supervisor Assoc. Prof. Dr. Yusuf Uludağ for his support and supervision during this study in METU and University of California, Davis. I would like to thank Prof. Dr. Robert L. Powell for his guidance for the carried part of this study in University of California, Davis.

I am very thankful to Middle East Technical University for ÖYP program and providing us doctorate education as a beginning of scientific career. I believe that science is the best way of serving my country and humanity for me.

Finally, I would like to express my gratitude to my wife Tesnim and my parents for their sincere help and support.

TABLE OF CONTENTS

ABSTRACT.....	iv
ÖZ	vi
ACKNOWLEDGMENTS	ix
TABLE OF CONTENTS.....	x
LIST OF TABLES	xiii
LIST OF FIGURES	xiv
LIST OF SYMBOLS	xviii
CHAPTERS	
1. INTRODUCTION.....	1
2. ULTRASOUND DOPPLER VELOCIMETRY AND DISCRETE SIGNAL PROCESSING.....	4
2.1 Ultrasound Doppler Velocimetry (UDV).....	4
2.2 Basic Principles of Discrete-Signal Analysis.....	11
2.2.1 Fourier Transform Representation of Signals.....	13
2.2.2 Random Signals and Their Statistics.....	14
2.2.2.1 Distribution and Probability Density Functions.....	15
2.2.2.2 Mean and Variance	16
3. INTRODUCTORY TURBULENCE AND VISCOELASTICITY	18
3.1 Introduction to Turbulence and Its Statistical Description	18
3.1.1 Navier-Stokes Equation and Reynolds Averaging of Turbulence	22
3.1.2 Statistics of Turbulence.....	23
3.1.3 Power Spectrum	25

3.1.4 Ergodicity of Turbulence	26
3.1.5 Turbulence Parameters.....	26
3.2 Viscoelastic Fluids and Linear Viscoelasticity	29
3.2.1 Maxwell Model.....	32
3.2.2 Kelvin Model	33
3.2.3 Generalized Maxwell Model.....	35
3.2.4 Relaxation Spectrum.....	37
3.2.5 Dynamic Oscillation Tests	38
4. ANALYTICAL AND NUMERICAL INVESTIGATION OF EFFECT OF CONSTANT AND OSCILLATING FLOWS ON SPECTRUM OF ULTRASOUND DOPPLER SIGNALS	42
4.1 Mathematical Representation of Sampled Ultrasound Signals.....	42
4.2 Measurement Volume of Constant Velocity Flow.....	45
4.3 Measurement Volume of Oscillating Velocity Flow	48
4.3.1 Limits of the Spectrum.....	50
4.3.2 Critical Point of the Spectrum.....	51
4.3.3 Simulations.....	51
4.3.4 Comparison of Simulation and Analytical Results	52
5. ANALYTICAL AND EXPERIMENTAL INVESTIGATION OF THE EFFECTS OF RANDOM VELOCITY STATISTICS ON ULTRASOUND DOPPLER SIGNALS.....	61
5.1. Velocity Probability Density Function (PDF)	61
5.2 Experimental Set-Up.....	64
5.3 Verification of PDF and Spectrum Relation by Experimental UDV Measurements	66
5.4. Velocity Auto-Correlation Function (ACF).....	70
5.5 Experimental Velocity ACC and Turbulence Measurements	76

5.5.1 Velocity ACC and Energy Spectrum.....	76
5.5.2 Turbulence Parameters.....	79
6. OBTAINING GENERALIZED MAXWELL MODEL PARAMETERS FOR A LINEAR VISCOELASTIC FLUID BY UDV: A THEORETICAL APPROACH	91
6.1 Obtaining Generalized Maxwell Model Viscosities Using UDV Spectrum	99
6.2 Effects of Material Type and Oscillation Frequency on Spectrum.....	101
7. CONCLUSIONS	106
REFERENCES.....	108
APPENDICES	
A. MATHEMATICAL DERIVATIONS	114
A.1 DFT of Sampled US Signals for Measurement Volume of Oscillating Velocity Flow.....	114
A.2 Auto-Correlation Function in Terms of Energy Spectrum.....	118
A.3 Velocity Auto-Correlation Function (ACF).....	118
A.4 DFT of Sampled US Signals for Measurement Volume of Viscoelastic Fluid Flow	120
B. SIGNAL PROCESSING TABLES	124
CURRICULUM VITAE	127

LIST OF TABLES

TABLES

Table 6.1: Linear viscoelastic parameters in Generalized Maxwell Model for LDPE ...	96
Table B.1: Properties of DFT	124
Table B.2: Some DFT pairs	124
Table B.3: Some useful relations in signal processing	126

LIST OF FIGURES

FIGURES

Figure 2.1.1: Ultrasonic beam and moving particle in this field.....	5
Figure 2.1.2: Position of ultrasonic transducer on a pipe, measurement volumes (channels) and signal processing architecture of Ultrasound Doppler Velocimeter	6
Figure 2.1.3: Artifact effect of far wall	9
Figure 2.1.4: Wall reflection and refraction.....	10
Figure 2.1.5: A typical power spectrum.....	10
Figure 3.1.2.1: PDF of turbulent velocity v	23
Figure 3.1.5.1: Eulerian ACC and time scales	27
Figure 3.2.1: Unsteady shear deformation of a Newtonian fluid (upper) and Hookean solid (lower) between two parallel plates.....	30
Figure 3.2.1.1: Maxwell model	32
Figure 3.2.2.1: Kelvin model	34
Figure 3.2.3.1: Generalized Maxwell model.....	35
Figure 3.2.5.1: Dynamic oscillation of fluid between two plates.	38
Figure 4.1.1: Representation of sampled signal values (right) of nine consecutive pulses (left) back reflected from a moving target (black point).....	43
Figure 4.3.4.1: Change of scaled maximum amplitude in ultrasonic spectrum with amplitude and frequency of oscillating velocity component.	53
Figure 4.3.4.2: Change of scaled total energy in ultrasonic spectrum with amplitude and frequency of oscillating velocity component..	55
Figure 4.3.4.3: Laminar velocity profile in pipe (upper). Spectrum for center of pipe (below).	57

Figure 4.3.4.4: Oscillating velocity profile in pipe with 20% amplitude and 80 Hz frequency (upper). Spectrum for center of pipe (below).....	58
Figure 4.3.4.5: Oscillating velocity profile in pipe with 20% amplitude and 40 Hz frequency (upper). Spectrum for center of pipe (below).....	59
Figure 4.3.4.6: Oscillating velocity profile in pipe with 20% amplitude and 20 Hz frequency (upper). Spectrum for center of pipe (below).....	60
Figure 5.2.1: Ultrasound Doppler Velocimeter-DOP 2125 (top left), ultrasound probes and ultrasonic coupling condom on pipe (bottom).....	65
Figure 5.2.2: Recirculation water flow system	66
Figure 5.3.1: Amplitude of ultrasound spectrum and fitted Gaussian function for $N_{Re}=16733$	68
Figure 5.3.2: Gaussian PDFs obtained from measured velocities and amplitude of ultrasound spectrum ($ S[u] $) through equation (5.1.5) for $N_{Re}=16733$	68
Figure 5.3.3: Amplitude of ultrasound spectrum and fitted Gaussian function for $N_{Re}=26295$	69
Figure 5.3.4: Gaussian PDFs obtained from measured velocities and amplitude of ultrasound spectrum ($ S[u] $) through equation (5.1.5) for $N_{Re}=26295$	69
Figure 5.4.1: Amplitude of spectrum of constant velocity from equation (A.3.1)	73
Figure 5.4.2: Velocity ACC for constant velocity from equation (5.4.3)	73
Figure 5.4.3: Amplitude of spectrum of fluctuating part of velocity for $A_f=10\%$ oscillation amplitude and $f_f=5\text{Hz}$ oscillation frequency from equation (A.3.1)	74
Figure 5.4.4: Velocity ACC of fluctuating part of velocity for $A_f=10\%$ oscillation amplitude and $f_f=5\text{Hz}$ oscillation frequency from equation (5.4.3).....	74
Figure 5.4.5: Amplitude of spectrum of fluctuating part of velocity for $A_f=10\%$ oscillation amplitude and $f_f=10\text{Hz}$ oscillation frequency from equation (A.3.1)	75
Figure 5.4.6: Velocity ACC of fluctuating part of velocity for $A_f=10\%$ oscillation amplitude and $f_f=10\text{Hz}$ oscillation frequency from equation (5.4.3).....	75
Figure 5.5.1.1: Velocity ACC of fluctuating part of measured velocities. Time resolution is 21.3 ms	77

Figure 5.5.1.2: Velocity ACC of fluctuating part of velocity. This is obtained from measured I-Q signals by using equation (5.4.3). Time resolution is 0.138 ms.....	77
Figure 5.5.1.3: Energy spectrum of turbulence at pipe center by using velocity ACC from equation (5.4.3). $N_{Re}=13148$	78
Figure 5.5.1.4: Energy distribution of turbulent length scales at pipe center. $N_{Re}=13148$	79
Figure 5.5.2.1: Mean longitudinal velocity at pipe center	80
Figure 5.5.2.2: Amplitude of velocity fluctuations in probe direction as percentage of longitudinal mean velocity (turbulence intensity) at pipe center	81
Figure 5.5.2.3: Eulerian integral length scale at pipe center from equation (3.1.5.8)	82
Figure 5.5.2.4: Eulerian micro length scale at pipe center from equation (3.1.5.6)...	82
Figure 5.5.2.5: Rate of energy dissipation at pipe center from equation (3.1.5.9).....	83
Figure 5.5.2.6: Kolmogorov length scale at pipe center from equation (3.1.7).....	83
Figure 5.5.2.7: Eddy diffusion coefficient at pipe center from equation (3.1.5.8)	84
Figure 5.5.2.8: Longitudinal average velocity in pipe measured by UDV for $N_{Re}=16733$ and fitted constrained polynomial.....	85
Figure 5.5.2.9: Normalized r.m.s. distribution in probe direction along diameter of pipe for $N_{Re}=16733$	86
Figure 5.5.2.10: Mean longitudinal velocities at $N_{Re}=16733$	87
Figure 5.5.2.11: Amplitude of velocity fluctuations as percentage of mean velocity (turbulence intensity) at $N_{Re}=16733$	87
Figure 5.5.2.12: Eulerian integral length scale at $N_{Re}=16733$ from equation (3.1.5.8)	88
Figure 5.5.2.13: Eulerian micro length scale at $N_{Re}=16733$ from equation (3.1.5.6)	88
Figure 5.5.2.14: Rate of energy dissipation at $N_{Re}=16733$ from equation (3.1.5.9) ..	89
Figure 5.5.2.15: Kolmogorov length scale at $N_{Re}=16733$ from equation (3.1.7).....	89
Figure 5.5.2.16: Eddy diffusion coefficient at $N_{Re}=16733$ from equation (3.1.5.8) ..	90
Figure 6.1: Oscillating piston system to drive an oscillating pipe flow.....	91

Figure 6.2: Phase shift of oscillating velocities with frequency of 10 Hz at the center of pipe compared to the negative pressure gradient (from Eq. (6.15)).	97
Figure 6.3: Numerically and analytically obtained amplitude of spectrum of ultrasonic signals taken from center of pipe for $f_f=10$ Hz oscillating flow ($P^\circ / f_f = 5000$).	98
Figure 6.4: Numerically and analytically obtained amplitudes at center of UDV spectrum (zero frequency) corresponding to different flow oscillation frequencies.	99
Figure 6.2.1: Numerically obtained amplitude of spectrum of ultrasonic signals taken from center of pipe for flow oscillating at 8 Hz ($P^\circ / f_f = 6250$).	102
Figure 6.2.2: Analyzed two different discrete relaxation spectrums of Generalized Maxwell Model for two different fluids.	103
Figure 6.2.3: Oscillating velocities at pipe center for three different fluids and two different oscillation frequencies (from Eq. (6.15)).	104
Figure 6.2.4: Numerically obtained Ultrasound Doppler spectrums from center of pipe for three different fluids and two different oscillation frequencies.	105

LIST OF SYMBOLS

A	: amplitude of emitted ultrasonic signals
A_f	: flow oscillation amplitude as % of mean velocity
A_o	: amplitude of received ultrasonic signals
c	: speed of sound in the flow medium
$d_{o,i}$: distance between probe and i^{th} measurement gate
d_i'	: change of position of particles because of flow at i^{th} measurement gate
$E[k]$: discrete energy spectrum
f_d	: Doppler frequency
f_f	: flow oscillation frequency (Hz)
f_o	: frequency of emitted ultrasonic signals
f_{prf}	: pulse repetition frequency ($1/ T_{\text{prf}}$)
$f_v(v)$: probability density function of random variable v
G	: relaxation modulus
G^*	: complex modulus
G'	: storage modulus (real part of G^*)
G''	: loss modulus (imaginary part of G^*)
$h[n]$: impulse response
$H(w)$: frequency response
I	: in-phase part of demodulated signals
j	: complex number ($\sqrt{-1}$):

J	: creep compliance
J_n	: n^{th} order Bessel function of 1 st kind
k	: discrete frequency
L_f	: Eulerian integral length scale
m_n	: n^{th} moment
n	: discrete time
N_c	: Number of cycles in a pulse
N_{pm}	: number of sended pulses
N_{Re}	: Reynolds number
P	: pressure
P^o	: amplitude of pressure oscillation
P_{max}	: maximum measurable depth
Q	: quadrature part of demodulated signals
r	: radial dimesion
$R_v(\tau)$: auto-correlation function of v
$R'_v(\tau)$: auto-correlation coefficient of v
$s[n]$: sampled discrete ultrasound signal
$S[k]$: discrete spectrum of sampled ultrasound signals
$S(w)$: power spectrum
t_d	: time delay of received ultrasound signals because of fluid motion
t_o	: sampling time for measurement gate (time of emission of n^{th} pulse is reference). Hence t_o is flying time of US signals from probe tip to the measurement gate and back to probe.
T_E	: Eulerian integral time scale
T_L	: Lagrangian integral time scale

T_{prf}	: Time period between emission of two consecutive pulses
$u[n]$: discrete time velocity in probe direction / unit step sequence
$U[k]$: discrete spectrum of $u[n]$
U_{τ}	: friction velocity
v, u, ϑ	: turbulent velocity of fluid along pipe axis, probe axis and radial direction respectively
$\bar{v}, \bar{u}, \bar{\vartheta}$: mean velocity of fluid along pipe axis, probe axis and radial direction respectively
v', u', ϑ'	: fluctuating part of velocity of fluid along pipe axis, probe axis and radial direction respectively
$\tilde{v}, \tilde{u}, \tilde{\vartheta}$: r.m.s. of fluctuating part of fluid velocity along pipe axis, probe axis and radial direction respectively
V_{max}	: maximum measurable velocity
w_0	: basic frequency in spectrum (frequency steps of $2\pi/N$)
z	: axial dimension / acoustic impedance

Abbreviations

ACC	: auto-correlation coefficient
ACF	: auto-correlation function
ADVP	: acoustic Doppler velocity profiler
CDF	: cumulative distribution function
DFT	: discrete Fourier transformation
DTFT	: discrete-time Fourier transformation
ESD	: energy spectral density
FFT	: fast Fourier transform
LDPE	: low density polyethylene
LDV	: laser Doppler velocimeter

LTI : linear time invariant
MRI : magnetic resonance imaging
ODE : ordinary differential equation
PDF : probability density function
PTV : particle tracking velocimeter
r.m.s. : root mean square
r.v. : random variable
UDV : ultrasound Doppler velocimeter
US : ultrasound

Greek Letters

$\delta[n]$: unit impulse function
 ε : energy dissipation rate (m^2/s^3)
 ϕ : phase of a signal
 γ : strain
 $\dot{\gamma}$: rate of strain or shear rate
 Γ : gamma function
 η : mean value / Kolmogorov length scale
 η^* : complex viscosity
 η' : dynamic viscosity (real part of η^*)
 η_0 : zero shear rate viscosity
 η_m : relaxation viscosity in generalized Maxwell model
 λ : wavelength of ultrasound
 λ_E : Eulerian micro time scale

- λ_f : Eulerian micro length scale
 λ_m : relaxation time
 μ : viscosity of fluid
 μ_n : n^{th} central moment
 ν : kinematic viscosity (m^2/s)
 θ : Doppler angle
 ρ : density of fluid
 σ : standard deviation
 τ : Kolmogorov time scale / time difference for auto-correlation
 τ_w : wall shear stress
 τ_{xy} : stress in the x direction on the surface which has normal in the y direction
 ϵ : eddy diffusivity (m^2/s)
 ϵ_m : eddy viscosity

Subscripts

- i : axial direction / index of measurement gate
 j : radial direction

Superscripts

- $*$: complex conjugate

Functions and Operators

- $\text{Arg}\{\}$, \sphericalangle : argument or phase operator
 $E\{\}$: expected value operator
 $\text{Im}\{\}$: imaginary part operator
 $\text{Overbar}(\bar{\quad})$: averaging operator
 $P\{\}$: probability operator

$\text{Re}\{\}$: real part operator
 $|\ |$: absolute value or amplitude operator
 $*$: convolution operator

CHAPTER 1

INTRODUCTION

Flow measurement is an important issue in many industrial processes to control the properties of fluids and for system design economy. Rheological properties of foods and chemicals in a continuous flow system are very important for control and quality purposes [1]. Although sampling and off-line measurement techniques are available, these are not real time analysis and slow. In-line velocity profile measurement is a quick and useful way to get shear deformation of fluid. This knowledge can be used to get rheological properties of fluid with simultaneous pressure measurements. Therefore in-line, non-invasive and fast measurement techniques are very useful not only for industrial applications but also for scientific studies [2]. Ultrasound Doppler velocimetry (UDV) is one of such techniques stands with many advantages over other techniques. Generally food and other industrial fluids are opaque. UDV is a suitable and low cost technique for measurement of such opaque materials.

Ultrasound Doppler velocimetry (UDV) technique (also called as ultrasound velocity profiler (UVP), acoustic Doppler velocity profiler (ADVP)) was originally used in medical applications [3], especially in researches of blood flow [4, 5]. After some pioneering studies published in early 1990's [6], fluid dynamics application of UDV in engineering field has considerably increased [7]. Different flow systems and fluids have been investigated such as hot liquid metals [8, 9], magnetic fluids [10], viscoelastic polymer melts [11], rheological properties of suspensions [12], multiphase flow applications [13, 14] and flow through a porous bed [15].

UDV is capable of obtaining velocity profile in short times (in a couple of ms), and of measuring velocity in opaque liquids. It is also a non-intrusive method. These features make this technique preferable compared to some older well established

methods such as laser Doppler velocimetry (LDV), magnetic resonance imaging (MRI) and particle tracking velocimetry (PTV) [16, 17].

In spite of its attractive features, UDV has some difficulties and limitations in flow measurements compared to the previously mentioned well established techniques. For example reflective particle concentration and size distribution have a strong impact on the quality of UDV data [18, 19]. Near wall measurements are not reliable because of high-pass filtering of signals employed to eliminate signals coming from wall interfaces. This process, on the other hand, decreases the sensitivity for low velocities encountered typically near the walls [13, 17, 20]. Time resolution of measurements is another limiting criterion for this technique which is bounded by the speed of sound in flow medium. Time resolution in LDV and MRI measurements is several times higher than that of UDV since signals propagate at the light speed in the former ones [17, 21, 22]. Time resolution is critical in quickly changing flow regimes like strong turbulent flows [23].

Spatial resolution is also crucial in flow measurements. In UDV diameter of ultrasound (US) probe and length of US pulse determine the spatial resolution of the measured velocity distribution. Beam shapes created by shape and size of probe has significant effects on spectrum of Doppler ultrasound [24]. Selection of correct size of probe compared to the size of the flow system is very important to obtain satisfactory spatial resolution. Shape of the measurement gates (pixels) is cylindrical with diameter close to that of probe and length equal to the half length of US pulses. Therefore point focusing is not possible for this technique like LDV which is critical in highly turbulent flows [25]. We can think of coming velocity information from a gate as averaging of all velocities within the volume. Coupling of US probe with flow conduit, gases within the fluid, knowing sound velocity in the flow medium are other important concerns of UDV technique [26].

Despite the listed resolution limitations of UDV compared to other methods, typically time and spatial resolutions about 20 ms and 0.7 mm are easily achieved in UDV measurements. These values correspond to a velocity resolution of 1 cm/s,

which is quite sufficient for most of the engineering studies including turbulent flows. Therefore UDV has already become a tool for process monitoring and control purposes. It is reported as a fast and useful in-line measurement tool to evaluate rheological properties of fluids by using with simultaneous pressure drop measurements [27, 28]. Capability of measuring velocity profiles of opaque liquids appears as an important advantage of UDV as most of the commercial chemicals and foods are opaque.

There are some studies which aimed to improve the signal processing algorithm of commercial UDV method [29]. Some of them consider time resolution of the method and others deal with measurement of transverse (vertical to probe) velocities by using correlation algorithms [5, 30].

Experimental studies regarding UDV are generally encountered in the literature [31, 32, 33]. However, theoretical or mathematical studies are very limited [34, 35]. Moreover many of experimental measurements are based on temporally averaged velocities discarding exact time change of velocities and turbulence. Also studies of flow of complex fluids like viscoelastic fluids are very rare in literature [36, 37]. The emerging point of this study is then, to utilize the interaction between the sound signals and flow field in order to characterize the flow. Here crucial point is to develop mathematical models for the flow effects on the sampled signals [38, 39].

This study can be divided into three main parts. First part includes theoretical analysis of effects of oscillating flows on US signals. Results are verified through computer simulations. This part was first step in investigating turbulent flow which was considered in the second part. Relation between relevant statistical properties (probability density function and auto-correlation function) of measured random velocities (turbulent velocity) and spectral properties of sampled US signals was established in this part. Experimental confirmation of these relations was also carried out after development of mathematical results. Finally another type of complex flow was considered. Effect of the relaxation spectrum of a flowing linear viscoelastic fluid on the spectrum of US signals was modeled.

CHAPTER 2

ULTRASOUND DOPPLER VELOCIMETRY AND DISCRETE SIGNAL PROCESSING

2.1 Ultrasound Doppler Velocimetry (UDV)

Doppler ultrasound technique initially used in medical field goes back to more than 30 years [40]. Non-invasive, fast and easy setting-up features of pulsed Doppler ultrasound technique increased its use in other flow measurements noticeably. In UDV single probe is used to emit and then receive (listen) ultrasonic pulses [6, 41]. Hence probe is switched to the listening mode after sending short sound pulses to receive back reflected echoes. Actually, Doppler expression in the name is misleading for the basic principle of this method. In UDV velocities are obtained from position shifts of reflecting particles in flow (i.e. time shifts of consecutive pulses) by sampling the incoming echoes at the same time relative to the burst emission. Therefore Doppler shift is not the case as opposed to laser Doppler velocimetry (LDV).

UDV measures the velocity vector which is in the direction of probe in measurement point. Since only this velocity component is creating Doppler effect on ultrasound (US) signals. Therefore orientation and coupling of US probe is important to obtain good measurements [13]. UDV samples the echo of ultrasound pulse signals from a definite gate (volume) at a definite time which depends on sound velocity in flow medium and distance of measurement gate. Phase of back sampled ultrasound is changing related to the velocity of particles in measurement gate. This phase shift reveals as time shift in time domain and as frequency shift in frequency domain according to Doppler equation. This frequency shift can be obtained after demodulating and low-pass filtering by taking the F.F.T. (Fast Fourier Transform) of

back sampled pulses. This frequency can be used to obtain velocity along probe in measurement gate according to the Doppler equation,

$$U = \frac{c.f_d}{2f_0} \quad (2.1.1)$$

Simultaneously demodulated and low-pass filtered echo signals are phase shifted by $\pi/2$ (quadrature part) to obtain flow direction.

For a single particle that is present along ultrasonic beam (Figure 2.1.1), its distance to the tip of transducer can be obtained from time difference (T_d) between emission and sampling of signals as,

$$P = \frac{c.T_d}{2} \quad (2.1.2)$$

where c is the sound velocity in flow medium.

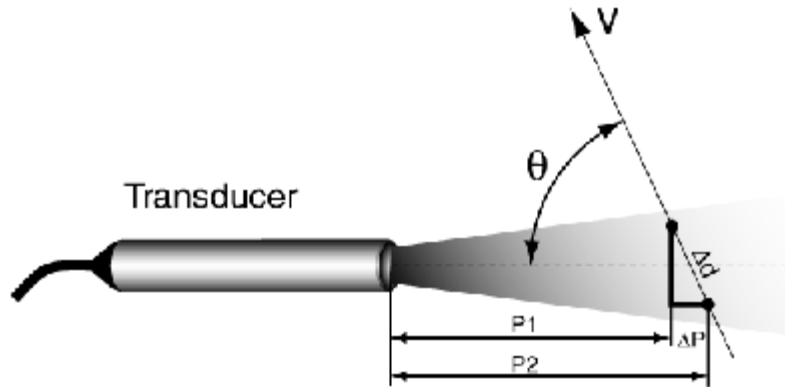


Figure 2.1.1: Ultrasonic beam and moving particle in this field

The displacement of the particle between two consecutive emissions separated by time of T_{prf} can be expressed as,

$$P_2 - P_1 = \frac{c}{2}(T_{d2} - T_{d1}) = V \cdot \cos \theta \cdot T_{prf}$$

If we change the time difference with phase shift,

$$\delta = 2\pi.f_0.(T_{d2} - T_{d1}) \Rightarrow V = \frac{c.\delta}{4\pi.f_0 \cos\theta.T_{prf}} = \frac{c.f_d}{2f_0 \cos\theta} \quad (2.1.3)$$

where f_d appears as frequency shift and this final equation is the same as the Doppler frequency shift equation since both are based on the same physical phenomenon. Therefore in the literature the term Doppler shift is used for the frequency change of US due to displacement of the source. In the case of randomly distributed particles, a combination of echoes from each particle will be received. Despite of random particle combination within measurement volume there should be a correlation between consecutive samples that is used to obtain velocity by digital signal processing techniques [42]. Figure 2.1.2 schematically shows the installation of probe on a pipe and order of signal processing algorithms.

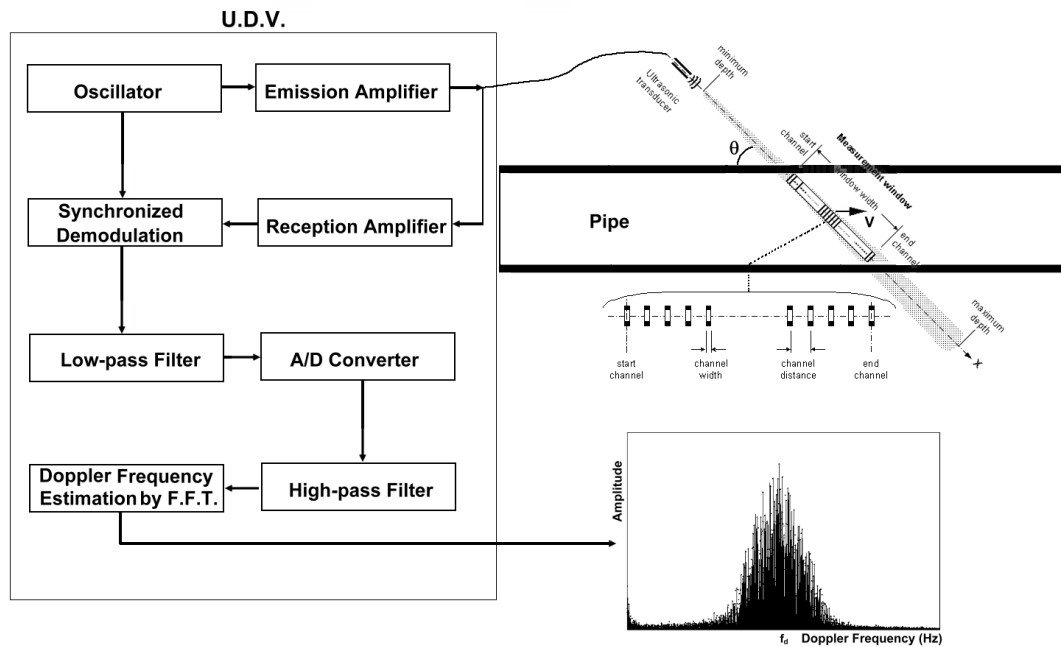


Figure 2.1.2: Position of ultrasonic transducer on a pipe, measurement volumes (channels) and signal processing architecture of Ultrasound Doppler Velocimeter

One of the most important features of the UDV technique is its ability to measure velocity values in many spatial points along ultrasonic emission axis. A window function is used to get the signals from wanted measurement range in the flow. Thereby receiver is switched to listening mode only for windowed time range. Channel width determines the spatial resolution and is given by the formula,

$$l_w = \frac{N_c \lambda}{2} \quad (2.1.4)$$

where N_c is the number of cycles per pulse, λ is the US wavelength. Width of channels can be half of the total length of pulse at maximum, since each signal must travel the same distance back to the receiver. Listening duration is equal to the time of traveling of length of pulse. Therefore width of channels maximum can be half of pulse length to capture signals throughout all desired region of the flow while excluding those originating beyond this region. Switching time of transducer is practically negligible compared to travelling time of pulses. Increasing number of cycles per pulse may cause channel width to be greater than channel distance leading to overlapping of two adjacent measurement channels. This phenomenon causes spatial averaging of velocities because of taking signals from neighboring channels of measurement channel which results in smoothing of velocity profile. This can be problematic for flows that have vigorous change of gradient.

Measurement window is distance between first and last measurement channels. This must be smaller than maximum measurable depth which is

$$P_{\max} = \frac{c}{2f_{\text{prf}}} \quad (2.1.5)$$

where f_{prf} is pulse repetition frequency (i.e. $1/T_{\text{prf}}$). Also Nyquist sampling theorem limits the maximum detectable Doppler frequency which is $f_{d,\max} = f_{\text{prf}}/2$. This means there would be a maximum detectable velocity given by equation (2.1.3).

$$V_{\max} = \frac{c f_{\text{prf}}}{4f_o} \quad (2.1.6)$$

Combining previous two equations gives the following constraint,

$$V_{\max} P_{\max} = \frac{c^2}{8f_0} \quad (2.1.7)$$

which means increasing either maximum velocity or maximum depth limit causes the decreasing of the other one. Decreasing f_0 is a way to increase both maximum limit values but this cause the decreasing of spatial resolution. Velocity resolution is defined by the resolution of discrete Doppler spectrum which can be represented as [43],

$$\Delta V = \frac{c}{2f_0 T_{pc}} \quad (2.1.8)$$

T_{pc} is profile calculation time and equals to $N \times T_{prf}$, where N is number of pulses that is used to determine velocity profile. Average time resolution of velocity measurements is equal to one profile calculation time (T_{pc}). The amplification of the received echo signals is needed to compensate attenuations due to physical medium. The signals from distant points experience more attenuation than those of closer locations. Parameters associated with signal amplification must be optimized to be able to get enough reflected signal energy for measurements. If the signals are weak, it might be useful to increase pulse repetition number (N) and/or number of cycles per pulse (N_c). But this will cause a decrease on time resolution and/or spatial resolution [44].

Ultrasonic waves emitted from probe propagate in a conical geometry. They are reflected and refracted by particles that have bigger size than their wavelength and have a different acoustic impedance ($z=\rho.c$). This will change the propagation direction of ultrasonic waves which is not desired in this technique. If the size of the particles is smaller than wavelength, they will cause reflections of a small amount of ultrasonic energy back. This small amount of sampled reflections practically doesn't affect the propagating waves [45].

Interface walls cause some artifacts on sampled signals. This makes measurements difficult for points close to the far interface. For example as shown in Figure 2.1.3 below some ultrasonic signals are back reflected directly from particle at C while some signals are following A-B-C-A path to turn back to transducer. Total time of flying of second path is corresponding to a measurement point outside of the wall which normally doesn't have any liquid or flow. This gives artificial velocity profile for depths beyond far wall interface. Hence one should be aware of the position of the wall interface.

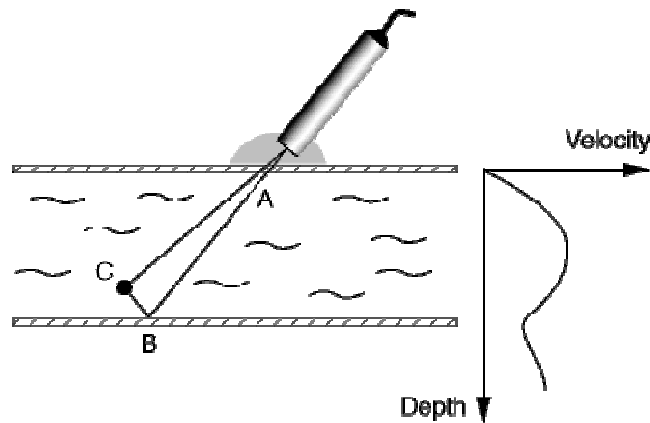


Figure 2.1.3: Artifact effect of far wall

Energy reflected by interfaces is stronger than the ones coming from particles in flow. Effects of stationary interfaces are eliminated by passing signals through a high pass filter. But this decreases the sensitivity to low velocities. If interface is moving and creates same frequency shift with flowing particles, it won't be possible to eliminate its effect on measured velocity field. Interfaces cause many reflections which will interfere with the reflections from particles.

Another important wall effect is amount of reflections and refractions when ultrasonic beam is passing from coupling medium to wall of conduit (Figure 2.1.4) [13].

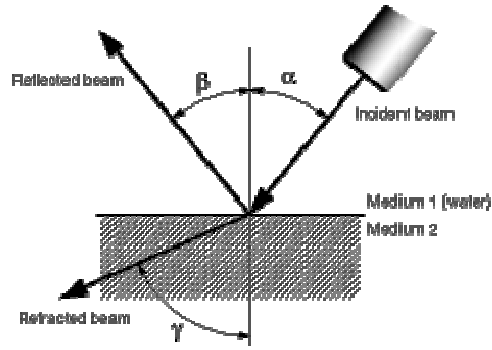


Figure 2.1.4: Wall reflection and refraction

There is a critical value of incident angle α after which total reflection is observed. Critical angle for water-PVC interface is around 27° .

Amplitude of demodulated echo signals (I and Q signals) taken from a measurement gate fluctuates due to particles of different sizes and different acoustic impedances. Sampled signal amplitude is a result of combined effect of these particles and demodulated signals will contain many Doppler frequencies because of different velocities within measurement volume. The frequency content of the sampled signals can be obtained from power spectrum which is FFT (Fast Fourier Transformation) of signals. Demodulated signals are passed through a high pass filter before computation of power spectrum for removing stationary components. Power spectrum (Figure 2.1.5) is given in logarithmic scale and frequency scale is converted to velocity by using Doppler equation (Eq. (2.1.3)).

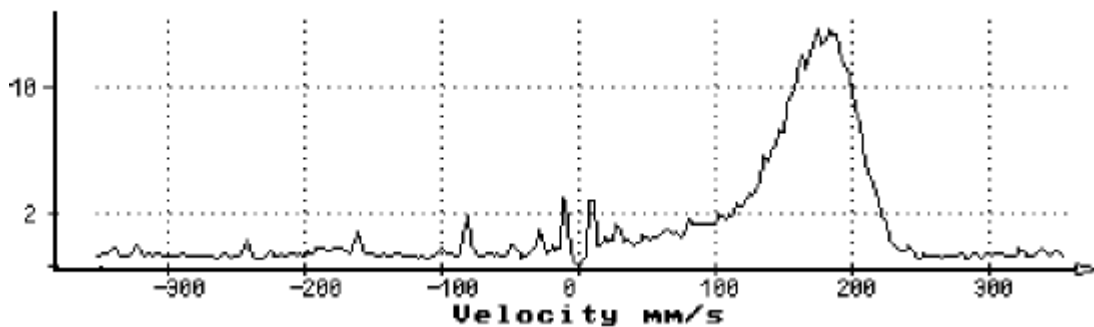


Figure 2.1.5: A typical power spectrum

2.2 Basic Principles of Discrete-Signal Analysis

In the modeling of the effect of various flow and fluid properties, effects on the UDV signals the starting point will be discrete representation of the UDV signals. In addition FFT of the discrete time domain signals will be extensively employed. Therefore it is deemed useful to introduce the basic discrete signal analysis below.

In all cases of signals information is contained in some pattern of variations and signals are represented as function of one or more independent variables. Independent variable in a mathematical representation may be either continuous or discrete. Continuous time signals are called as *analog signals*. Besides discrete-time signals are called as *digital signals*. Discrete time signals can be created by sampling continuous time signals or directly from a discrete time process [46]. Discrete time signals are represented as sequences of numbers. The n^{th} number in a sequence x is denoted as $x[n]$. n is an integer and such a sequence is obtained from periodic sampling of analog signals. Hence relation between discrete and analog values is $x[n]=x_a(n.T)$ where T is *sampling period*. $X[n]$ is only defined for integer values of n and undefined for non-integer values. Original analog signal can be reconstructed from sequence of samples if the samples are taken frequently enough. Any sequence can be expressed as,

$$x[n] = \sum_{k=-\infty}^{\infty} x[k]\delta[n-k] \quad (2.2.1)$$

where $\delta[n]$ is *unit impulse* function which is one when $n=0$ and zero otherwise. Unit step sequence is defined as,

$$u[n] = \begin{cases} 1 & n \geq 0 \\ 0 & n < 0 \end{cases} \text{ or} \quad (2.2.2)$$

$$u[n] = \sum_{k=-\infty}^{\infty} u[k]\delta[n-k] = \sum_{k=0}^{\infty} 1 \times \delta[n-k]$$

Unit impulse function can be represented in terms of unit step sequences as follows,

$$\delta[n] = u[n] - u[n-1] \quad (2.2.3)$$

Sinusoidal and complex exponential sequences are very important in signal analysis since they are occurring widely in physical systems. A sinusoidal sequence has general form,

$$x[n] = A \cos(\omega_0 n + \phi) \quad (2.2.4)$$

and a complex exponential sequence is,

$$x[n] = |A| e^{j(\omega_0 n + \phi)} = |A| \cos(\omega_0 n + \phi) + j|A| \sin(\omega_0 n + \phi) \quad (2.2.5)$$

where ω_0 is frequency in radians and ϕ is phase of signals. n is always integer in here and this creates some differences on signals compared to continuous time signals. For example an oscillatory signal with frequency ω_0 and $\omega_0 + 2\pi r$ (r is integer) are indistinguishable from one another. Hence we need to consider only frequencies within interval of 2π such as $-\pi < \omega_0 < \pi$. Another difference between continuous and discrete sinusoidal signals is interpretation of high and low frequencies. Oscillation of a continuous time sinusoidal signal is getting more and more rapid while oscillation frequency is increasing. However a discrete time sinusoidal signal oscillates more rapidly as ω_0 increases from 0 to π and oscillates more slowly as ω_0 increases from π to 2π . Since frequencies of 0 and 2π are identical in discrete case. Therefore the 0 frequency is referred to lowest frequency and π to highest frequency for discrete signals.

If $x[n]$ is input, output of a linear time-invariant (LTI) system can be represented as,

$$y[n] = \sum_{k=-\infty}^{\infty} x[k] h[n-k] \quad (2.2.6)$$

where $h[n]$ is impulse ($\delta[n]$) response of the system and $h[n-k]$ is response to $\delta[n-k]$. Equation (2.2.6) is called as *convolution sum* and depicted as,

$$y[n] = x[n] * h[n] \quad (2.2.7)$$

Complex exponential and sinusoidal sequences play important role for representing discrete time signals. This is because complex exponentials are eigenfunctions of LTI systems. Response to a sinusoidal input is sinusoidal with the same frequency and with amplitude and phase determined by the system. This fundamental property of LTI systems makes useful representation of signals in terms of complex exponentials (Fourier representation). For example if input sequence is $x[n]= e^{j\omega n}$, output of the LTI system with impulse response $h[n]$ will be,

$$y[n] = \sum_{k=-\infty}^{\infty} h[k]e^{j\omega(n-k)} = e^{j\omega n} \underbrace{\sum_{k=-\infty}^{\infty} h[k]e^{-j\omega k}}_{H(\omega)} \quad (2.2.8)$$

where *frequency response* $H(\omega)$ is eigen value and $e^{j\omega n}$ is eigen function of the system. $H(\omega)$ is generally complex and shows how amplitude of complex exponential input changes. Also $H(\omega)$ is periodic in frequency with period 2π .

2.2.1 Fourier Transform Representation of Signals

Wide range of signals can be represented as linear combination of complex exponentials as,

$$x[n] = \sum_k a_k e^{j\omega_k n} \quad (2.2.1.1)$$

One way is to use Discrete Time Fourier Transform (DTFT):

$$x[n] = \frac{1}{2\pi} \int_{-\pi}^{\pi} X(\omega) e^{j\omega n} d\omega \quad \text{inverse DTFT \{synthesis equation\}} \quad (2.2.1.2)$$

$$\text{where } X(\omega) = \sum_{n=-\infty}^{\infty} x[n] e^{-j\omega n} \quad \text{DTFT}$$

Frequency weighting function $X(\omega)$, which determines the contribution of each complex exponential to synthesize $x[n]$, is complex and can be written in polar notation as,

$$X(\omega) = |X(\omega)| e^{j\angle X(\omega)} \quad (2.2.1.3)$$

where $|X(w)|$ and $\angle X(w)$ are amplitude and phase of Fourier transform respectively. If any sequence is absolute summable i.e. $\sum_{n=-\infty}^{\infty} |x[n]| < \infty$ then Fourier transform exists.

Sequences taken from measurements are generally with finite duration. Fourier representation of these signals is referred to as *discrete Fourier transform* (DFT). DFT is a sequence also by itself which is composed of samples of Fourier transform of signal. Time domain discrete sequence is accepted to be periodic with total number of samples (N) and frequency domain DFT sequence will also be periodic with N in this transform. Frequency domain components appear at integer multiples of basic frequency $w_0=2\pi/N$. Discrete frequency is depicted with k while discrete time with n. DFT pairs are as follows,

$$x[n] = \frac{1}{N} \sum_{k=0}^{N-1} X[k] e^{j(2\pi/N)kn} \quad \text{inverse DFT \{synthesis equation\}} \quad (2.2.1.4)$$

$$\text{where } X[k] = \sum_{n=0}^{N-1} x[n] e^{-j(2\pi/N)kn} \quad \text{DFT}$$

2π stands for maximum sampling frequency which determines the limit of detectable frequency after DFT. *Nyquist sampling theorem* says that minimum sampling frequency of a continuous time signal must be two times highest frequency that shown in Fourier spectrum in order to get continuous signal back from its samples ($f_s \geq 2f_N$). You can see properties of DFT and some DFT pairs in APPENDIX B.

2.2.2 Random Signals and Their Statistics

A *random variable* (r.v.) is a function that assigns a value to the outcome of a random process (experiment). For example turbulent velocity (\mathbf{v}) at a measurement point is a r.v. This turbulent velocity is a time function. Values of random turbulent velocity at a specific time will be obtained by realization of turbulent flow several times with same boundary conditions and by measuring velocities at designated time. These measured values will give the ensemble of random turbulent velocity at a

specified time. All statistical analysis should be done on this ensemble of values. A *discrete random variable* can take only specific, isolated numerical values, like the outcome of tossing a die. On the other hand a *continuous random variable* can take any values within a continuous interval, like temperature in a room. Each assigned value of a r.v. has a probability. For example $P\{\mathbf{v}=\mathbf{v}\}$ shows the probability of random velocity \mathbf{v} of being \mathbf{v} . Similarly $P\{\mathbf{v}\leq\mathbf{v}\}$ shows the probability of random velocity \mathbf{v} of being equal or less than \mathbf{v} . For any r.v. \mathbf{x} , $P\{\mathbf{x}=\infty\} = P\{\mathbf{x}=-\infty\} = 0$.

2.2.2.1 Distribution and Probability Density Functions

Cumulative Distribution Function (CDF) of r.v. \mathbf{x} is defined as [51, Ch.4, 5],

$$F_x(\mathbf{x}) = P\{\mathbf{x}\leq\mathbf{x}\} \text{ defined for } -\infty \leq \mathbf{x} \leq \infty$$

Some properties of distribution function:

- 1) $F_x(+\infty) = 1$, $F_x(-\infty) = 0$
- 2) If $x_1 < x_2$ then $F_x(x_1) \leq F_x(x_2)$
- 3) $P\{\mathbf{x}>\mathbf{x}\} = 1 - F_x(\mathbf{x})$
- 4) $P\{x_1 < \mathbf{x} \leq x_2\} = F_x(x_2) - F_x(x_1)$
- 5) r.v. \mathbf{x} is continuous if $F_x(\mathbf{x})$ is continuous. \mathbf{x} is discrete type if $F_x(\mathbf{x})$ is a staircase function.

Derivative of $F_x(\mathbf{x})$ is called as Probability Density Function (PDF) of r.v. \mathbf{x} ,

$$f_x(\mathbf{x}) = \frac{dF_x(\mathbf{x})}{d\mathbf{x}} \tag{2.2.2.1.1}$$

If \mathbf{x} is discrete r.v. taking the values x_i with probabilities p_i [46, App.A],

$$f_x(\mathbf{x}) = \sum_i p_i \delta(\mathbf{x} - x_i) \tag{2.2.2.1.2}$$

where $p_i = P\{\mathbf{x}=x_i\}$

Some properties of PDF:

$$1) f_x(x) \geq 0$$

$$2) F_x(x) = \int_{-\infty}^x f_x(\xi) d\xi \text{ and } F_x(\infty) = \int_{-\infty}^{\infty} f_x(x) dx = 1$$

$$3) F_x(x_2) - F_x(x_1) = \int_{x_1}^{x_2} f_x(x) dx = P\{x_1 < \mathbf{x} \leq x_2\}$$

Normal or Gaussian is one of the most commonly encountered PDFs which is,

$$f_x(x) = \frac{1}{\sigma\sqrt{2\pi}} e^{-(x-\eta)^2/2\sigma^2} \quad (2.2.2.1.3)$$

where η is mean value and σ is standard deviation. PDF of a r.v. \mathbf{y} which is a function of r.v. \mathbf{x} can be related to the PDF of \mathbf{x} as following,

For $\mathbf{y}=\mathbf{g}(\mathbf{x})$, if x_1, x_2, \dots, x_n are roots of this equation {i.e. $y=\mathbf{g}(x_1)=\mathbf{g}(x_2)= \dots =\mathbf{g}(x_n)$ } and $g'(x)$ is derivative of $g(x)$ with respect to x .

$$f_y(y) = \frac{f_x(x_1)}{|g'(x_1)|} + \frac{f_x(x_2)}{|g'(x_2)|} + \dots + \frac{f_x(x_n)}{|g'(x_n)|} \quad (2.2.2.1.4)$$

2.2.2.2 Mean and Variance

The mean or expected value of a r.v. \mathbf{x} is defined by

$$\eta_x = E\{\mathbf{x}\} = \int_{-\infty}^{\infty} x f_x(x) dx \quad (2.2.2.2.1)$$

For discrete type r.v. this integral can be written as a sum.

$$E\{\mathbf{x}\} = \sum_i x_i p_i \quad (2.2.2.2.2)$$

where \mathbf{x} takes discrete values x_i with probability p_i . Expected value of the function $\mathbf{y}=\mathbf{g}(\mathbf{x})$ of r.v. \mathbf{x} will be,

$$\eta_y = E\{\mathbf{g}(\mathbf{x})\} = \int_{-\infty}^{\infty} \mathbf{g}(x) f_x(x) dx \quad (2.2.2.2.3)$$

If x is discrete type,

$$E\{\mathbf{g}(\mathbf{x})\} = \sum_i \mathbf{g}(x_i) P\{\mathbf{x} = x_i\} \quad (2.2.2.2.4)$$

Linearity property of expected value operation gives,

$$E\{a_1 \mathbf{g}_1(\mathbf{x}) + a_2 \mathbf{g}_2(\mathbf{x}) + b\} = a_1 E\{\mathbf{g}_1(\mathbf{x})\} + a_2 E\{\mathbf{g}_2(\mathbf{x})\} + b \quad (2.2.2.2.5)$$

The variance of a random variable \mathbf{x} is,

$$\sigma_x^2 = E\{(x - \eta_x)^2\} = \int_{-\infty}^{\infty} (x - \eta_x)^2 f_x(x) dx \quad (2.2.2.2.6)$$

σ_x is called as standard deviation of r.v. \mathbf{x} . For discrete type \mathbf{x} ,

$$\sigma_x^2 = \sum_i (x_i - \eta_x)^2 p_i \quad (2.2.2.2.7)$$

Moments are another interest of r.v. studies. n^{th} moment is defined as,

$$m_n = E\{\mathbf{x}^n\} = \int_{-\infty}^{\infty} x^n f_x(x) dx \quad (2.2.2.2.8)$$

n^{th} central moment is,

$$\mu_n = E\{(\mathbf{x} - \eta)^n\} = \int_{-\infty}^{\infty} (x - \eta)^n f_x(x) dx \quad (2.2.2.2.9)$$

CHAPTER 3

INTRODUCTORY TURBULENCE AND VISCOELASTICITY

3.1 Introduction to Turbulence and Its Statistical Description

Definition of turbulence given by Taylor and Von Karman [47] is: “Turbulence is an irregular motion generally appears in fluids when they pass over a solid surface or even over a stream of same fluid.” Because of this irregularity it is not possible to describe the turbulent motion as a function of time and space in detail. Both Eulerian (fixed point measurements) and Lagrangian (moving particle measurements) velocities are irregular function of time in turbulent fluid motions. But turbulence is not an absolutely irregular motion since it can be described by the statistical laws. Turbulent flow of viscous fluids is a dissipative kind of motion which converts kinetic energy into heat. Hence without an external energy source turbulence is going to decay. Viscosity also makes turbulence more homogeneous. Gradient of average velocity for homogeneous turbulence would be constant throughout the flow field. If statistical properties don't have any directional preference, turbulence is called as *isotropic* turbulence. Gradient of average velocity for isotropic turbulence would be zero. If mean velocity has a gradient, the turbulence is then termed as *anisotropic* [47, Ch.1]. Flows with constant periodicity (regular pattern) which are called as *pseudo turbulent flows* can be used to simulate and understand real turbulent flows.

Turbulent flows can have different scales of patterns which are called as *scale of turbulence*. These scales are determined by the velocities and size of geometry in which turbulence occurs. For example time scale of pipe turbulence would be in the order of ratio of pipe diameter to mean velocity. Spatial scale is going to be in the order of pipe diameter. Another parameter characterizing the turbulence is intensity of turbulence which is given by root-mean square values of turbulent fluctuations

with respect to time (v'). By definition mean value of velocity fluctuations ($\overline{v'}$) is zero. Turbulent velocity can be decomposed into summation of average value and fluctuating part (Reynold's decomposition) as,

$$v = \overline{V} + v' \quad (3.1.1)$$

Root-mean square (r.m.s.) of fluctuations,

$$\tilde{v} = \sqrt{\overline{v'^2}} \quad (3.1.2)$$

Relative intensity of turbulence at a point is defined as,

$$\frac{\tilde{v}}{\overline{V}} \quad (3.1.3)$$

Average velocity value can be obtained by taking time average if turbulent flow field is stationary random (i.e. statistical properties are constant). Otherwise average must be taken over large number of experiments with the same initial and boundary conditions. This is called as ensemble average. Space averaging can be possible if turbulence is homogeneous. These averaging techniques are useful for Eulerian velocity measurements. Averaging over large number of particles or ensemble averaging must be used for Lagrangian measurements. Lagrangian measurements are convenient to study turbulent transport or diffusion. Time averaging at a fixed point (x_0) can be expressed mathematically as,

$$\overline{V}(x_0) = \lim_{T \rightarrow \infty} \frac{1}{2T} \int_{-T}^T v(x_0, t) dt \quad (3.1.4)$$

Practically it is not possible to take time interval T as infinity but it should be large enough compared to turbulent time scale. Hence

$$\overline{V}(x_0) = \frac{1}{2T} \int_{-T}^T v(x_0, t) dt \quad (3.1.5)$$

Turbulence consists of superposition of eddies of many sizes. But the size of the smallest eddies are determined by the viscosity of fluid since velocity gradients are biggest for these eddies which creates viscous shear stress and cease eddies. These smallest eddies in turbulent motion corresponds to minimum scales and maximum frequencies. Kinetic energy is distributed among these eddies of different sizes and frequencies which is called as *energy spectrum*. Size of the biggest eddies are determined by the size of the flow geometry where as size of smallest ones are determined by viscosity and mean velocity. Increasing mean velocity decreases the size of smallest eddies. Turbulent flows have a strong diffusive nature which makes turbulent transport more prominent. Turbulent kinetic energy is transferred through eddies from bigger to smaller and finally it is dissipated by viscous forces.

Turbulent flows in circular pipes arise from laminar flows because of instabilities at Reynolds numbers ($R \times V \times \rho / \mu$) of around 2000. Diffusive nature of turbulence can be described by means of effective diffusivity (eddy diffusivity) but this causes to treat the turbulence as a property of fluid rather than a property of flow [48]. Conceptually this is not correct but it is sometimes useful in engineering applications. Dimensional analysis gives the scale of eddy diffusivity as follows,

$$\epsilon \sim \tilde{v} L \quad (3.1.6)$$

where L is characteristic length scale (integral scale) of the flow. Expressions like this with experimentally determined coefficients are used in practical applications. Since small scale motions have much smaller time scales compared to large scale motions we can assume them as statistically independent. Hence small scale motions are only dependent on the rate of energy supplying from main flow and kinematic viscosity. We can assume energy supply as equal to energy dissipation in small scale motions. This is the basis for *Kolmogorov's equilibrium theory* of small scale structures. Hence *Kolmogorov microscales* can be expressed by using turbulent energy dissipation rate (ϵ , m^2/s^3) and kinematic viscosity (ν , m^2/s) as follows,

$$\eta = \left(\frac{v^3}{\varepsilon}\right)^{1/4} \text{ is Kolmogorov length scale} \quad (3.1.7)$$

$$\tau = (v / \varepsilon)^{1/2} \text{ is Kolmogorov time scale}$$

$$V = (v.\varepsilon)^{1/4} \text{ is Kolmogorov velocity scale}$$

Kolmogorov scales are the smallest turbulent scales that occur in a turbulent flow and viscous dissipation is very strong at this scale [47, pp.223]. Reynolds Number with reference to this length and velocity scales is one.

$$N_{Re} = \frac{V.\eta}{v} = 1 \quad (3.1.8)$$

Energy supply rate of the largest eddies can be given by multiplication of their kinetic energy and fluctuation frequency since they lose their energy generally after one cycle. Hence energy dissipation rate is of order,

$$\varepsilon \sim \tilde{v}^2 . \tilde{v} / L = \tilde{v}^3 / L \quad (3.1.9)$$

This shows that viscous energy dissipation can be predicted from large scale dynamics and it is independent of viscosity. Hence we can conclude viscous dissipation as a passive process that proceeds at a determined rate by inviscid inertial large eddy motions. The non-linear mechanism of turbulence is dissipative since it creates smaller and smaller eddies until eddy sizes become so small that viscous dissipation dominates. Scale separation of small and large scale eddies are increasing with increasing Reynolds number. Therefore statistical independence of small scale eddies become clearer at high Reynolds numbers. The main difference between two different turbulent flows with different Reynolds numbers and same integral scale is the size of the smallest eddies. Higher Reynolds number flows have finer small scale structures. Most of the vorticity is associated with small scale eddies while most of the energy is associated with large scale eddies. Vorticity of small scale motions should be proportional to reciprocal of their time scale since vorticity has the unit of frequency.

3.1.1 Navier-Stokes Equation and Reynolds Averaging of Turbulence

Navier-Stokes equation for a Newtonian and incompressible fluid by invoking the equation of continuity ($\partial v_i / \partial x_i = 0$) is going to be,

$$\rho \left(\frac{\partial v_i}{\partial t} + v_j \frac{\partial v_i}{\partial x_j} \right) = - \frac{\partial P}{\partial x_i} + \mu \frac{\partial^2 v_i}{\partial x_j \partial x_j} \quad (3.1.1.1)$$

After decomposing velocity and pressure terms as summation of mean and fluctuation values (Reynold's decomposition) and taking time average of both sides, equation of motion for average quantities will be,

$$\rho \left(\frac{\partial \bar{V}_i}{\partial t} + \bar{V}_j \frac{\partial \bar{V}_i}{\partial x_j} \right) = - \frac{\partial \bar{P}}{\partial x_i} + \frac{\partial}{\partial x_j} \left(\mu \frac{\partial \bar{V}_i}{\partial x_j} - \rho \overline{v_i' v_j'} \right) \quad (3.1.1.2)$$

$\overline{v_i' v_j'}$ appears as another stress term in addition to the pressure and viscous stresses. These double fluctuating velocity correlations are called as *Reynold's stresses*. If $\overline{v_i' v_j'} \neq 0$, v_i and v_j are correlated otherwise they are uncorrelated. Degree of correlation is determined by *correlation coefficient* which is,

$$c_{ij} = \overline{v_i' v_j'} / \sqrt{\overline{v_i'^2} \overline{v_j'^2}} \quad (3.1.1.3)$$

Correlation is perfect if $c_{ij} = \pm 1$. If there is no correlation (i.e. $c_{ij} = 0$), there would be no turbulent momentum transport. But this correlation is not likely to be zero since turbulent momentum transport is a key property of turbulence. These fluctuations exchange momentum between turbulence and mean flow although mean momentum of turbulent velocity fluctuations is zero.

Reynolds stress tensor brings nine additional unknowns to the equation of motion. Hence we need some additional relations for these stresses. Relating them to the shear rates has been used frequently [48, 49]. Following relation from mixing length theory can be proposed as a closure equation for Reynolds stresses,

$$-\rho \overline{v_i' v_j'} = \underbrace{\rho \cdot c_1 \cdot \tilde{v}_j \cdot \ell}_{\epsilon_m} \frac{\partial \bar{V}_i}{\partial x_j} \quad (3.1.1.4)$$

where ϵ_m is eddy viscosity which relates turbulent stresses to mean velocity gradient. c_1 is a numerical coefficient and ℓ is mixing length. Eddy viscosity is a flow property rather than fluid. Hence it changes within the flow field.

3.1.2 Statistics of Turbulence

Turbulence is generally treated as statistically steady which means average of fluctuating values are not function of time. A statistically steady function is called as *stationary*. The probability of a random variable v of being between v and $v+dv$ is given by probability density function (PDF) of it ($f_v(v)$) (Figure 3.1.2.1).

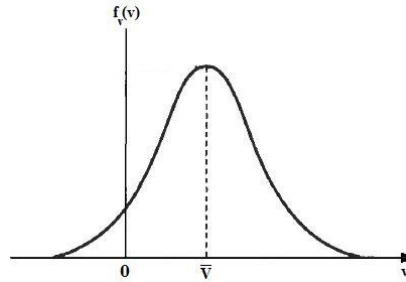


Figure 3.1.2.1: PDF of turbulent velocity v

Hence summation of PDF from minus infinity to plus infinity must be one which is the probability of being between $-\infty$ and $+\infty$ for random variable. Gaussian (normal) type of PDF is one of the mostly encountered and used distributions in turbulence studies. Mathematical representation of a Gaussian PDF for a turbulent velocity v is [50, pp.47],

$$f_v(v) = \frac{1}{\sqrt{2\pi}\sigma} e^{-(v-\bar{v})^2/(2\sigma^2)} \quad (3.1.2.1)$$

Mean values can be evaluated by using PDF. Mean values of several powers of a random variable are called as moments. First moment is mean value which is defined as,

$$\bar{V} = \int_{-\infty}^{+\infty} v \cdot f_v(v) dv \quad (3.1.2.2)$$

$f_v(v)$ is PDF of fluctuating turbulent velocity which can be depicted as $f_v(\bar{V} + v')$. Hence PDF of fluctuations ($f_{v'}(v')$) is shifted version of PDF of fluctuating velocity in the amount of mean value (\bar{V}). Moments formed with $f_{v'}(v')$ and v'^n are called as central moments. First central moment is zero as expected. Second central moment is called as *variance* which is mean-square deviation from mean value. It is defined as,

$$\sigma^2 = \overline{v'^2} = \int_{-\infty}^{+\infty} v'^2 f_{v'}(v') dv' = \int_{-\infty}^{+\infty} v'^2 f_v(v) dv \quad (3.1.2.3)$$

Square-root of σ^2 is called as *standard deviation* which is a measure of width of PDF. Second central moment is not affected by the anti-symmetry of PDF. Third central moment ($\overline{v'^3}$) on the other hand totally depends on the symmetry of PDF. If PDF is symmetric around the origin $\overline{v'^3} = 0$. Non-dimensional measure of asymmetry is called as *skewness* which is,

$$S = \overline{v'^3} / \sigma^3 \quad (3.1.2.4)$$

Another way of showing correlations is to use PDF for auto-correlation (variance) or joint PDF for correlation of different functions (covariance).

$$\overline{v_i' v_j'} = \int_{-\infty}^{+\infty} \int_{-\infty}^{+\infty} v_i' v_j' f_{v_i', v_j'}(v_i', v_j') dv_i' dv_j' \quad (3.1.2.5)$$

If $\overline{v_i' v_j'} = 0$, v_i' and v_j' are uncorrelated but not necessarily independent of each other. Two variables are statistically independent if,

$$f_{v_i', v_j'}(v_i', v_j') = f_{v_i'}(v_i') f_{v_j'}(v_j') \quad (3.1.2.6)$$

The correlation between values of a function at two different times ($\overline{v'(t)v'(t')}$) is called as *auto-correlation*. For stationary variables, origin of time doesn't make any difference on auto-correlation function (ACF). Time difference ($\tau=t'-t$) is the only parameter that affects ACF. Since

$$R_{v'}(\tau) = R_{v'}(-\tau) = \overline{v'(t)v'(t')} = \overline{v'(t')v'(t)} \quad (3.1.2.7)$$

ACF must be symmetric function of τ . Auto-correlation coefficient (ACC) for stationary variables is defined as,

$$R'_{v'}(\tau) = R'_{v'}(-\tau) = \frac{\overline{v'(t)v'(t')}}{\overline{v'^2(t)}} = \frac{\overline{v'(t)v'(t')}}{\overline{v'^2(t')}} \quad (3.1.2.8)$$

Schwartz's inequality states that,

$$|R'_{v'}(\tau)| \leq R'_{v'}(0) = 1 \quad (3.1.2.9)$$

3.1.3 Power Spectrum

Fourier transform of ACF is called as *power spectral density* or simply *power spectrum* ($S(w)$). Power spectrum must be real and symmetric since ACF is symmetric (even function) and real respectively. Area under $S(w)$ is $2\pi.R_{v'}(0) = 2\pi.\overline{v'^2}$. Mathematically $S(w)$ is defined by,

$$S(w) = \int_{-\infty}^{+\infty} R_{v'}(\tau) e^{-j\tau w} d\tau \quad (3.1.3.1)$$

or inverse transform gives: $R_{v'}(\tau) = \frac{1}{2\pi} \int_{-\infty}^{+\infty} S(w) e^{j\tau w} dw$

Power spectrum $S(w)$ may be thought of as the energy distribution of $v'(t)$ in a frequency range. Hence it shows the frequency content of the time domain velocity fluctuations.

3.1.4 Ergodicity of Turbulence

It is not easy always to take ensemble sampling of a process. Because ensemble sampling requires conducting of many experiments to find out the statistical properties of measured function. For example ensemble sampling is almost not possible for a turbulent velocity. Time sampling is the mostly used technique for turbulence. A process is called as *ergodic*, if time statistical properties of the process approach to ensemble statistical properties while measurement time goes to infinity [51, pp.427]. Hence implicitly we assume turbulent velocity as an ergodic random variable in equation (3.1.5). An ergodic random variable is uncorrelated and statistically independent of itself for large time differences.

3.1.5 Turbulence Parameters

Eulerian velocity ACC (Figure 3.1.5.1) is time correlation for fixed point velocity measurements which is,

$$R'_{u'}(\tau) = \frac{\overline{u'(t) \cdot u'(t + \tau)}}{\overline{u'^2(t)}} \quad (3.1.5.1)$$

Where u' is fluctuating Eulerian velocity in the direction of UDV probe. Over bar indicates time averaging and there is not a reference time [47].

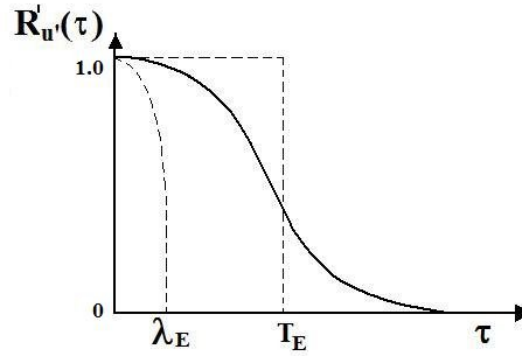


Figure 3.1.5.1: Eulerian ACC and time scales

T_E is Eulerian integral time scale over which statistics of flow process are correlated. It corresponds to the main energy containing (largest) eddies and defined as [52, Ch.5],

$$T_E = \int_0^{\infty} R'_u'(\tau) d\tau \quad (3.1.5.2)$$

For homogeneous and stationary turbulence if $\bar{U} \gg u'$ Eulerian integral length scale is [47, pp.46, 47]

$$L_f = \bar{U} \cdot T_E \quad (3.1.5.3)$$

where \bar{U} is mean velocity along probe.

Another time scale is Eulerian micro time scale (λ_E) which is defined by the curvature of the $R'_u'(\tau)$ at the origin,

$$-\frac{2}{\lambda_E^2} = \left. \frac{d^2 R'_u'(\tau)}{d\tau^2} \right|_{\tau=0} \quad (3.1.5.4)$$

If we take the Tylor series expansion of $R'_u'(\tau)$ about $\tau=0$ and truncate the higher order terms, for small τ [48, pp.211],

$$R'_{u'}(\tau) \approx 1 - \frac{\tau^2}{\lambda_E^2} \quad (3.1.5.5)$$

λ_E corresponds to the smallest eddies in the flow. Hence it is related to the rate of dissipation of turbulent energy (ϵ) [53]. Again for homogeneous and stationary turbulence we can write Eulerian micro length scale (λ_f) as,

$$\lambda_f = \bar{U} \lambda_E \quad (3.1.5.6)$$

where \bar{U} is mean velocity along probe.

For homogeneous and stationary flow field and $\tau > T_L$ (T_L is Lagrangian integral time scale) eddy diffusion coefficient is,

$$\epsilon = \overline{v'^2(t)} T_L \quad (3.1.5.7)$$

where the first term is square of Lagrangian r.m.s. value.

Although T_L and T_E are not the same the shape of Eulerian and Lagrangian velocity ACCs are similar and using Eulerian r.m.s. value and integral time scale (T_E) gives a good estimation of ϵ [54], [55, Ch.2],

$$\epsilon = \overline{u'^2(t)} T_E \quad (3.1.5.8)$$

For isotropic turbulence a good estimate of energy dissipation rate is [48, pp.67],

$$\epsilon = \frac{15 \cdot \overline{v \cdot u'^2}}{\lambda_f^2} = \frac{15 \cdot \overline{v \cdot u'^2}}{\bar{U}^2 \cdot \lambda_E^2} \quad (3.1.5.9)$$

3.2 Viscoelastic Fluids and Linear Viscoelasticity

Viscoelastic fluids are such fluids that show a combination of viscous and elastic responses for an imposed deformation. Stress is function of both strain (γ) and rate of strain ($\dot{\gamma}$) for these fluids. If stress and strain relation is linear fluid is called as linear viscoelastic fluid. Linear viscoelasticity is a case only for small deformations (strains). First consider an experiment on a Newtonian fluid between two parallel planes (Figure 3.2.1). Upper plane moves with velocity of $V(t)$ and let's assume two planes are close to each other and viscosity is high enough so that velocity distribution between two planes is linear in y direction. Then shear stress because of this shearing motion will be function of time only and is given by,

$$\tau_{yx}(t) = \mu \frac{\partial V_x(y,t)}{\partial y} = \mu \dot{\gamma}_{yx}(t) \quad (3.2.1)$$

Where μ is viscosity and $\dot{\gamma}_{yx}$ is rate of strain tensor which is time function for unsteady flows.

Secondly consider a Hookean elastic solid between two parallel planes (Figure 3.2.1). There is no net stress at time t_0 and upper plane undergoes a small displacement $U(t_0,t)$ with time so that displacement of material between planes is linear function of y . Then shear stress for Hookean solid can be given as,

$$\tau_{yx}(t) = G \frac{\partial U_x(y, t_0, t)}{\partial y} = G \gamma_{yx}(t_0, t) \quad (3.2.2)$$

where G is elastic modulus and note that strain tensor (γ_{yx}) is time function referring to time t_0 . A Hookean solid remembers its past until time t_0 whereas a Newtonian fluid doesn't have any memory of past events [56].

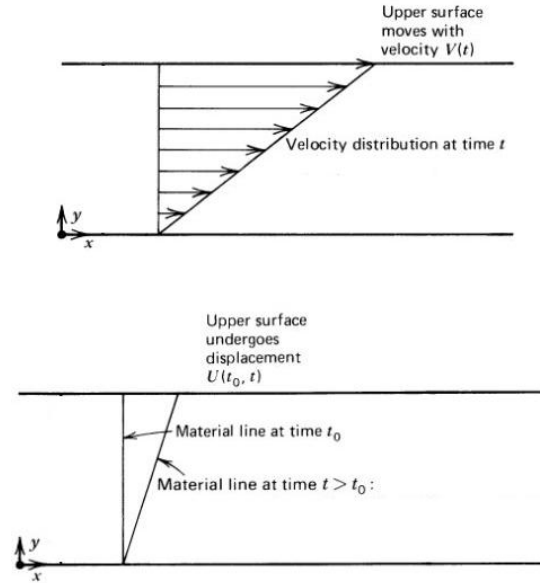


Figure 3.2.1: Unsteady shear deformation of a Newtonian fluid (upper) and Hookean solid (lower) between two parallel plates.

Relaxation test is one of the methods to characterize the time dependent behavior of a viscoelastic material. A sudden strain (γ_0) is applied and kept constant during relaxation test and there is no previous history of stress. It will be observed that the stress needed to maintain constant strain is decreasing with time (relaxation). For example stress will go to zero for an ideal thermoplastic polymer and to a constant value for a thermoset (cross-linked) polymer. Since stress is function of time and strain is constant, modulus will be function of time and it is called as relaxation modulus which is,

$$G(t) = \frac{\tau_{yx}(t)}{\gamma_0} \quad (3.2.3)$$

Limit values of relaxation modulus for a cross-linked polymer are called as initial modulus (G_0 when $t=0$) and equilibrium modulus (G_∞ when $t \rightarrow \infty$).

Another test is creep test for viscoelastic materials. A constant stress (τ_0) is applied during test and strain increases with time which defines the parameter creep compliance (J) as,

$$J(t) = \frac{\gamma_{yx}(t)}{\tau_0} \quad (3.2.4)$$

In a creep test, strain will approach a constant value for a thermoset while it will increase continuously for a thermoplastic. Creep recovery is an important test also to see what happens to strain when stress is removed. Strain will go back to zero for an ideal thermoset material after a sufficient time. However a residual deformation (strain) will always remain for a thermoplastic material. In relaxation or creep test initial behavior of viscoelastic material is analogous to the behavior of elastic solid.

$$G(t = 0) = \frac{\tau_0}{\gamma_0}, \quad J(t = 0) = \frac{\gamma_0}{\tau_0} \quad (3.2.5)$$

After long enough time in a creep test, time derivative of strain will be constant for a thermoplastic material which is characteristic of a fluid.

Some mechanical models are used to understand creep and relaxation of viscoelastic liquids. The simplest mechanical models consist of a spring for elastic behavior and a damper (a dashpot that contains Newtonian fluid) for viscous behavior. Axial elongation of a Hookean bar can be represented by a linear spring for elastic behavior of viscoelastic material. We can use elastic modulus instead of spring constant if force applied on spring is changed with normal stress and elongation of spring with strain (Eq. (3.2.2)). Viscous behavior of viscoelastic material can be represented by a Newtonian fluid within a dashpot that moves according to Newton's law of viscosity. Spring and damper elements can be combined in several ways to simulate the viscoelastic behavior. These models are very useful to understand the stress-strain relation in viscoelastic materials. The simplest combinations are serial connection (Maxwell model) and parallel connection (Kelvin model) of two elements [57].

3.2.1 Maxwell Model

This model consists of a spring and a dashpot element in series (Figure 3.2.1.1). This model will give a sudden strain and then continuously increasing strain in a creep test like thermoplastic polymers. The stress will decay to zero in a relaxation for this model similar to thermoplastic polymers.

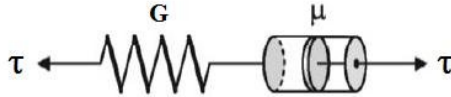


Figure 3.2.1.1: Maxwell model

Relation between stress and strain for a mechanical model can be obtained by using equilibrium and kinematic conditions for the model and constitutive equations for the elements. For Maxwell model equilibrium says stress in spring and stress in damper are equal to stress applied to system. Kinematic condition is summation of strains of both elements gives the total strain on system. Combination of these equations will give the relation between stress and strain as,

$$\tau_{yx} + \frac{\mu}{G} \frac{\partial \tau_{yx}}{\partial t} = \mu \dot{\gamma}_{yx} \quad (3.2.1.1)$$

Hence stress-strain relation for a Maxwellian material is a differential equation. This is linear combination of the deformation rates for viscous behavior (first term on left) and elastic behavior (second term) [58]. Coefficient of stress rate is defined as relaxation time (λ) which is a characteristic time constant. If we change the viscosity (μ) with zero shear rate viscosity (η_0) then,

$$\tau_{yx} + \lambda \frac{\partial \tau_{yx}}{\partial t} = \eta_0 \dot{\gamma}_{yx} \quad (3.2.1.2)$$

For steady-state motions this equation simplifies to constitutive equation of Newtonian fluids. For dominant elastic behavior sudden changes in stress will be

more important (second term at left side). Solution of simplified differential equation is going to give constitutive equation of Hookean solids.

Solution of equation (3.2.1.2) for creep experiment (applying constant sudden shear stress- τ_0) will be,

$$\gamma_{yx}(t) = \gamma_0 + \frac{\tau_0 t}{\eta_0} = \tau_0 \left(\frac{1}{G} + \frac{t}{\eta_0} \right) = \tau_0 J(t) \quad (3.2.1.3)$$

Solution of Maxwell constitutive equation for relaxation experiment (applying constant sudden shear strain- γ_0) will be,

$$\tau_{yx}(t) = \tau_0 e^{-t/\lambda} = \gamma_0 G e^{-t/\lambda} = \gamma_0 G(t) \quad (3.2.1.4)$$

These are the behavior of thermoplastic materials. Stress for relaxation experiment will be τ_0/e , when time is equal to λ (relaxation time). This knowledge allows one to determine relaxation time directly from experimental measurements. Real viscoelastic materials actually have a distribution of relaxation times.

General solution of equation (3.2.1.2) (first order linear differential equation) will be,

$$\tau_{yx}(t) = \int_{-\infty}^t \left\{ \frac{\eta_0}{\lambda} e^{-(t-t')/\lambda} \right\} \dot{\gamma}_{yx}(t') dt' \quad (3.2.1.5)$$

Note that the term within braces is time dependent relaxation modulus for Maxwell fluid. Stress at time t depends on the history of rate of strain for all past times as well as rate of strain for current time. There is a weighting factor (relaxation modulus) in front of the rate of strain. It is decaying exponentially while time is going back which shows fading memory of material.

3.2.2 Kelvin Model

This model consists of a spring and a dashpot element in parallel (Figure 3.2.2.1) and it is generally used for creep phenomena. This model will give an increasing strain but not a sudden jump in a creep test. Since damper (dashpot element) won't allow it.

Kelvin elements will creep to a constant equilibrium strain similar to the response of a thermoset polymer. The stress will decay to an equilibrium value in a relaxation for this model like thermoset polymers. Simple stress relaxation test is not possible for this model since damper prevents sudden increase in strain.

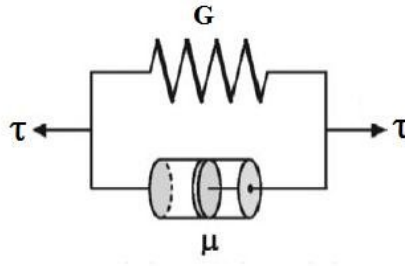


Figure 3.2.2.1: Kelvin model

Equilibrium condition for this model says total stress is equal to the summation of stresses on both elements. Kinematic condition is strain on each element is equal to each other and to the strain of the system. If we combine equilibrium, kinematic and constitutive equations for this model, result will be,

$$\tau_{yx} = G\gamma + \eta_0 \frac{\partial \gamma}{\partial t} \quad (3.2.2.1)$$

Solution of this equation for creep loading will be,

$$\gamma(t) = \frac{\tau_0}{G} (1 - e^{-t/\lambda}) = \tau_0 J(t) \quad (3.2.2.2)$$

There is not an initial elasticity for this model since damper prevents sudden strain of system. Also because of this reason Kelvin model is not useful to understand the relaxation phenomenon. Strain goes to a constant equilibrium value ($\gamma_\infty = \tau_0/G$) for a very large time which is the behavior of a thermoset polymer. This time λ is called as retardation time and can be determined experimentally.

3.2.3 Generalized Maxwell Model

Several Maxwell elements can be connected in parallel (Figure 3.2.3.1) to represent the actual stress-strain behavior of viscoelastic materials.

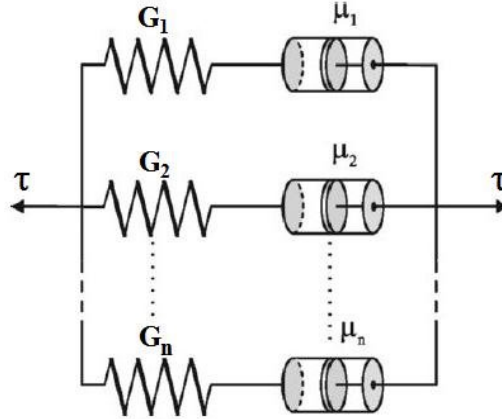


Figure 3.2.3.1: Generalized Maxwell model

Equilibrium and kinematic conditions for this system are,

$$\begin{aligned}\tau &= \tau_1 + \tau_2 + \dots + \tau_n \\ \gamma &= \gamma_1 = \gamma_2 = \dots = \gamma_n\end{aligned}\tag{3.2.3.1}$$

Differential equations for each Maxwell elements will be,

$$\begin{aligned}\tau_{yx,1} + \lambda_1 \frac{\partial \tau_{yx,1}}{\partial t} &= \eta_{o,1} \dot{\gamma}_{yx,1} \\ \tau_{yx,2} + \lambda_2 \frac{\partial \tau_{yx,2}}{\partial t} &= \eta_{o,2} \dot{\gamma}_{yx,2} \\ &\vdots \\ \tau_{yx,n} + \lambda_n \frac{\partial \tau_{yx,n}}{\partial t} &= \eta_{o,n} \dot{\gamma}_{yx,n}\end{aligned}\tag{3.2.3.2}$$

These equations can be combined to obtain an \$n^{\text{th}}\$ order differential equation of stress. One should solve this \$n^{\text{th}}\$ order differential equation to get a relation between stress and strain or solve each first order differential equations to get stresses for each Maxwell element. Summation of stresses of Maxwell elements is going to give

the total stress of the system. Solution of differential equations for a relaxation test will be,

$$\begin{aligned}
 \tau_{yx,1}(t) &= \gamma_o G_1 e^{-t/\lambda_1} \\
 \tau_{yx,2}(t) &= \gamma_o G_2 e^{-t/\lambda_2} \\
 &\vdots \\
 \tau_{yx,n}(t) &= \gamma_o G_n e^{-t/\lambda_n}
 \end{aligned}
 \tag{3.2.3.3}$$

Superposition of these solutions will give the stress behavior of the system.

$$\begin{aligned}
 \tau_{yx}(t) &= \gamma_o G_1 e^{-t/\lambda_1} + \gamma_o G_2 e^{-t/\lambda_2} + \dots + \gamma_o G_n e^{-t/\lambda_n} = \gamma_o \sum_{k=1}^n G_k e^{-t/\lambda_k} \\
 \Rightarrow G(t) &= \sum_{k=1}^n G_k e^{-t/\lambda_k} = \sum_{k=1}^n \frac{\eta_{o,k}}{\lambda_k} e^{-t/\lambda_k}
 \end{aligned}
 \tag{3.2.3.4}$$

As many Maxwell elements as possible in the system, representation of actual behavior will be more accurate. Integration of equation (3.2.3.2) to solve each stress term and knowing that total stress is the addition of all stresses on Maxwell elements will give the following integral form of Generalized Maxwell Model,

$$\tau_{yx}(t) = \int_{-\infty}^t \left\{ \sum_{k=1}^n \frac{\eta_{o,k}}{\lambda_k} e^{-(t-t')/\lambda_k} \right\} \dot{\gamma}_{yx}(t') dt'
 \tag{3.2.3.5}$$

Again the term within braces is time dependent relaxation modulus of system composed of many Maxwell elements. When we compare integral form of equations (3.2.1.5) and (3.2.3.5), we see that they are in the same form: integral over all past times of relaxation modulus multiplied by rate of deformation. Thereby we can write a generalized expression for linear viscoelastic fluids as follows,

$$\tau_{yx}(t) = \int_{-\infty}^t G(t-t') \dot{\gamma}_{yx}(t') dt'
 \tag{3.2.3.6}$$

$G(t-t')$ is relaxation modulus. First term in this integral depends on nature of fluid and second depends on nature of flow. This equation is the starting point for the description of the rheology of incompressible viscoelastic fluids for small

displacement motions. For steady-state shear flow (i.e. for constant velocity gradient $\dot{\gamma}_{yx}$) preceding equation will be,

$$\tau_{yx} = \int_{-\infty}^t \overbrace{G(t-t')}^s dt' \dot{\gamma}_{yx} = \underbrace{\int_0^{\infty} G(s) ds}_{\eta_0} \dot{\gamma}_{yx} = \eta_0 \dot{\gamma}_{yx} \quad (3.2.3.7)$$

This is a behavior of Newtonian fluids.

3.2.4 Relaxation Spectrum

Combination of many Maxwell elements will have a distribution of relaxation times with amplitudes of G_k corresponding to relaxation times λ_k . This distribution is called as discrete relaxation spectrum. Molecular weight distribution of polymeric materials creates this relaxation spectrum. Hence wider molecular weight distribution is wider relaxation spectrum for a polymeric viscoelastic material [59, pp.59, 60]. If number of Maxwell elements (n) would be increased infinitely, equation (3.2.3.4) can be written in continuous form as,

$$G(t) = \int_0^{\infty} G_k(\lambda) e^{-t/\lambda} d\lambda \quad (3.2.4.1)$$

Here $G_k(\lambda)$ is called as relaxation spectrum. It is a continuous and kind of a probability density function. For example $G_k(\lambda) = G_1 \delta(\lambda - \lambda_1)$ is relaxation spectrum for a single Maxwell element which will give relaxation modulus as $G(t) = G_1 e^{-t/\lambda_1}$. Relaxation spectrum for generalized Maxwell model would be,

$$G_k(\lambda) = \sum_{k=1}^n G_k \delta(\lambda - \lambda_k) \quad (3.2.4.2)$$

Sufficient number of elements can represent a real viscoelastic material [57, pp.208-210].

3.2.5 Dynamic Oscillation Tests

Viscoelastic properties are often determined by steady-state oscillation tests. Let's assume a viscoelastic fluid between two plates that upper one is imposing an oscillative motion to the fluid (Figure 3.2.5.1).

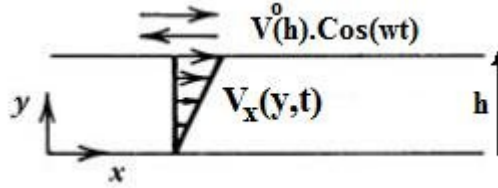


Figure 3.2.5.1: Dynamic oscillation of fluid between two plates.

Upper plate is oscillating with amplitude of $V^0(h)$ and radial frequency of w . We expect fluid between plates to oscillate with same frequency w and with decreasing amplitude towards bottom plate because of viscous effects but with different phases in y direction because of viscoelastic effects. Shear strain, shear rate and shear stress will be in complex notation,

$$\gamma_{yx}(y, t) = \text{Re}\{-j\gamma_{yx}^0(y)e^{j\omega t}\} \text{ where } \gamma_{yx}^0 \text{ is complex}$$

$$\text{and at } y = h \Rightarrow \gamma_{yx}(h, t) = \gamma_{yx}^0(h) \sin(\omega t)$$

$$\dot{\gamma}_{yx}(y, t) = \frac{d\gamma_{yx}(y, t)}{dt} = \text{Re}\{\underbrace{\omega \gamma_{yx}^0(y)}_{\dot{\gamma}_{yx}^0(y)} e^{j\omega t}\} = \frac{dV_x(y, t)}{dy}$$

$$\Rightarrow \int_0^{V_x(y,t)} dV_x = \int_0^y \text{Re}\{\dot{\gamma}_{yx}^0(y) e^{j\omega t}\} dy = \text{Re}\{e^{j\omega t} \underbrace{\int_0^y \dot{\gamma}_{yx}^0(y) dy}_{V^0(y)}\}$$

$$V_x(y, t) = \text{Re}\{V^0(y)e^{j\omega t}\} \quad (3.2.5.1)$$

where $V^0(y)$ is complex and at $y = h$ it is real so;

$$V_x(h, t) = V^0(h) \cos(\omega t)$$

Moreover shear stress to maintain the oscillatory motion is not necessarily in phase with shear rate which is due to viscoelasticity. There is no phase difference between shear stress and shear strain for an elastic material while it is 90° for a Newtonian fluid. This phase shift is between 0° and 90° for a viscoelastic fluid.

$$\tau_{yx}(y, t) = \text{Re}\{\tau_{yx}^o(y) e^{j\omega t}\} \quad (3.2.5.2)$$

where τ_{yx}^o is complex. Constitutive equation is,

$$\tau_{yx}(y, t) = \int_{-\infty}^t G(t-t') \frac{\partial V_x(y, t')}{\partial y} dt' \quad (3.2.5.3)$$

If we combine last two equations and put velocity from previous derivations,

$$\begin{aligned} \text{Re}\{\tau_{yx}^o(y) e^{j\omega t}\} &= \int_{-\infty}^t \underbrace{G(t-t')}_s \frac{\partial \text{Re}\{e^{j\omega t'} \int \dot{\gamma}_{yx}^o(y) dy + c\}}{\partial y} dt' \\ \tau_{yx}^o(y) e^{j\omega t} &= - \int_{-\infty}^0 G(s) e^{j\omega t} e^{-j\omega s} \dot{\gamma}_{yx}^o(y) ds \\ \tau_{yx}^o(y) &= \underbrace{\int_0^{\infty} G(s) e^{-j\omega s} ds}_{\eta^*(\omega)} \dot{\gamma}_{yx}^o(y) \end{aligned} \quad (3.2.5.4)$$

where $\eta^* = \eta' - j\eta''$ is complex viscosity and η' is called as dynamic viscosity. Then time dependent shear stress is going to be,

$$\tau_{yx}(y, t) = \text{Re}\{(\eta' - j\eta'') \dot{\gamma}_{yx}^o(y) e^{j\omega t}\} \quad (3.2.5.5)$$

At upper plate (i.e. $y=h$) this will be,

$$\tau_{yx}(h, t) = \eta' \dot{\gamma}_{yx}^o(h) \cos(\omega t) + \eta'' \dot{\gamma}_{yx}^o(h) \sin(\omega t) \quad (3.2.5.6)$$

First term is called as viscous part since it is in-phase with shear rate (rate of strain). Second term is elastic part hence it is in-phase with shear strain. For a Newtonian fluid $\eta''=0$, $\eta'=\mu$. If we assume a linear relationship between stress and strain, we can write the shear stress as following,

$$\tau_{yx}(h, t) = \text{Re} \left\{ \underbrace{-jG^* \gamma_{yx}^o(h)}_{\tau_{yx}^o} e^{j\omega t} \right\} \quad (3.2.5.7)$$

Where G^* is complex modulus and note that stress is in-phase with strain (sine oscillatory) in the limit of elastic solid (G^* is real). Also we can write the following linear relationship between stress and rate of strain,

$$\tau_{yx}(h, t) = \text{Re} \left\{ \underbrace{\eta^* \dot{\gamma}_{yx}^o(h)}_{\tau_{yx}^o} e^{j\omega t} \right\} \quad (3.2.5.8)$$

Here stress is in-phase with rate of strain (cosine oscillatory) in the limit of Newtonian fluid (η^* is real). From last two expressions,

$$\begin{aligned} -jG^* \cancel{\gamma_{yx}^o(h)} &= \eta^* \dot{\gamma}_{yx}^o(h) = \eta^* \omega \cancel{\gamma_{yx}^o(h)} \\ \Rightarrow G^* &= j\omega \eta^* \Rightarrow G' + jG'' = j\omega(\eta' - j\eta'') \\ \Rightarrow G' &= \omega \eta'' \text{ and } G'' = \omega \eta' \end{aligned} \quad (3.2.5.9)$$

Therefore we can write shear stress also in terms of real and imaginary parts of complex modulus as follows,

$$\tau_{yx}(h, t) = \text{Re} \left\{ -j(G' + jG'') \gamma_{yx}^o(h) e^{j\omega t} \right\} = G'' \gamma_{yx}^o \cos(\omega t) + G' \gamma_{yx}^o \sin(\omega t) \quad (3.2.5.10)$$

First term on the right side is in phase with rate of strain which is viscous response and second term is in phase with strain which is elastic response. Thereby G' is called as storage modulus and G'' as loss modulus. For an elastic solid $G''=0$ and $G'=G$ hence shear stress will be,

$$\tau_{yx}(h, t) = G \gamma_{yx}^o(h) \sin(\omega t) \quad (3.2.5.11)$$

Now let's try to write complex viscosity for Generalized Maxwell Model. Since relaxation modulus for this model is,

$$G(s) = \sum_{k=1}^{\infty} \frac{\eta_{0,k}}{\lambda_k} e^{-s/\lambda_k} \quad (3.2.5.12)$$

Complex viscosity is going to be,

$$\begin{aligned}
 \eta^* &= \int_0^\infty \sum_{k=1}^\infty \frac{\eta_{o,k}}{\lambda_k} e^{-s/\lambda_k} e^{-j\omega s} ds = \sum_{k=1}^\infty \frac{\eta_{o,k}}{\lambda_k} \int_0^\infty e^{-s(\frac{1}{\lambda_k} + j\omega)} ds = \sum_{k=1}^\infty \frac{\eta_{o,k}}{\lambda_k} \left(-\frac{1}{(\frac{1}{\lambda_k} + j\omega)} e^{-s(\frac{1}{\lambda_k} + j\omega)} \right) \Bigg|_0^\infty \\
 &= \sum_{k=1}^\infty \frac{\eta_{o,k}}{\lambda_k} \frac{1}{(\frac{1}{\lambda_k} + j\omega)} = \sum_{k=1}^\infty \frac{\eta_{o,k}}{\lambda_k} \frac{\lambda_k}{1 + \lambda_k j\omega} \approx \sum_{k=1}^M \frac{\eta_{o,k}}{1 + \lambda_k j\omega} = \sum_{k=1}^M \frac{\eta_{o,k}(1 - \lambda_k j\omega)}{1 + (\lambda_k \omega)^2} \\
 \eta^* &= \underbrace{\sum_{k=1}^M \frac{\eta_{o,k}}{1 + (\lambda_k \omega)^2}}_{\eta'} - j \underbrace{\sum_{k=1}^M \frac{\eta_{o,k} \lambda_k \omega}{1 + (\lambda_k \omega)^2}}_{\eta''} \tag{3.2.5.13}
 \end{aligned}$$

CHAPTER 4

ANALYTICAL AND NUMERICAL INVESTIGATION OF EFFECT OF CONSTANT AND OSCILLATING FLOWS ON SPECTRUM OF ULTRASOUND DOPPLER SIGNALS

4.1 Mathematical Representation of Sampled Ultrasound Signals

It is assumed that the flow medium is homogeneous, linear and lossless for US signals in analytical derivations and numerical simulations. Also back sampled signals were assumed as coming from identical particles within a measurement volume. We expect a Gaussian type distribution of back sampled signal energy because of particle distribution in measurement volume. Considering this effect will make analytical derivations highly complicated. Assuming all particles following fluid perfectly means just considering maximum energy component in the Gaussian distribution which is related to mean velocity in the volume. This is practically an accurate approximation.

A series of pulses are sent and then back reflected echoes are sampled to analyze in UDV (Figure 4.1.1). Although sampling time is the same for a measurement gate, sampled data would change if reflecting particles move. This position change causes phase change in sound signals and results in a frequency shift in frequency domain. Therefore Fourier transform of sampled signals gives a characteristic frequency-amplitude distribution (Doppler spectrum) related to velocity at the measurement point through Doppler equation.

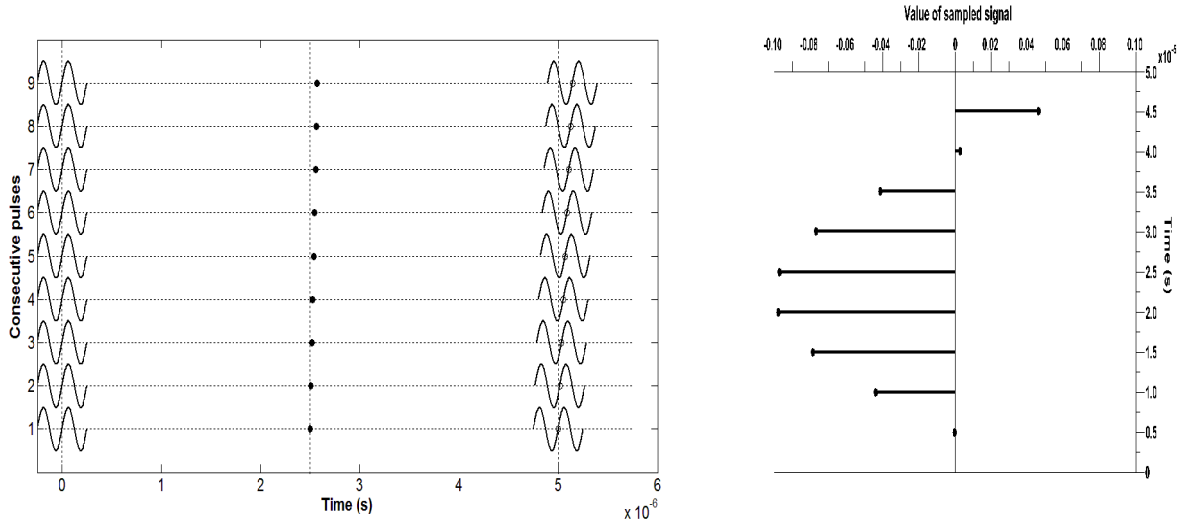


Figure 4.1.1: Representation of sampled signal values (right) of nine consecutive pulses (left) back reflected from a moving target (black point).

If N_c is the number of cycles and center of these cycles is set at zero time then emitted signals can be designated as,

$$s''(t) = A e^{j2\pi f_o (t + \frac{N_c}{2f_o})} \quad (4.1.1)$$

But this is valid if emission is continuous. For emission of finite length pulses we must multiply this with a function $E(t)$ which is,

$$E(t) = \begin{cases} 1 & \text{when } -\frac{N_c}{2f_o} \leq t \leq \frac{N_c}{2f_o} \\ 0 & \text{else} \end{cases} \quad (4.1.2)$$

Negative is used for time before the reference time of zero. Then emitted signals will be,

$$s'(t) = s''(t).E(t) = A e^{j2\pi f_o (t + \frac{N_c}{2f_o})} .E(t) \quad (4.1.3)$$

Received signals would be the time delayed form of emitted signals since they are back reflected from particles in flow medium. This time delay (t_d) depends on the

position of particles in measurement volume. Also amplitude change on signal will be occurred because of attenuations. If received signals have amplitude of A_o then they are,

$$s(t) = \frac{A_o}{A} s'(t - t_d) = A_o e^{j2\pi f_o (t + \frac{N_c}{2f_o} - t_d)} \cdot E(t - t_d) \quad (4.1.4)$$

Sampling time is fixed (t_o) which is total time of flight of an US pulse. It depends on the distance (d_o) between probe tip and measurement volume and sound speed (c).

$$t_o = 2 \frac{d_o}{c} \quad (4.1.5)$$

If the real distance of reflecting particles in measurement volume is,

$$d = d_o + d' \quad (4.1.6)$$

Time delay will be,

$$t_d = 2 \frac{d_o + d'}{c} \quad (4.1.7)$$

Then sampled signals become,

$$\begin{aligned} s(t_o) &= A_o e^{j2\pi f_o (t_o + \frac{N_c}{2f_o} - t_d)} \cdot E(t_o - t_d) \\ &= A_o e^{j2\pi f_o (\frac{2d_o}{c} + \frac{N_c}{2f_o} - \frac{2d_o}{c} - \frac{2d'}{c})} \cdot E(\frac{2d_o}{c} - \frac{2d_o}{c} - \frac{2d'}{c}) \\ &= A_o e^{j2\pi f_o (\frac{N_c}{2f_o} - \frac{2d'}{c})} \cdot E(-\frac{2d'}{c}) \end{aligned} \quad (4.1.8)$$

where

$$E(-\frac{2d'}{c}) = \begin{cases} 1 & \text{when } -\frac{c.N_c}{4f_o} \leq d' \leq \frac{c.N_c}{4f_o} \\ 0 & \text{else} \end{cases} \quad (4.1.9)$$

Note that $\frac{c.N_c}{4f_o}$ is a quarter of the total cycle length. We can show d' as $d' = u.t'$

where u is velocity of particles along probe axis and t' is total time of motion of

particles (reference is emission of first pulse). If n is number of samples, total motion time (t') for each sample will be,

$$t'[n] = (n-1)T_{\text{prf}} + \frac{d_o}{c} \quad (4.1.10)$$

Then sampled signals in discrete form can be represented as,

$$s[n] = A_o e^{j2\pi f_o \left(\frac{N_c}{2f_o} - \frac{2}{c} u[(n-1)T_{\text{prf}} + \frac{d_o}{c}] \right)} \cdot E\left(-\frac{2}{c} u[(n-1)T_{\text{prf}} + \frac{d_o}{c}]\right) \quad (4.1.11)$$

where

$$E\left(-\frac{2}{c} u[(n-1)T_{\text{prf}} + \frac{d_o}{c}]\right) = \begin{cases} 1 & \text{when } -\frac{c.N_c}{4f_o} \leq u[(n-1)T_{\text{prf}} + \frac{d_o}{c}] \leq \frac{c.N_c}{4f_o} \\ 0 & \text{else} \end{cases}$$

$$= \begin{cases} 1 & \text{when } \left| u[(n-1)T_{\text{prf}} + \frac{d_o}{c}] \right| \leq \frac{c.N_c}{4f_o} \\ 0 & \text{else} \end{cases}$$

$$= \begin{cases} 1 & \text{when } n \leq \left[\frac{1}{T_{\text{prf}}} \left(\frac{c.N_c}{4f_o |u|} - \frac{d_o}{c} \right) + 1 \right] \\ 0 & \text{else} \end{cases} \quad (4.1.12)$$

4.2 Measurement Volume of Constant Velocity Flow

Let z and i be the axial flow direction (in a pipe or a channel) and number of measurement volume (gate) respectively. There is only axial flow component for laminar (constant velocity) pipe or channel flow. But even if measurement gate has other velocity components since derived equations show the analysis of velocity component in probe direction, they are still useful. If the distance (in the direction of US beams) between probe tip and measurement gate i is $d_{o,i}$, sampled U.S. signals can be represented by equations (4.1.8) and (4.1.9).

Let's assume, particles in the gate can be represented by a single particle initially at the center ($d_{o,i}$) of the gate. The position of particle with respect to US probe changes with time because of fluid motion. d_i' is the component along US beams of this time

and velocity dependent position change for i^{th} gate. Then distance (d_i) between probe tip and particle in measurement gate will be,

$$d_i = d_{o,i} + d'_i \text{ where } d'_i = d'_i(t, \mathbf{V}_i) \text{ and } \mathbf{V}_i = \mathbf{V}_i(t) \quad (4.2.1)$$

\mathbf{V}_i is fluid velocity in vector form for i^{th} gate. For laminar flow there is only axial velocity component i.e. $\mathbf{V}_i = \mathbf{v}_{z,i}$. So particle migration in the direction of US beams can be depicted as,

$$d'_i = \int_0^t V_i \cos \theta dt \quad (4.2.2)$$

and for axial flow,

$$d'_i = \int_0^t v_{z,i} \cos \theta dt \quad (4.2.3)$$

where V_i , $v_{z,i}$ are magnitudes of vectors and θ is angle between probe axis and velocity vector \mathbf{V}_i . t is absolute time starting at the emission of first pulse. This time is time of encountering of US signals with particles for n^{th} pulse, so t has discrete values. It can be related to the discrete time (or pulse number) by,

$$t = \frac{d_{o,i}}{c} + (n-1)T_{\text{prf}} \quad (4.2.4)$$

where T_{prf} is time period between two pulse emissions. If we combine all equations above and write the sampled signals in discrete form,

$$s[n] = A_o e^{j2\pi f_o \left(\frac{N_c}{2f_o} - \frac{2}{c} \left(\int_0^{\frac{d_{o,i} + (n-1)T_{\text{prf}}}{c}} v_{z,i} \cos \theta dt \right) \right)} \quad (4.2.5)$$

We assumed E function is one for all taken samples. Otherwise there won't be sampled signals. This equation is valid for any medium attenuation and any axial velocity function. First assume that attenuated signals always have amplitude of A_o . We don't consider the effects of velocity distribution of multiple particles and shape of US beams. For laminar flow $v_{z,i}$ is constant with respect to time. Then the signal is,

$$\begin{aligned}
s[n] &= A_0 e^{j(\pi N_c - \frac{4\pi f_0}{c} [\frac{d_{o,i}}{c} + \frac{(n-1)T_{prf}}{m}] v_{z,i} \cos \theta)} \\
\Rightarrow s[m+1] &= A_0 e^{j(\pi N_c - \frac{4\pi f_0}{c} [\frac{d_{o,i}}{c} + mT_{prf}] v_{z,i} \cos \theta)}
\end{aligned} \tag{4.2.6}$$

It should be noted that n is changing between 1 and N_{prn} (total number of transmitted pulses) while m is changing between 0 and $N_{prn}-1$. Hence m represents discrete time. Discrete Fourier Transform of $s[m+1]$ then becomes,

$$\text{D.F.T.}\{s[m+1]\} = A_0 \text{D.F.T.}\{e^{j(\pi N_c - \frac{4\pi f_0}{c} [\frac{d_{o,i}}{c} + mT_{prf}] v_{z,i} \cos \theta)}\} = A_0 \cdot e^{j(a_1 - a_2)} N_{prn} \delta[k + \frac{a_3 \cdot N_{prn}}{2\pi}]$$

$$\text{where } a_1 = \pi N_c, \quad a_2 = \frac{4\pi f_0}{c} \frac{d_{o,i}}{c} v_{z,i} \cos \theta \quad \text{and} \quad a_3 = \frac{4\pi f_0}{c} v_{z,i} \cos \theta \cdot T_{prf}$$

$$\text{since D.F.T.}\{s[m]\} = \text{D.F.T.}\{s[m+1]\} e^{-j \frac{2\pi}{N_{prn}} k \cdot 1}$$

$$\text{D.F.T.}\{s[m]\} = S[k] = A_0 N_{prn} e^{j(a_1 - a_2)} \delta[k + \frac{a_3 \cdot N_{prn}}{2\pi}] \cdot e^{ja_3}$$

$$= A_0 N_{prn} e^{j(a_1 - a_2 + a_3)} \delta[k + \frac{a_3 \cdot N_{prn}}{2\pi}] \tag{4.2.7}$$

$$\text{when } k = -\frac{a_3 \cdot N_{prn}}{2\pi}, \quad w = k \cdot w_0 = -\frac{a_3 \cdot N_{prn}}{2\pi} \frac{2\pi}{N_{prn}} = -a_3$$

$$\text{and since } a_3 = 4\pi \frac{f_0}{c} v_{z,i} \cos \theta \cdot T_{prf} \quad (\text{in radian})$$

$$f = -4\pi \frac{f_0}{c} v_{z,i} \cos \theta \cdot T_{prf} \frac{f_{prf}}{2\pi} = -\frac{2f_0 v_{z,i} \cos \theta}{c}$$

This is Doppler frequency in Hz corresponding to the constant flow velocity. 2π is corresponding to the maximum sampling frequency which is f_{prf} in D.F.T. Then at this Doppler frequency the signal is,

$$S[k] \Big|_{k = -\frac{a_3 N_{prn}}{2\pi}} = A_0 N_{prn} e^{j(a_1 - a_2 + a_3)}$$

$$S[k] \Big|_{k \neq -\frac{a_3 N_{prn}}{2\pi}} = 0$$

$$\text{Amplitude of signal } \left| S\left[-\frac{a_3 N_{\text{prn}}}{2\pi}\right] \right| = A_o N_{\text{prn}} \quad (4.2.8)$$

$$\begin{aligned} \text{Phase of signal } \text{Arg}\left\{S\left[-\frac{a_3 N_{\text{prn}}}{2\pi}\right]\right\} &= a_1 - a_2 + a_3 \\ &= \pi N_c - 4\pi \frac{f_o}{c} \frac{d_{o,i}}{c} v_{z,i} \cos \theta + 4\pi \frac{f_o}{c} v_{z,i} \cos \theta T_{\text{prf}} \\ &= \pi N_c + 4\pi \frac{f_o}{c} v_{z,i} \cos \theta \left(T_{\text{prf}} - \frac{d_{o,i}}{c}\right) \end{aligned} \quad (4.2.9)$$

As it is seen from this result coherent velocity value is captured by the phase of signal spectrum.

4.3 Measurement Volume of Oscillating Velocity Flow

Before investigating the effects of turbulence or velocity fluctuations on the UDV signal, a simpler case involving an oscillating velocity is considered. The axial velocity is composed of a constant mean value and a superimposed oscillating part with a specific amplitude and frequency represented as,

$$v_{z,i} = \bar{v}_{z,i} + A_f \bar{v}_{z,i} \sin(2\pi f_f t) \quad (4.3.1)$$

where $\bar{v}_{z,i}$ is mean velocity, A_f is a percentage of $\bar{v}_{z,i}$ so that $A_f \bar{v}_{z,i}$ represents amplitude of the oscillating part and f_f is oscillation frequency in terms of Hz. If there is only axial component of the velocity ($v_{z,i}$), from equation (4.2.5) sampled US signals in discrete form become,

$$s[n] = A_o e^{j2\pi f_o \left(\frac{N_c}{2f_o} - \frac{2}{c} \int_0^{\frac{d_{o,i} + (n-1)T_{\text{prf}}}{c}} (\bar{v}_{z,i} \cos \theta + A_f \bar{v}_{z,i} \cos \theta \sin(2\pi f_f t)) dt\right)} \quad (4.3.2)$$

where all E values are again assumed as one for the sampling period. After evaluating the integral and making simplifications,

$$s[n] = A_o e^{j(a_7 - a_3(n-1) + a_4 \cos(a_5 + a_6(n-1)))} \quad (4.3.3)$$

$$\text{where } a_1 = \pi N_c, a_2 = \frac{4\pi f_o^-}{c} v_{z,i} \cos \theta \frac{d_{o,i}}{c},$$

$$a_3 = \frac{4\pi f_o^-}{c} v_{z,i} \cos \theta T_{\text{prf}}, a_4 = \frac{4\pi f_o^-}{c} v_{z,i} \cos \theta \frac{A_f}{2\pi f_f}$$

$$a_5 = 2\pi f_f \frac{d_{o,i}}{c}, a_6 = 2\pi f_f T_{\text{prf}}, a_7 = a_1 - a_2 - a_4$$

After decomposing sampled signals in equation (4.3.3) into cosine and sine parts, evaluating DFT of both parts and combining results (details can be seen in Appendix A.1) give the DFT of sampled signals as,

$$\begin{aligned} S[k] = & A_o N_{\text{prn}} J_o(a_4) \cdot e^{j(a_7+a_3)} \delta\left[k + \frac{N_{\text{prn}} a_3}{2\pi}\right] \\ & + A_o N_{\text{prn}} e^{ja_7} \sum_{l=1}^{\infty} (-1)^l J_{2l}(a_4) (e^{j(2l(a_5-a_6)+a_3)} \delta\left[k + \frac{N_{\text{prn}}(a_3 - 2la_6)}{2\pi}\right] \\ & + e^{-j(2l(a_5-a_6)-a_3)} \delta\left[k + \frac{N_{\text{prn}}(a_3 + 2la_6)}{2\pi}\right]) \\ & + A_o N_{\text{prn}} e^{j(a_7+\frac{\pi}{2})} \sum_{l=0}^{\infty} (-1)^l J_{2l+1}(a_4) \cdot (e^{j((2l+1)(a_5-a_6)+a_3)} \delta\left[k + \frac{N_{\text{prn}}(a_3 - (2l+1)a_6)}{2\pi}\right] \\ & + e^{-j((2l+1)(a_5-a_6)-a_3)} \delta\left[k + \frac{N_{\text{prn}}(a_3 + (2l+1)a_6)}{2\pi}\right]) \end{aligned} \quad (4.3.4)$$

Amplitude of the signal is,

$$\begin{aligned} |S[k]| = & A_o N_{\text{prn}} \left| J_o(a_4) \right|_{k=-\frac{N_{\text{prn}} a_3}{2\pi}} + A_o N_{\text{prn}} \sum_{l=1}^{\infty} \left| J_{2l}(a_4) \right|_{k=-\frac{N_{\text{prn}}(a_3-2la_6)}{2\pi}, k=-\frac{N_{\text{prn}}(a_3+2la_6)}{2\pi}} \\ & + A_o N_{\text{prn}} \sum_{l=0}^{\infty} \left| J_{2l+1}(a_4) \right|_{k=-\frac{N_{\text{prn}}(a_3-(2l+1)a_6)}{2\pi}, k=-\frac{N_{\text{prn}}(a_3+(2l+1)a_6)}{2\pi}} \end{aligned} \quad (4.3.5)$$

Phase of the signal is,

$$\begin{aligned}
\angle\{S[k]\} &= (a_7 + a_3) \Big|_{k=-\frac{N_{\text{prn}} a_3}{2\pi}} + \sum_{l=1}^{\infty} (2l(a_5 - a_6) + a_3 + a_7 + l\pi) \Big|_{k=-\frac{N_{\text{prn}}(a_3 - 2l a_6)}{2\pi}} \\
&+ \sum_{l=1}^{\infty} (2l(a_6 - a_5) + a_3 + a_7 + l\pi) \Big|_{k=-\frac{N_{\text{prn}}(a_3 + 2l a_6)}{2\pi}} + \sum_{l=0}^{\infty} ((2l+1)(a_5 - a_6) + a_3 + a_7 + \frac{\pi}{2} + l\pi) \Big|_{k=-\frac{N_{\text{prn}}(a_3 - (2l+1)a_6)}{2\pi}} \\
&+ \sum_{l=0}^{\infty} ((2l+1)(a_6 - a_5) + a_3 + a_7 + \frac{\pi}{2} + l\pi) \Big|_{k=-\frac{N_{\text{prn}}(a_3 + (2l+1)a_6)}{2\pi}} \tag{4.3.6}
\end{aligned}$$

4.3.1 Limits of the Spectrum

It may be interesting to examine the behavior of the oscillating flow UDV signal at some critical oscillation amplitudes and frequencies.

$$a_4 = \frac{2f_o}{c} v_{z,i} \cos \theta \frac{A_f}{f_f}, \quad a_6 = 2\pi f_f T_{\text{prf}}$$

For a moderate f_f ,

$$\text{when } A_f \rightarrow \infty, a_4 \rightarrow \infty, |J_n(a_4)| \rightarrow 0 \Rightarrow |S[k]|_{\text{for all } k} \rightarrow 0$$

$$\text{when } A_f \rightarrow 0, a_4 \rightarrow 0, \begin{matrix} |J_{n \neq 0}(a_4)| \rightarrow 0 \\ |J_0(a_4)| \rightarrow 1 \end{matrix} \Rightarrow S[k] \Big|_{k=-\frac{N_{\text{prn}} a_3}{2\pi}} \rightarrow A_o N_{\text{prn}} e^{j(a_7 + a_3)} = A_o N_{\text{prn}} e^{j(a_1 - a_2 + a_3)}$$

This is same with spectrum of constant velocity flow (Eq. (4.2.7)).

For a moderate A_f ,

$$\text{when } f_f \rightarrow \infty, \begin{matrix} a_4 \rightarrow 0 \\ a_6 \rightarrow \infty \end{matrix}, \begin{matrix} |J_{n \neq 0}(a_4)| \rightarrow 0 \\ |J_0(a_4)| \rightarrow 1 \end{matrix} \Rightarrow S[k] \Big|_{k=-\frac{N_{\text{prn}} a_3}{2\pi}} \rightarrow A_o N_{\text{prn}} e^{j(a_1 - a_2 + a_3)}$$

This is again constant velocity (laminar flow) spectrum.

$$\text{when } f_f \rightarrow 0, \begin{matrix} a_4 \rightarrow \infty \\ a_6 \rightarrow 0 \end{matrix}, |J_n(a_4)| \rightarrow 0 \Rightarrow |S[k]|_{\text{for all } k} \rightarrow 0$$

Both limits of oscillation frequency goes to zero and amplitude goes to infinity give the same amplitude of zero for all spectrum. This makes impossible the determination of mean flow velocity. This may be caused from infinite amplitude of flow oscillation will spreads the coherent US energy as noise. Also limited sampling of very slowly changing flow won't be enough to capture its Doppler spectrum.

4.3.2 Critical Point of the Spectrum

If we look at the amplitude of spectrum ($|S[k]|$) and change of Bessel function of first kind (J_n) for integer orders (i.e. $n=0, 1, 2, \dots$), there seems a critical value for a_4 around 1.45. After this value, amplitudes of side frequency components start to dominate the amplitude of spectral component corresponding to the mean velocity. Therefore if this value is exceeded by increasing flow oscillation amplitude and/or decreasing oscillation frequency, the ambiguity of spectrum increases in terms of determining mean flow.

4.3.3 Simulations

The effect of particles moving with the fluid was simulated by a MATLAB program, which is based on the tracking of particles during the experiment. All particles in measurement volume were assumed to have the same velocity. Amplitude of transmitted ultrasonic pulses (A) was taken as unity and attenuation due to physical medium was neglected. During measurement period new particle cluster was assumed to be entering the measurement volume after previous cluster leaves the measurement volume. Hence 'E' function can always be taken as one for homogeneously distributed particles in fluid and continuous flow.

Simulation program determines the position of particle cluster when ultrasonic pulse comes to the measurement volume. Afterwards it determines the sampled signal value according to the particle position. Therefore it can simulate sampled signal sequence coming from any flow medium if the velocity can be mathematically

represented. After getting sampled signals their spectral analysis are conducted to obtain ultrasonic spectrum and velocity distribution.

4.3.4 Comparison of Simulation and Analytical Results

Spectrum, maximum amplitude change and total energy change were obtained from both analytical equation (4.3.5) and simulation for center of pipe (i.e. $r=0$ mm). Radius of pipe is 0.023 m and parabolic velocity profile was assumed for $N_{Re}=2662$. Parabolic velocity profile seems to be reasonable for transition from laminar flow to turbulent. Local mean velocity at pipe center is 0.1157 m/s and UDV parameters are: $N_c=8$, $N_{prn}=4096$, $f_{prf}=7246$ Hz, $\theta=70^\circ$, 33 measurement gates.

Maximum amplitude corresponding to mean velocity in ultrasonic signal spectrum is decreasing towards the corner of increasing oscillation amplitude and decreasing frequency (i.e. increasing a_4) (Figure 4.3.4.1). This means there is attenuation on the energy of spectral component corresponding to mean velocity because of oscillating part. Smoother results in the case of analytical solution is due to the continuous functions involved as opposed to the simulation results which are obtained by sampling discrete signals with respect to time.

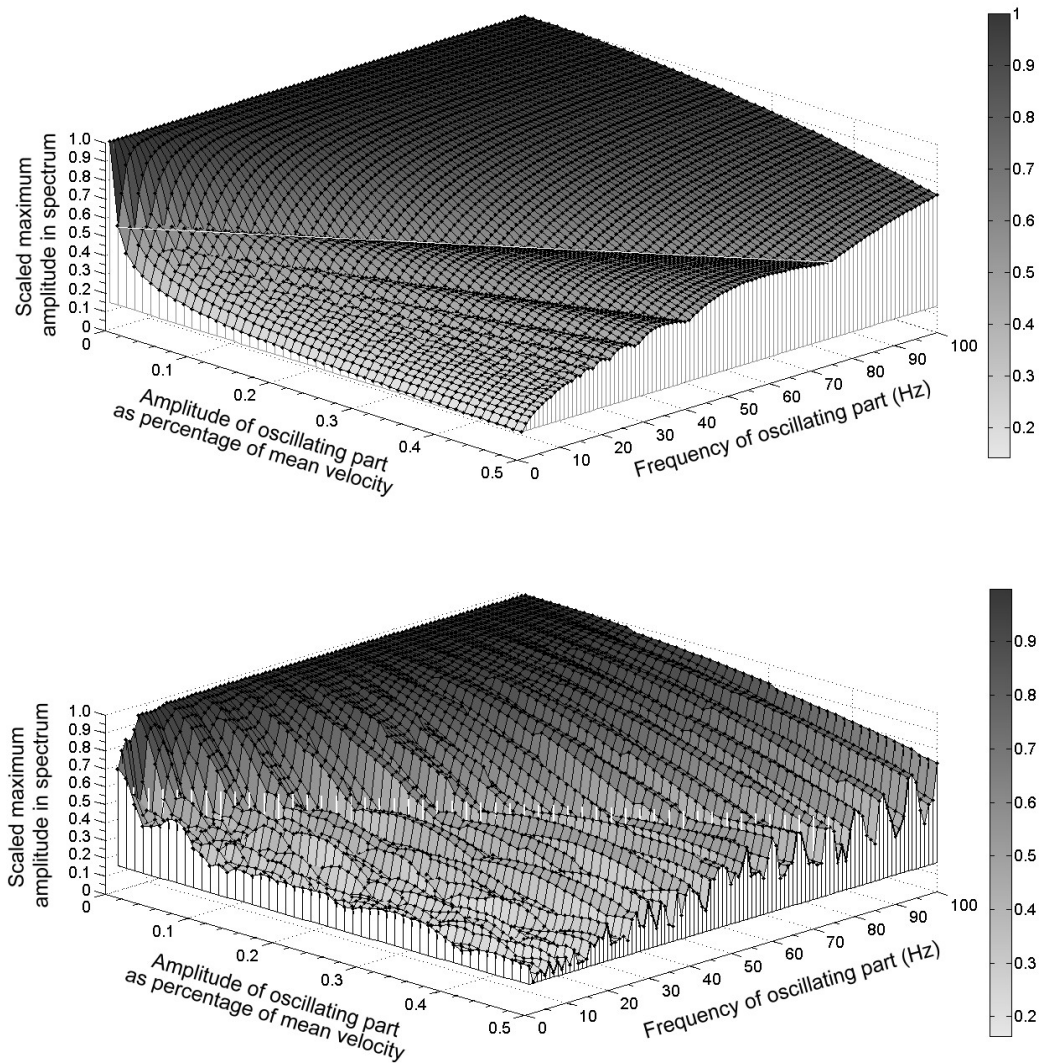


Figure 4.3.4.1: Change of scaled maximum amplitude in ultrasonic spectrum with amplitude and frequency of oscillating velocity component. Upper one is from analytical equation (4.3.5), lower one is from simulation. These surfaces are for measurement gate at the center of pipe. White line of fences shows the border where a_4 is getting bigger than 1.45

Total energy of signals in spectrum is constant for all oscillating velocity components (Figure 4.3.4.2) which can be defined as,

$$E_{\text{tot}} = \sum_{k=0}^{N_{\text{pm}}-1} \frac{|S[k]|^2}{N_{\text{pm}}} \quad (4.3.4.1)$$

where $\frac{|S[k]|^2}{N_{\text{pm}}}$ is energy spectral density (ESD).

Since it was assumed in the analysis that there is not any attenuation due to physical medium, all transmitted energy is recovered back in the reflected signal.

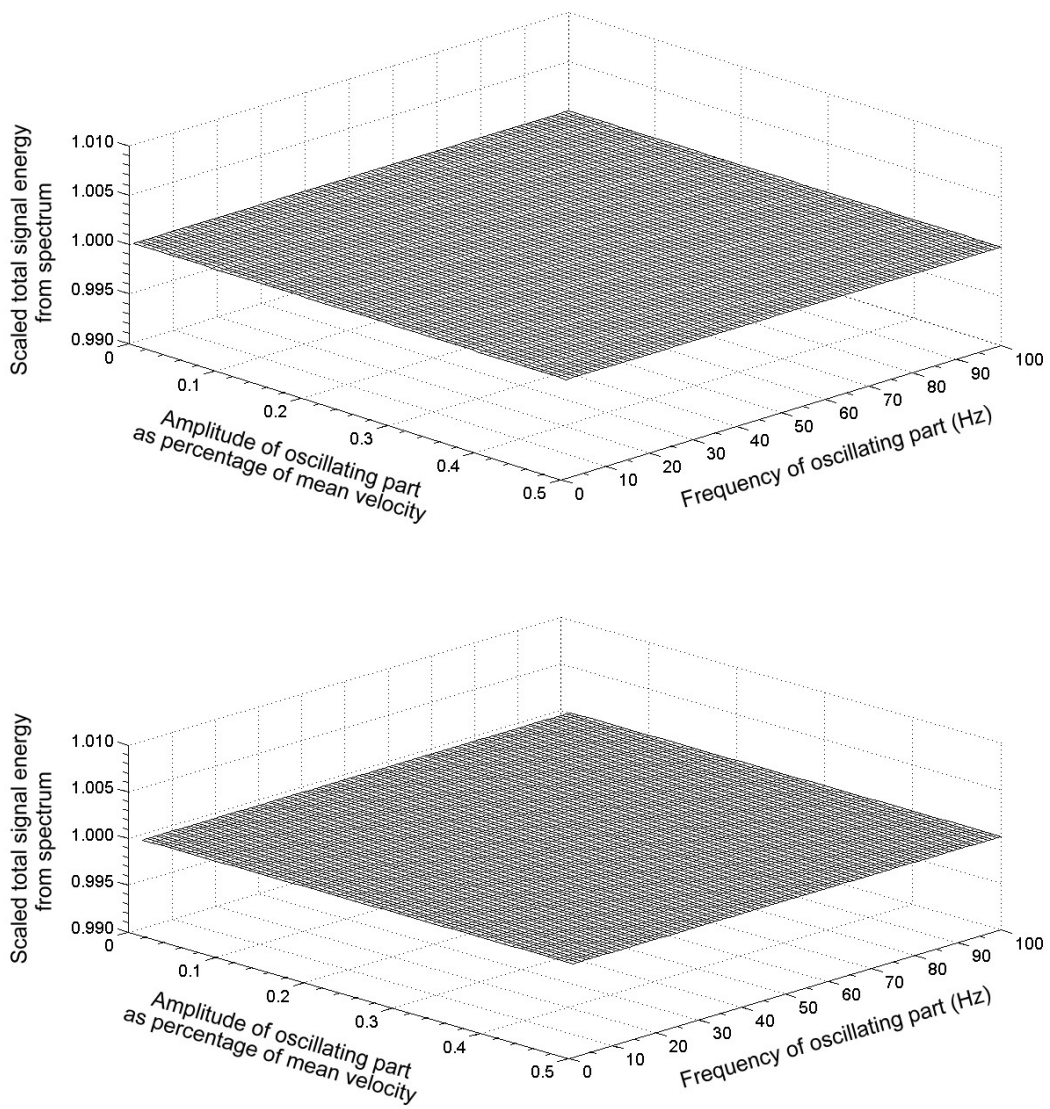


Figure 4.3.4.2: Change of scaled total energy in ultrasonic spectrum with amplitude and frequency of oscillating velocity component. Upper one is from analytical equation (4.3.5), lower one is from simulation. These surfaces are for measurement gate at the center of pipe.

Parabolic mean velocity profiles obtained from spectrum of each gates and spectrum of US signals coming from maximum velocity gate (pipe center) are shown below (Figures 4.3.4.3 – 4.3.4.6). Velocity scale corresponds to the Doppler frequency distribution (through Doppler Eq. (2.1.3)) for a discrete gate at a radial position. An oscillating part was superimposed on this parabolic velocity value for each measurement gate at a specified amplitude and frequency. Spectrums of gate at the pipe center obtained by simulation and analytically are well compatible. As it is seen some part of spectral energy is distributed between main (dominant) spectral components in simulation because of discrete frequency interval which is set by sampling frequency and number of samples. Superimposed oscillation components are distributing the spectral energy to other frequencies and creating ghosts. Spectrums of this kind of flows are dominated by the mean flow component and ghost components at multiples of flow oscillation frequency around Doppler frequency of mean flow. However their amplitudes are determined by the ratio of oscillation amplitude to frequency.

As it is seen from simulation and analytical results, separation of ghosts from mean velocity profile is determined by oscillation frequency of fluctuating part. While keeping other parameters constant, decreasing oscillation frequency (or increasing a_4) increases the intensity of ghosts and decreases the intensity of mean velocity profile. Increasing oscillation amplitude has the same effect on intensity of ghosts and mean velocity as decreasing oscillation frequency (Figure 4.3.4.1). Intensity of ghosts towards center of the pipe is increasing since oscillation amplitude was taken as percentage of local mean velocity.

Number of ghosts around mean velocity profile is increasing and they are becoming more and more dominant with increasing a_4 value (Figures 4.3.4.3 – 4.3.4.6). This means ambiguity for the determined velocity profile is increasing. After a certain limit of a_4 (~ 1.45), it becomes unreliable to determine mean velocity profile by UDV signals.

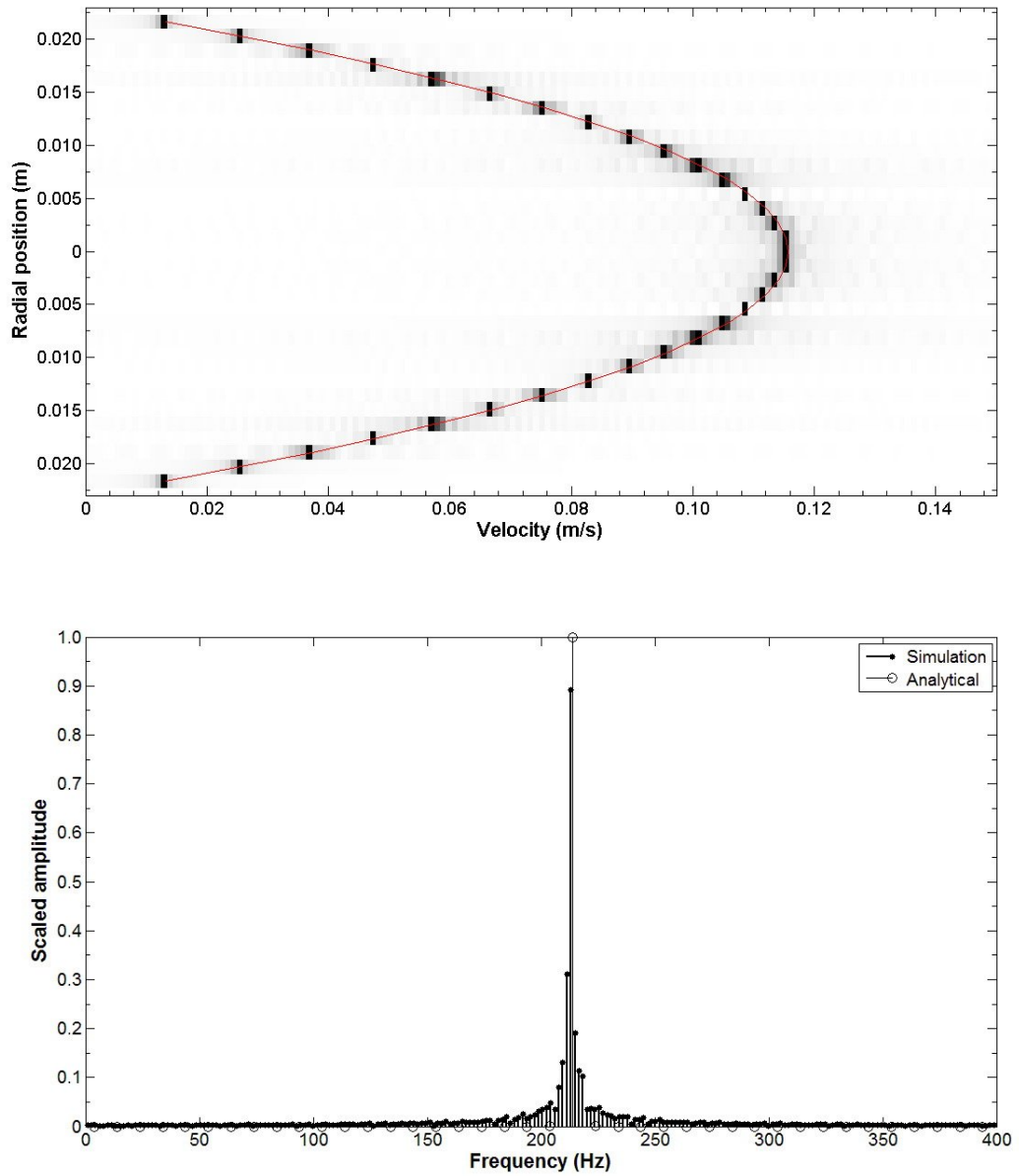


Figure 4.3.4.3: Laminar velocity profile in pipe (upper): red line shows mean velocity profile, black-white colors show the distribution of frequencies (velocities) for related gates by UDV simulation. Darker regions correspond to the bigger amplitudes. Spectrum for center of pipe (below): both spectrums obtained analytically and from simulation are seen.

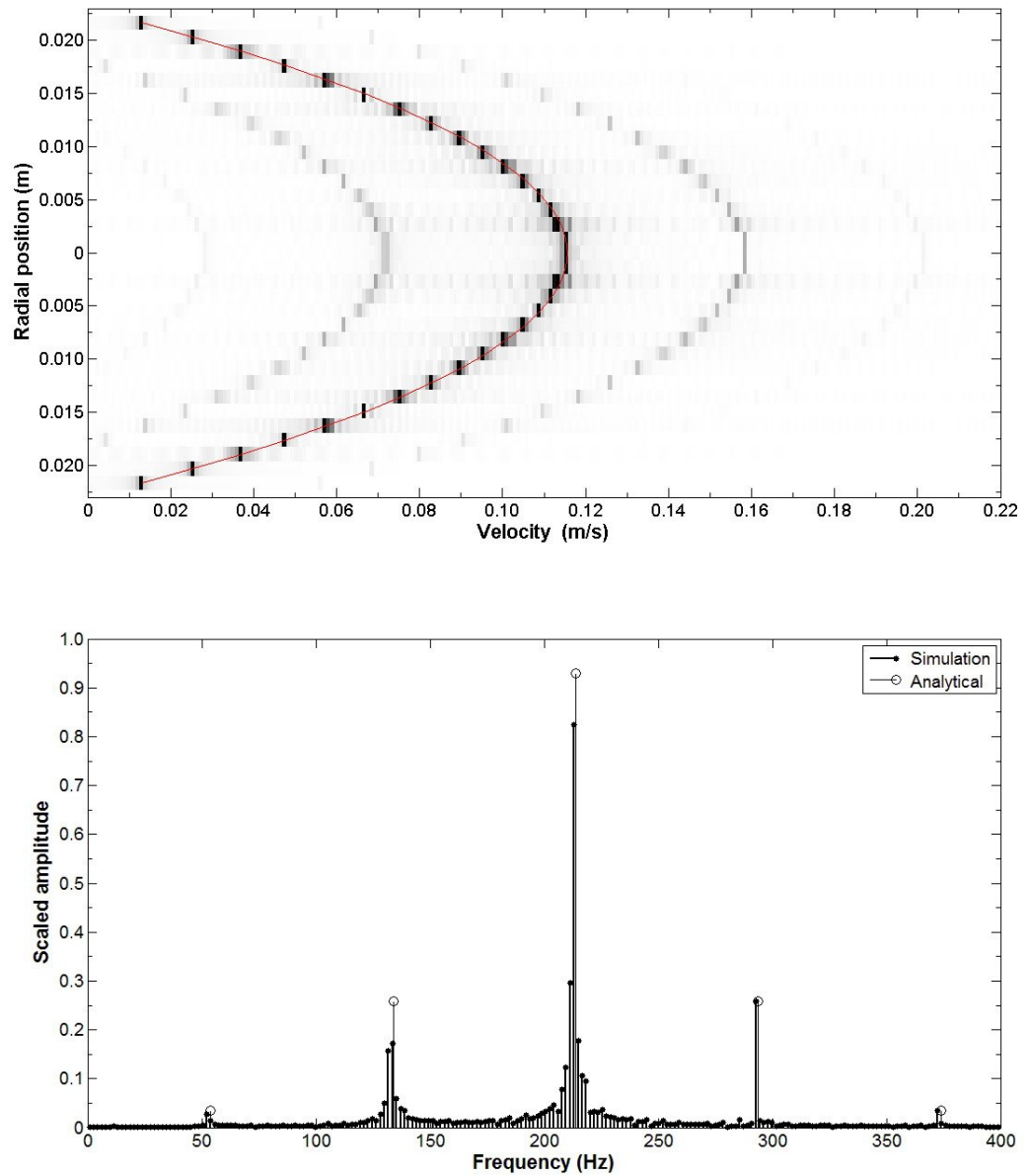


Figure 4.3.4.4: Oscillating velocity profile in pipe with 20% amplitude and 80 Hz frequency (upper): a_4 is 0.53, red line shows mean velocity profile, black-white colors show the distribution of frequencies (velocities) for related gates by UDV simulation. Darker regions correspond to the bigger amplitudes. Spectrum for center of pipe (below): both spectrums obtained analytically and from simulation are seen.

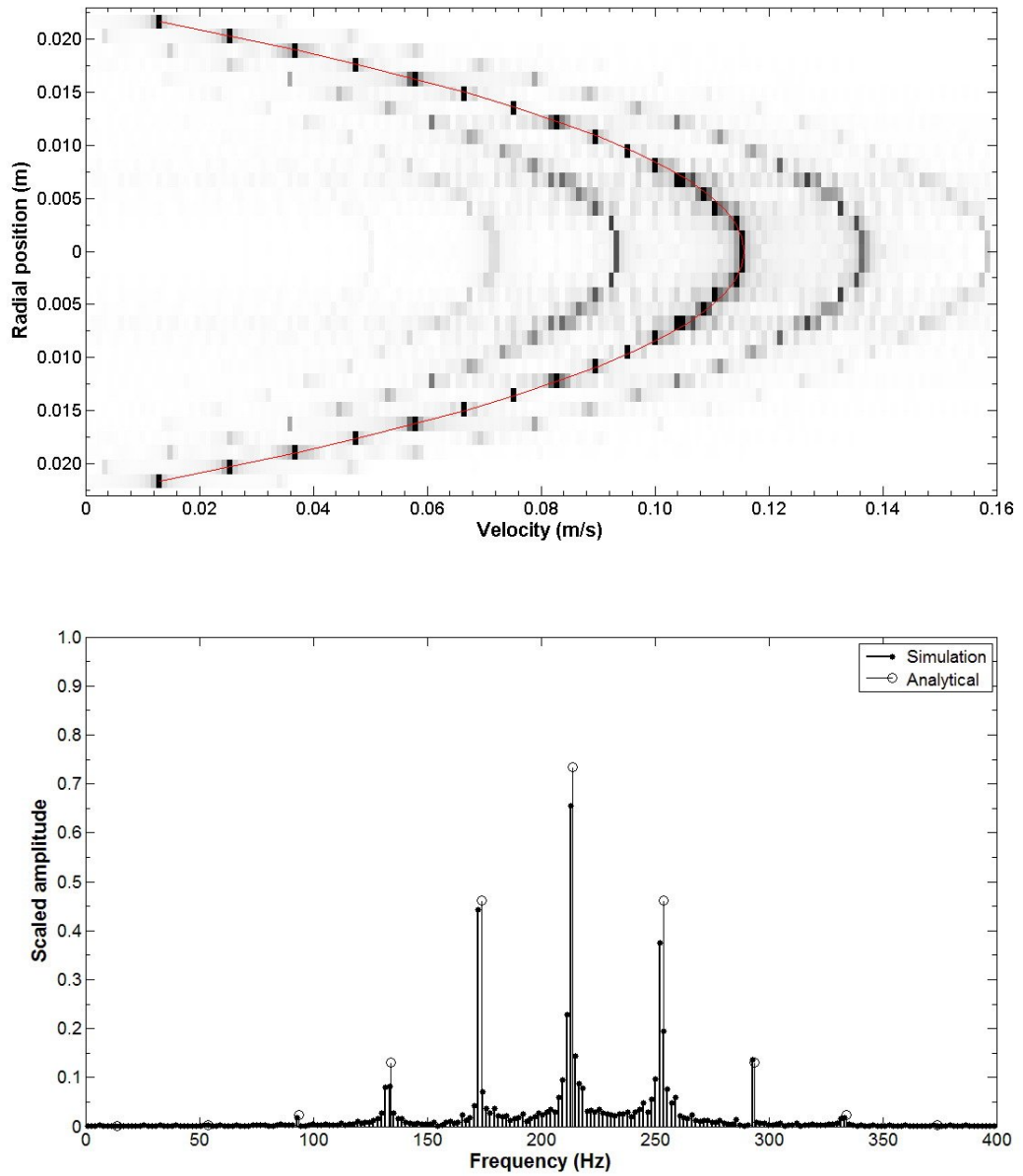


Figure 4.3.4.5: Oscillating velocity profile in pipe with 20% amplitude and 40 Hz frequency (upper): a_4 is 1.07, red line shows mean velocity profile, black-white colors show the distribution of frequencies (velocities) for related gates by UDV simulation. Darker regions correspond to the bigger amplitudes. Spectrum for center of pipe (below): both spectrums obtained analytically and from simulation are seen.

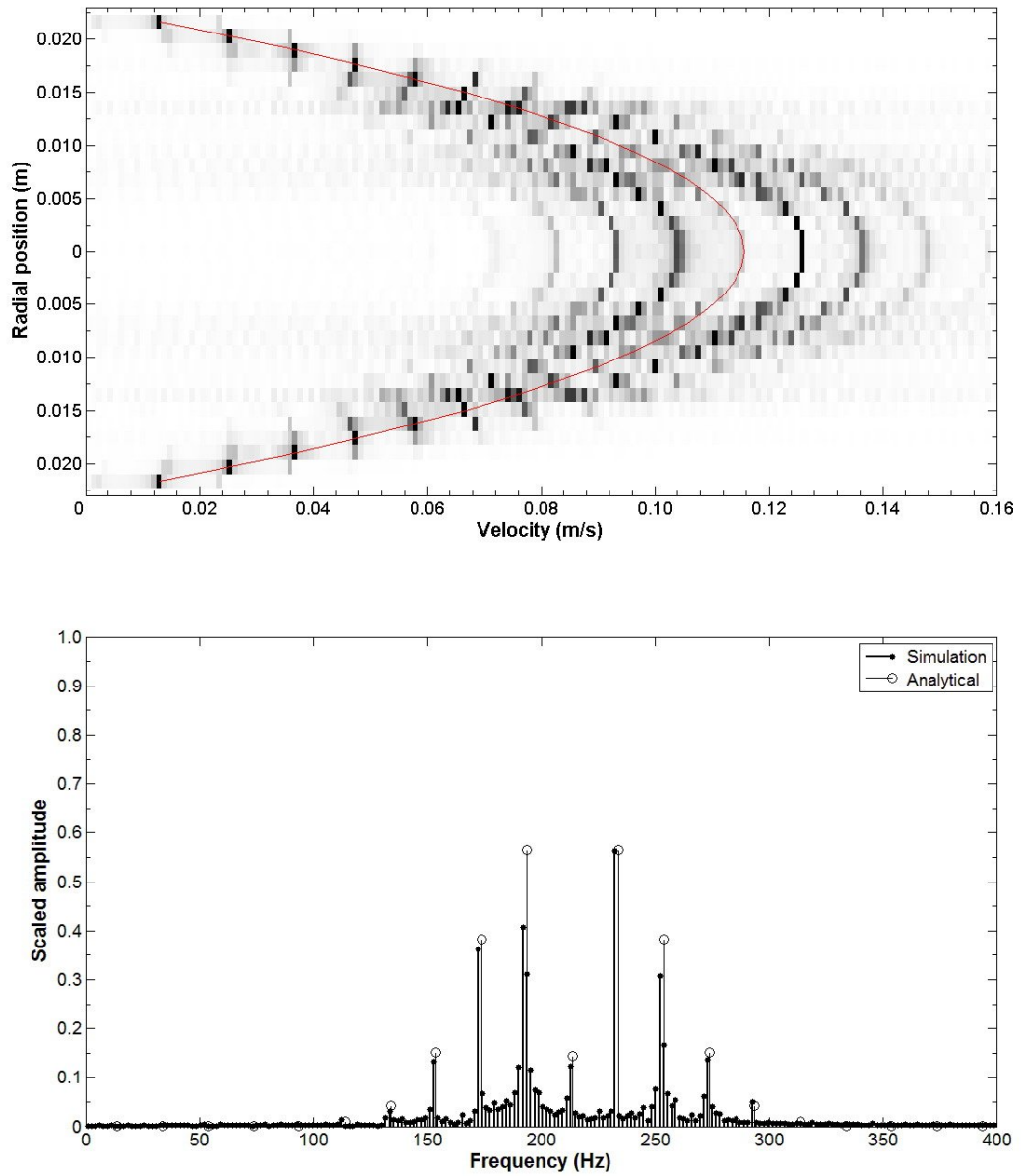


Figure 4.3.4.6: Oscillating velocity profile in pipe with 20% amplitude and 20 Hz frequency (upper): a_4 is 2.14, red line shows mean velocity profile, black-white colors show the distribution of frequencies (velocities) for related gates by UDV simulation. Darker regions correspond to the bigger amplitudes. Spectrum for center of pipe (below): both spectrums obtained analytically and from simulation are seen.

CHAPTER 5

ANALYTICAL AND EXPERIMENTAL INVESTIGATION OF THE EFFECTS OF RANDOM VELOCITY STATISTICS ON ULTRASOUND DOPPLER SIGNALS

5.1. Velocity Probability Density Function (PDF)

The following derivations start from equations (4.1.11) and (4.1.12) that represents sampled ultrasonic signals in discrete form.

$$\begin{aligned}
 s[n] &= A_o e^{j(\pi N_c - \frac{4\pi f_o}{c} u[(n-1)T_{prf} + \frac{d_{o,i}}{c}])} \overbrace{E[n]}^1 = A_o e^{\underbrace{j(\pi N_c)}_{\gamma_1} - \underbrace{\frac{4\pi f_o T_{prf}}{c} u(n-1)}_{\gamma_2} - \underbrace{\frac{4\pi f_o d_{o,i}}{c^2} u}_{\gamma_3}} \\
 s[n] &= A_o e^{j(\gamma_1 - \gamma_2 \cdot u \cdot n + \gamma_2 \cdot u - \gamma_3 \cdot u)} = A_o e^{\underbrace{j(\gamma_1 - \gamma_2 \cdot u \cdot n + \gamma_2 \cdot u - \gamma_3 \cdot u)}_{\gamma_4}} = A_o e^{j(\gamma_1 - \gamma_2 \cdot u \cdot n + \gamma_4 \cdot u)}
 \end{aligned} \tag{5.1.1}$$

Here velocity fluctuations can be handled in two ways: Velocity u can either be taken as a random variable or it can be decomposed to \bar{u} (average velocity) and u' (fluctuating random part). For the first case, discrete auto-correlation function (ACF) of the US signal $s[n]$ is,

$$R_s[\tau] = E\{s[n]s^*[n + \tau]\} \tag{5.1.2}$$

where E is expected value operator and $*$ denotes complex conjugate.

$$R_s[\tau] = E\{A_o e^{j(\gamma_1 - \gamma_2 \cdot u \cdot n + \gamma_4 \cdot u)} \cdot A_o e^{-j(\gamma_1 - \gamma_2 \cdot u \cdot (n+\tau) + \gamma_4 \cdot u)}\} = A_o^2 E\{e^{j(\gamma_2 \cdot u \cdot \tau)}\} = A_o^2 \int_{-\infty}^{\infty} e^{j\gamma_2 \cdot u \cdot \tau} f_u(u) \cdot du$$

where $f_u(u)$ is the PDF of random velocity u . Since $\gamma_2 \cdot u$ has unit of radial frequency

(radians/s), lets $w = \gamma_2 \cdot u \Rightarrow u = \frac{w}{\gamma_2} \Rightarrow du = \frac{1}{\gamma_2} dw$ and by using the relation between

PDFs of two random variables [51, pp.93],

$$f_u(u) = \frac{f_w(\gamma_2 \cdot u)}{\left| \frac{1}{\gamma_2} \right|} = \gamma_2 \cdot f_w(\overbrace{\gamma_2 \cdot u}^w)$$

$$\Rightarrow R_s[\tau] = A_o^2 \int_{-\infty}^{\infty} e^{j \cdot w \cdot \tau} \cdot \cancel{\gamma_2} \cdot f_w(w) \cdot \frac{1}{\cancel{\gamma_2}} dw = A_o^2 \underbrace{\int_{-\infty}^{\infty} e^{j \cdot w \cdot \tau} \cdot f_w(w) \cdot dw}_{2\pi \times \text{I.F.T.} \{f_w(w)\}}$$

Since we are analyzing N_{prn} discrete signals we should write this in discrete form.

$$\Rightarrow R_s[\tau] = A_o^2 \cdot \cancel{N_{\text{prn}}} \cdot \frac{1}{\cancel{N_{\text{prn}}}} \sum_{k=0}^{N_{\text{prn}}-1} f_k[k] e^{j \cdot \frac{2\pi}{N_{\text{prn}}} k \cdot \tau} = A_o^2 \sum_{k=0}^{N_{\text{prn}}-1} f_k[k] e^{j \cdot \frac{2\pi}{N_{\text{prn}}} k \cdot \tau} \quad (5.1.3)$$

We can also write ACF in terms of energy spectrum as follows (see Appendix A.2 for derivation),

$$R_s[\tau] = \frac{1}{N_{\text{prn}}} \sum_{k=0}^{N_{\text{prn}}-1} \frac{|S[-k]|^2}{N_{\text{prn}}} \cdot e^{j \cdot \frac{2\pi}{N_{\text{prn}}} k \cdot \tau} = \frac{1}{N_{\text{prn}}} \sum_{k=0}^{N_{\text{prn}}-1} E[-k] \cdot e^{j \cdot \frac{2\pi}{N_{\text{prn}}} k \cdot \tau} \quad (5.1.4)$$

where $E[-k]$ is energy spectral density (ESD) at $-k$. Therefore ACF is inverse DFT of energy spectrum. If we equalize expressions (5.1.3) and (5.1.4) for ACF,

$$R_s[\tau] = A_o^2 \sum_{k=0}^{N_{\text{prn}}-1} f_k[k] \cdot e^{j \cdot \frac{2\pi}{N_{\text{prn}}} k \cdot \tau} = \frac{1}{N_{\text{prn}}} \sum_{k=0}^{N_{\text{prn}}-1} \frac{|S[-k]|^2}{N_{\text{prn}}} \cdot e^{j \cdot \frac{2\pi}{N_{\text{prn}}} k \cdot \tau}$$

$$\Rightarrow A_o^2 f_k[k] = \frac{|S[-k]|^2}{N_{\text{prn}}^2} \Rightarrow f_k[k] = \frac{|S[-k]|^2}{A_o^2 \cdot N_{\text{prn}}^2} \Rightarrow f_{k \cdot w_o}[k \cdot w_o] = \frac{|S[-k \cdot w_o]|^2}{A_o^2 \cdot N_{\text{prn}}^2}$$

where w_o is basic frequency of sampling.

$$\frac{1}{\gamma_2} f_u[u = k \cdot w_o / \gamma_2] = \frac{|S[-k \cdot w_o]|^2}{A_o^2 \cdot N_{\text{prn}}^2} \quad \text{since } \gamma_2 = \frac{4\pi f_o T_{\text{prf}}}{c}$$

$$f_u\left[\frac{c}{4\pi f_o T_{\text{prf}}} k w_o\right] = \frac{4\pi f_o T_{\text{prf}}}{c} \frac{|S[-k \cdot w_o]|^2}{A_o^2 \cdot N_{\text{prn}}^2} \quad (5.1.5)$$

This result shows the mathematical relation between PDF of random velocity and amplitude of Doppler US spectrum. It is clear from this result that PDF of random

velocity is directly related to the energy spectrum of US signals after scaling with some measurement parameters. Frequency axis is converted to velocity axis through Doppler relation according to equation (5.1.5). This is a meaningful result since each random velocity value at the measurement gate is expected to create a spectral component in US spectrum with an intensity related with its probability.

To validate the expression by a simple case, amplitude of US spectrum for laminar flow from previous derivations (Eq. (4.2.8)) can be substituted for the US signal spectrum. Then,

$$f_u \left[\frac{c}{4\pi f_o T_{prf}} \left(\frac{2f_o V_{z,i} \cos\theta N_{prn} T_{prf}}{c} \right) \frac{2\pi}{\underbrace{N_{prn}}_{w_o}} \right] = \frac{4\pi f_o T_{prf}}{c} \frac{(A_o N_{prn})^2}{A_o^2 N_{prn}^2}$$

$$\Rightarrow f_u[u = V_{z,i} \cos\theta] = \frac{4\pi f_o T_{prf}}{c} \text{ and } f_u[u \neq V_{z,i} \cos\theta] = 0 \quad (5.1.6)$$

This result implicates that PDF is unit impulse at $V_{z,i} \cos\theta$ which is the laminar velocity value along probe axis. This is an expected result. If the analytical result of oscillating flow spectrum (Eq. (4.3.5)) is substituted in equation (5.1.5),

$$f_u[u] = \frac{4\pi f_o T_{prf}}{c} |J_o(a_4)|^2 \Big|_{u=V_{z,i} \cos\theta}$$

$$+ \frac{4\pi f_o T_{prf}}{c} \sum_{l=1}^{\infty} |J_{2l}(a_4)|^2 \Big|_{u=\frac{c}{2f_o} \left(\frac{2f_o}{c} \bar{v}_{z,i} \cos\theta - 2l f_f \right), u=\frac{c}{2f_o} \left(\frac{2f_o}{c} \bar{v}_{z,i} \cos\theta + 2l f_f \right)}$$

$$+ \frac{4\pi f_o T_{prf}}{c} \sum_{l=0}^{\infty} |J_{2l+1}(a_4)|^2 \Big|_{u=\frac{c}{2f_o} \left(\frac{2f_o}{c} \bar{v}_{z,i} \cos\theta - (2l+1) f_f \right), u=\frac{c}{2f_o} \left(\frac{2f_o}{c} \bar{v}_{z,i} \cos\theta + (2l+1) f_f \right)} \quad (5.1.7)$$

where $a_4 = \frac{2f_o}{c} \bar{v}_{z,i} \cos\theta \frac{A_f}{f_f}$

Equation (5.1.7) shows a PDF which is distributed around mean velocity. Maximum PDF value is seen at mean velocity value.

If $u = \bar{u} + u'$ is considered, the relation between PDF of u' and amplitude of Doppler US spectrum becomes,

$$f_{u'}\left[\frac{c}{4\pi f_o T_{prf}} kw_o - \bar{u}\right] = \frac{4\pi f_o T_{prf}}{c} \frac{|S[-k.w_o]|^2}{A_o^2 . N_{pm}^2} \quad (5.1.8)$$

This PDF is shifted version of PDF of whole random variable u by the amount of \bar{u} . If the spectrum of constant velocity flow (without any fluctuation) is substituted in equation (5.1.8),

$$f_{u'}[u' = \underbrace{V_{z,i} \cos\theta}_u - \bar{u} = 0] = \frac{4\pi f_o T_{prf}}{c} \quad \text{and} \quad f_{u'}[u' \neq 0] = 0 \quad (5.1.9)$$

PDF of fluctuating part of random velocity has impulse at zero. This means there is no fluctuating part for constant velocity flow as expected.

5.2 Experimental Set-Up

Experimental measurements of velocity, In-phase and Quadrature (I-Q) signals were performed by means of a water flow system (Figure 5.2.2) and DOP 2125 UDV (Signal Processing, Switzerland). PVC pipe of 46 mm inside diameter and 2 mm thickness was used in the flow system. Length of measurement point from pipe entrance is 4.5 meters and a part of 1.5 meters from pipe exist was left to prevent end effects. This entrance length is quite enough to have a fully developed turbulent flow for used interval of Reynolds numbers [61, Ch.8]. Rotameter, pressure transducer and two storage tanks were used in the flow system. Height of upper tank is 3 meters from bottom one. Flow was driven by a centrifuge water pump. Flow rate was controlled by a gate valve. 4 MHz ultrasonic probe with inclination of 70^0 (Doppler angle) was located in a condom filled with water on pipe. This gave the best US coupling in our studies. Probe didn't have any direct contact with the pipe in order to prevent the effect of flow system vibrations on probe position. Level of upper tank was kept constant by overflowing water. Normal tap water with added Griltex copolyamide particles (60% $50\mu\text{m}$ – 40% $80\mu\text{m}$, Signal Processing, Switzerland) was

used. Concentration of 10 g Griltex/140 L water gave good measurement results. Some pictures of ultrasound Doppler velocimeter, ultrasonic probes and their coupling are depicted below (Figure 5.2.1).

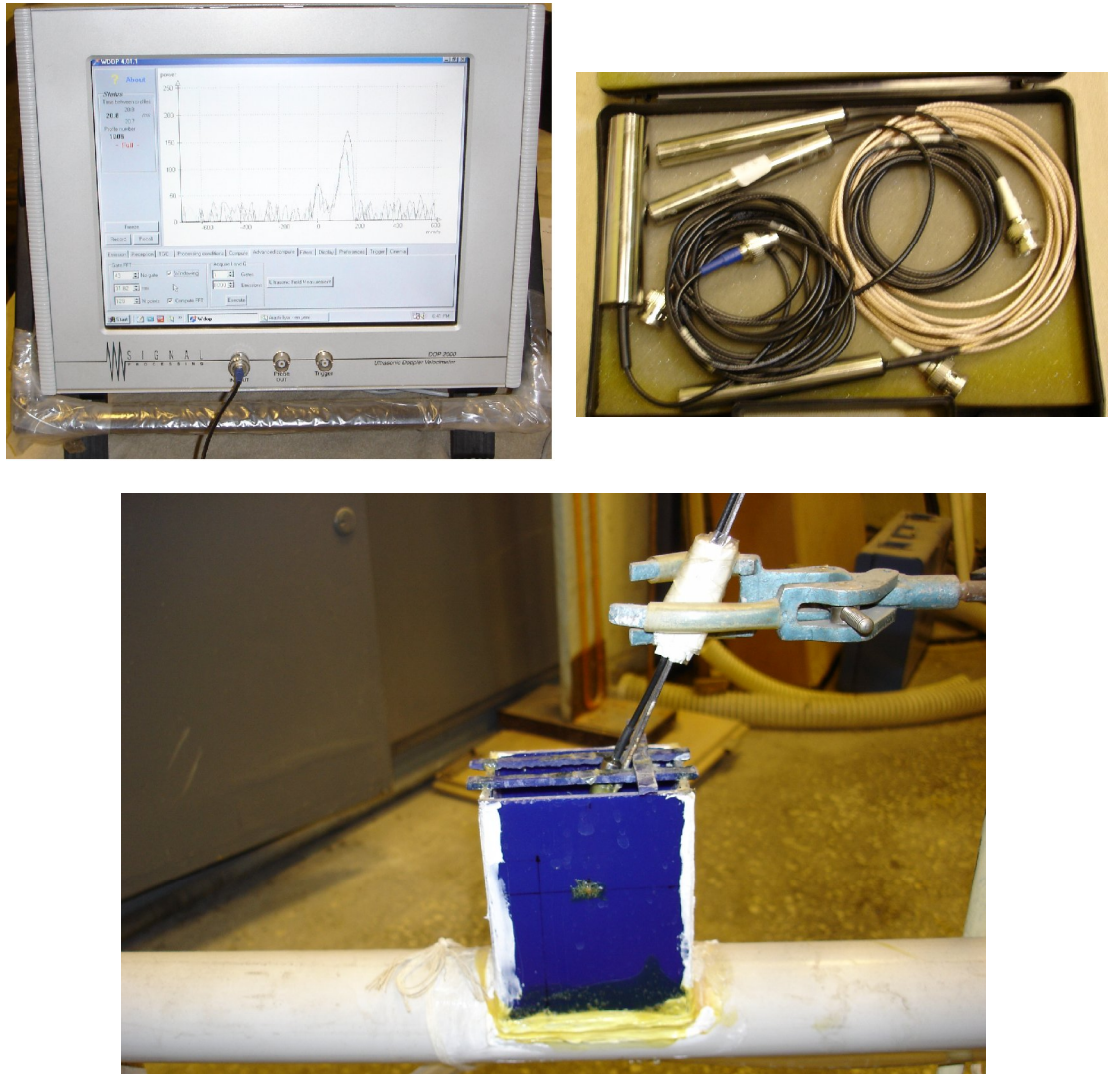


Figure 5.2.1: Ultrasound Doppler Velocimeter-DOP 2125 (top left), ultrasound probes and ultrasonic coupling condom on pipe (bottom).

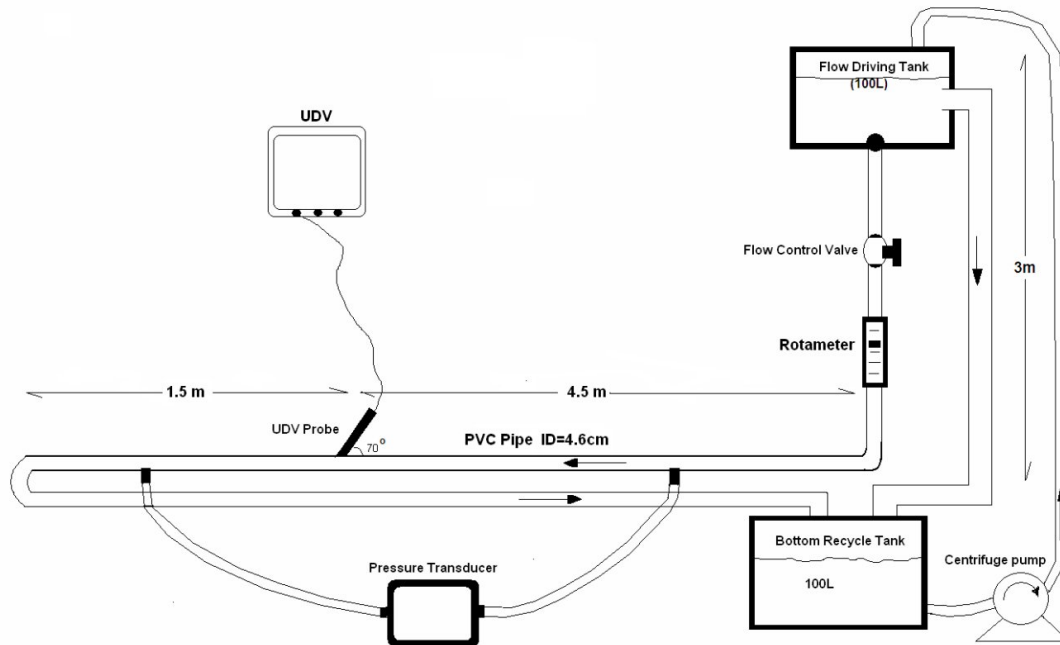


Figure 5.2.2: Recirculation water flow system

5.3 Verification of PDF and Spectrum Relation by Experimental UDV Measurements

Experimentally velocity and I-Q signal measurements were carried out to verify the relation (5.1.5) between PDF of velocity and spectrum of sampled ultrasound signals. Measurements were done at two different Reynolds Numbers and at the center of pipe (ID=46 mm). A Gaussian PDF was assumed for measured 4096 velocities. Also spectrum of sampled raw signals was displayed from FFT of total signal (i.e. $I + jQ$). A Gaussian function was fitted to the amplitude of this spectrum and both Gaussian curves of spectrum and velocity PDF were compared with equation (5.1.5). All measurements and calculations were done for the velocity component in the probe direction. UDV measurement parameters are,

I-Q signal measurements: $N_{pm}=8000$, $c=1480$ m/s, $f_o=4$ MHz, $T_{prf}=0.138$ ms, $\theta=70^\circ$

Velocity measurements: 4096 velocity, 128 pulses/velocity, $c=1480$ m/s, $f_0=4$ MHz, $T_{\text{prf}}=0.138$ ms, $\theta=70^\circ$

Spectrum of sampled ultrasound signals is,

$$S[k.w_0] = \text{F.F.T.}\{I + jQ\} \quad (5.3.1)$$

Frequency axis was converted to velocity by Doppler equation

$$u = -\frac{k.w_0 c}{2f_0} \times 10^3 \text{ mm/s} \quad (5.3.2)$$

Negative sign is used to ensure that velocities away from probe become positive. Amplitude of sampled signals was obtained by using the following averaging operation.

$$A_0 = \sqrt{I^2 + Q^2} \quad (5.3.3)$$

Spectrum of US signal is presented in the form of amplitude versus velocity for Reynolds number of 16733 in Figure 5.3.1. The figure can also be considered as the distribution of various velocities occurring in the fluctuating flow. In the figure solid line represents a fitted Gaussian function. Close fit indicates that the distribution of the velocities around the average follows a Gaussian pattern which is clearly depicted in Figure 5.3.2. In the figure PDFs obtained from measured velocities and from US spectrum are shown. The first one is obtained after processing the US signals to extract the velocity data while the second one is calculated directly from the sampled signals. Velocity PDFs obtained from measured velocities are slightly narrower compared to the one obtained from ultrasound spectrum. This might be due to longer durations and averaging while measuring velocities. It should be noted that time resolution for measured velocities are $128 \times T_{\text{prf}}$ whereas it is T_{prf} for sampled ultrasonic signals (I-Q), which means higher time resolutions in the case of US spectrum. Although both PDFs are well correlated, the one obtained from ultrasound spectrum seems more reliable because of higher time resolution.

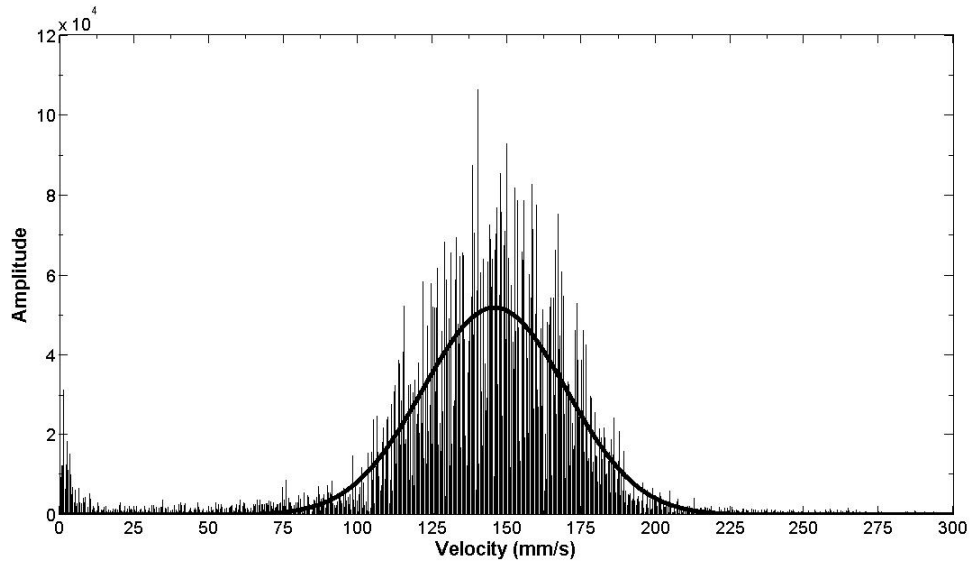


Figure 5.3.1: Amplitude of ultrasound spectrum and fitted Gaussian function for

$N_{Re}=16733$. Gaussian function is:
$$\left| S\left[u = -\frac{c.k.w_o}{4\pi f_o T_{prf}}\right] \right| = 5.175 \times 10^4 e^{-\frac{(u-145.9)^2}{33.96}}$$

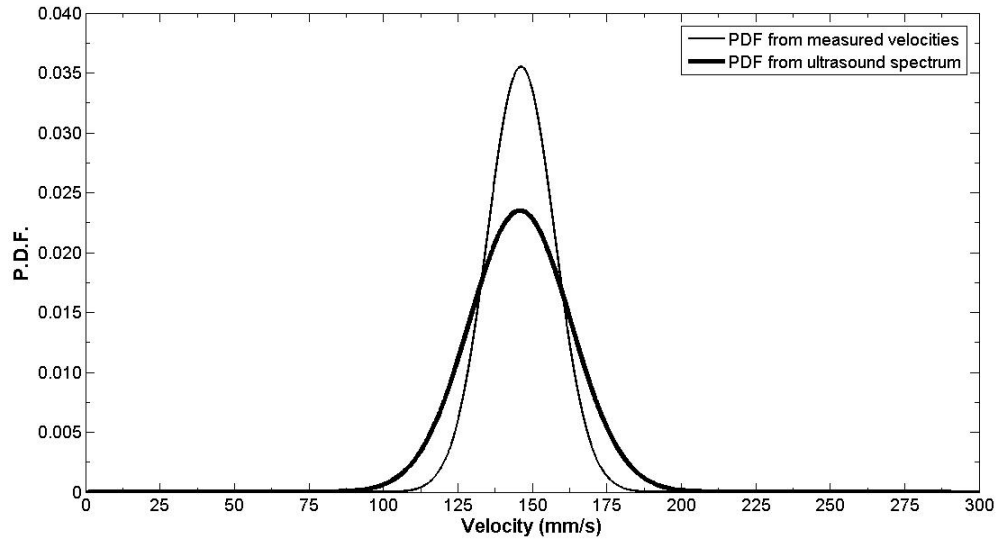


Figure 5.3.2: Gaussian PDFs obtained from measured velocities and amplitude of ultrasound spectrum ($|S[u]|$) through equation (5.1.5). $A_o=91$, mean velocity at pipe center is 146.2 mm/s and standard deviation is 11.2 mm/s for $N_{Re}=16733$.

Received average signal amplitude (A_o) is increasing from 91 to 147 while N_{Re} is increasing from 16733 to 26295. Increasing N_{Re} also increases the standard deviation of US spectrum and velocity PDF as shown in Figures 5.3.3 and 5.3.4 respectively.

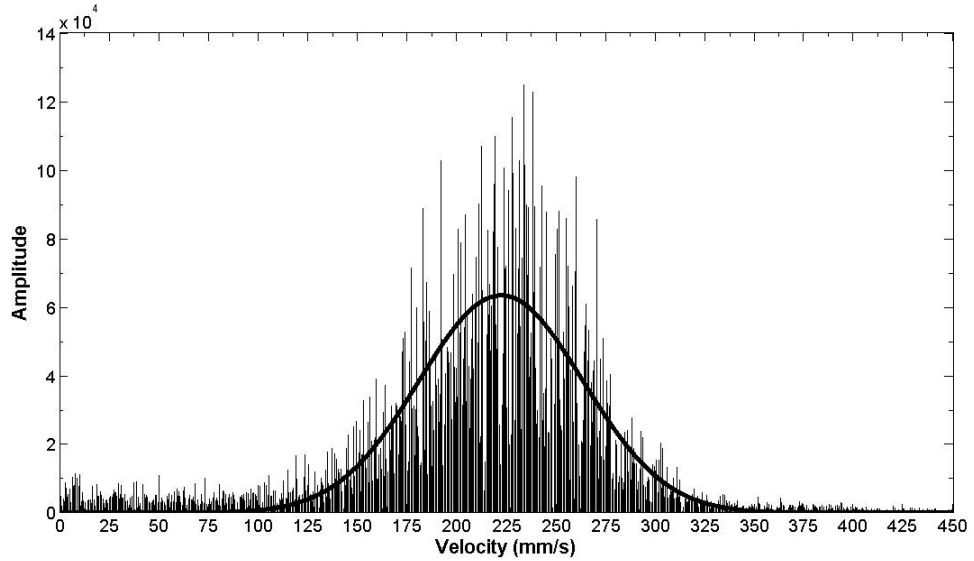


Figure 5.3.3: Amplitude of ultrasound spectrum and fitted Gaussian function for

$$N_{Re}=26295. \text{Gaussian function is: } \left| S[u = -\frac{c.k.w_o}{4\pi f_o T_{prf}}] \right| = 6.336 \times 10^4 e^{-\left(\frac{u-222.0}{58.36}\right)^2}$$

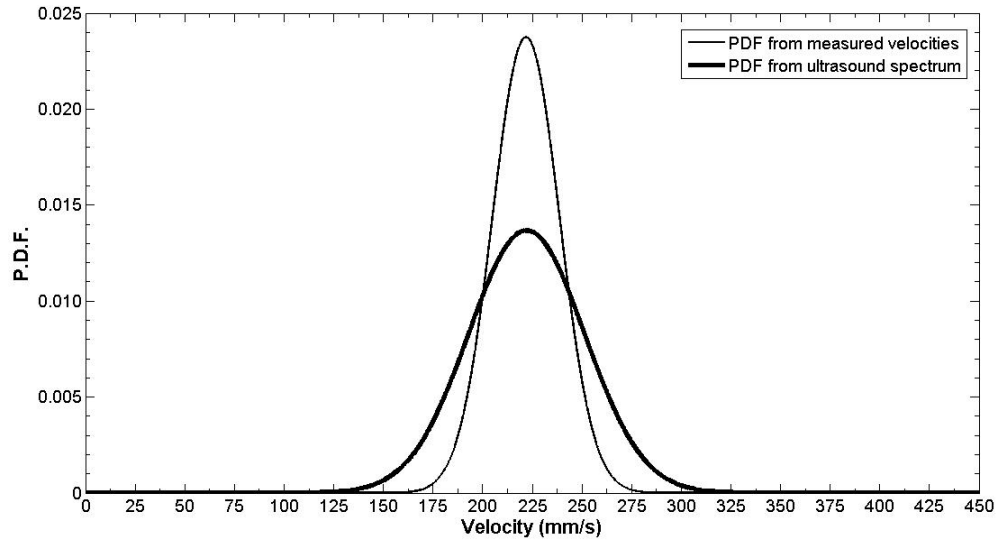


Figure 5.3.4: Gaussian PDFs obtained from measured velocities and amplitude of ultrasound spectrum ($|S[u]|$) through equation (5.1.5). $A_o=147$, mean velocity at pipe center is 221.8 mm/s and standard deviation is 16.8 mm/s for $N_{Re}=26295$.

5.4. Velocity Auto-Correlation Function (ACF)

Velocity auto-correlation function (ACF) of velocity component (u) in the direction of probe axis is investigated in this section. U has been taken as a random variable (r.v.) throughout this analysis and it is positive when going away from probe. In the case of pipe flow, statistical properties of axial flow velocity (v) can be deduced from statistical properties of u, since $u=v.\cos\theta$ where θ is angle between probe axis and axial flow direction. Derivations were started from equation (5.1.1) which represents sampled ultrasonic signals in discrete and complex form for a measurement volume of i. it should be noted that u is random variable and some function of discrete time n in this equation. For the signals of $E[n] = 1$,

$$\frac{s[n]}{A_o} = e^{j(\gamma_1 - \gamma_2 u.n + \gamma_4 u)} \Rightarrow \ln\left(\frac{s[n]}{A_o}\right) = j(\gamma_1 - \gamma_2 u.n + \gamma_4 u)$$

If $s[n]$ is demodulated complex Doppler signal, it can be expressed in terms of In-phase (I) and Quadrature (Q) parts as, $s[n]=I[n]+jQ[n]=A_o[n]e^{j\phi[n]}$. Amplitude and phase of $s[n]$ in terms of I and Q signals will be,

$$|s[n]| = \sqrt{I^2[n] + Q^2[n]} = A_o[n] \quad (5.4.1)$$

$$\phi[n] = \angle \{s[n]\} = \text{Tan}^{-1} \left\{ \frac{Q[n]}{I[n]} \right\} \quad (5.4.2)$$

Therefore we can show I and Q parts of $s[n]$ as,

$$I = A_o[n] \cos(\phi[n]) , Q = A_o[n] \sin(\phi[n]) .$$

$$\Rightarrow \ln\left(\frac{A_o[n] e^{j\phi[n]}}{A_o[n]}\right) = j(\gamma_1 - \gamma_2 u.n + \gamma_4 u)$$

$$\angle \phi[n] = \angle (\gamma_1 - \gamma_2 u.n + \gamma_4 u)$$

After taking DFT of both sides to find the spectrum of random velocity u, obtained velocity auto correlation function is (see Appendix A.3 for details),

$$R_u[\tau] = \text{D.F.T.}^{-1} \{S_u[k]\} = \frac{1}{N_{\text{prn}}} \sum_{k=0}^{N_{\text{prn}}-1} \left\{ \lim_{N_{\text{prn}} \rightarrow \infty} \frac{1}{N_{\text{prn}}} |U[k]|^2 \right\} e^{j \frac{2\pi}{N_{\text{prn}}} k \cdot \tau}$$

$$R_u[\tau] = \text{D.F.T.}^{-1} \left\{ \lim_{N_{\text{prn}} \rightarrow \infty} \frac{1}{N_{\text{prn}}} \left| N_{\text{prn}} \bar{u} \delta[k] + \frac{j \cdot 2\pi}{N_{\text{prn}} \gamma_2} e^{-\frac{j \cdot 2\pi \cdot \gamma_4}{N_{\text{prn}} \cdot \gamma_2} k} \int_0^k (\phi_4 - \gamma_1 N_{\text{prn}} \delta[k]) e^{\frac{j \cdot 2\pi \cdot \gamma_4}{N_{\text{prn}} \cdot \gamma_2} k} dk \right|^2 \right\} \quad (5.4.3)$$

The amplitude of $U[k]$ {i.e. $|U[k]|$ } cannot be obtained analytically from equation (5.4.3) since it depends on phases of each part of $U[k]$. But it can be evaluated numerically by putting discrete phase sequence $\{\text{Tan}^{-1}(Q/I)\}$ which is obtained from UDV.

We can check equation (5.4.3) analytically and numerically. If flow is constant velocity flow from equation (4.2.6),

$$\phi_4[k] = \text{D.F.T.} \{s[n]\} = \text{D.F.T.} \{\gamma_1 - \gamma_2 \bar{u} \cdot n + \gamma_4 \bar{u}\} \quad (5.4.4)$$

where \bar{u} is constant velocity and n is discrete time between 1 and N_{prn} .

$$\begin{aligned} \phi_4[k] &= \gamma_1 N_{\text{prn}} \delta[k] + \gamma_4 \bar{u} N_{\text{prn}} \delta[k] - \gamma_2 \bar{u} \left(\frac{N_{\text{prn}}^2}{2\pi} j \frac{d\delta[k]}{dk} \right) \\ &\Rightarrow \int_0^k (\phi_4 - \gamma_1 N_{\text{prn}} \delta[k]) e^{\frac{j \cdot 2\pi \cdot \gamma_4}{N_{\text{prn}} \cdot \gamma_2} k} dk = \int_0^k (\gamma_4 \bar{u} N_{\text{prn}} \delta[k] - \gamma_2 \bar{u} \frac{N_{\text{prn}}^2}{2\pi} j \frac{d\delta[k]}{dk}) e^{\frac{j \cdot 2\pi \cdot \gamma_4}{N_{\text{prn}} \cdot \gamma_2} k} dk = \\ &\gamma_4 \bar{u} N_{\text{prn}} \delta[k] - j \frac{N_{\text{prn}}^2 \gamma_2 \bar{u}}{2\pi} \int_0^k \frac{d\delta[k]}{dk} e^{\frac{j \cdot 2\pi \cdot \gamma_4}{N_{\text{prn}} \cdot \gamma_2} k} dk = \\ &\gamma_4 \bar{u} N_{\text{prn}} \delta[k] - j \frac{N_{\text{prn}}^2 \gamma_2 \bar{u}}{2\pi} \left(- \int_0^k \frac{j \cdot 2\pi \cdot \gamma_4}{N_{\text{prn}} \cdot \gamma_2} e^{\frac{j \cdot 2\pi \cdot \gamma_4}{N_{\text{prn}} \cdot \gamma_2} k} \delta[k] dk \right) = \\ &\gamma_4 \bar{u} N_{\text{prn}} \delta[k] + j \frac{N_{\text{prn}}^2 \gamma_2 \bar{u}}{2\pi} \frac{j \cdot 2\pi \cdot \gamma_4}{N_{\text{prn}} \gamma_2} \delta[k] = \gamma_4 \bar{u} N_{\text{prn}} \delta[k] - \gamma_4 \bar{u} N_{\text{prn}} \delta[k] = 0 \end{aligned}$$

(where integration by parts i.e. $\int_{\text{cycle}} f[k] \delta'[k] dk = \underbrace{f[k] \delta[k]}_{\substack{\text{around} \\ k=0}} \Big|_{\text{cycle}} - \int_{\text{cycle}} f'[k] \delta[k] dk$ is

used)

Since integral in equation (A.3.1) is zero,

$$\Rightarrow U[k] = N_{\text{prn}} \bar{u} \delta[k] \Rightarrow R_u[\tau] = \text{D.F.T.}^{-1} \left\{ \frac{1}{N_{\text{prn}}} N_{\text{prn}} \bar{u}^2 \delta[k] \right\} = \bar{u}^2 \text{ for all } \tau$$

Velocity ACF is constant for all time lags. This shows constant velocity is fully correlated with itself which is an expected result.

If we put analytical phase expressions $\{\text{Tan}^{-1}(Q/I)\}$ from previous derivations for constant velocity (Eq. (4.2.6)) and single frequency oscillating (Eq. (4.3.3)) flows and solve numerically, the velocity spectrums (from Eq. (A.3.1)) and velocity auto-correlation coefficients (ACC) (from Eq. (5.4.3)) are obtained as in Figures 5.4.1 to 5.4.6.

$$\text{For constant velocity flow: } \text{Tan}^{-1}\left(\frac{Q}{I}\right) = \gamma_1 - \gamma_2 \bar{u}.n + \gamma_4 \bar{u}$$

$$\text{For oscillating velocity flow: } \text{Tan}^{-1}\left(\frac{Q}{I}\right) = \gamma_1 - \gamma_2 \bar{u}.n + \gamma_4 \bar{u} - a_4 + a_4 \cos(a_5 + a_6(n-1))$$

$$\text{where } a_4 = \frac{2f_o \bar{u} A_f}{c.f_f}, a_5 = \frac{2\pi f_f d_{o,i}}{c}, a_6 = 2\pi f_f T_{\text{prf}}$$

A_f is oscillation amplitude as percentage of mean velocity and f_f is oscillation frequency as Hz. For the parameters of mean velocity of $\bar{u}=0.01\text{m/s}$, $N_{\text{prn}}=8001$, $N_c=4$, $f_o=4\text{MHz}$, $c=1480\text{m/s}$, $T_{\text{prf}}=0.138\text{ms}$ and $d_{o,i}=0.035\text{m}$, obtained velocity spectrums and velocity ACCs would be as following.

Spectrum of constant velocity (Figure 5.4.1) contains only an impulse function at zero frequency and velocity is fully correlative with itself (Figure 5.4.2) as expected.

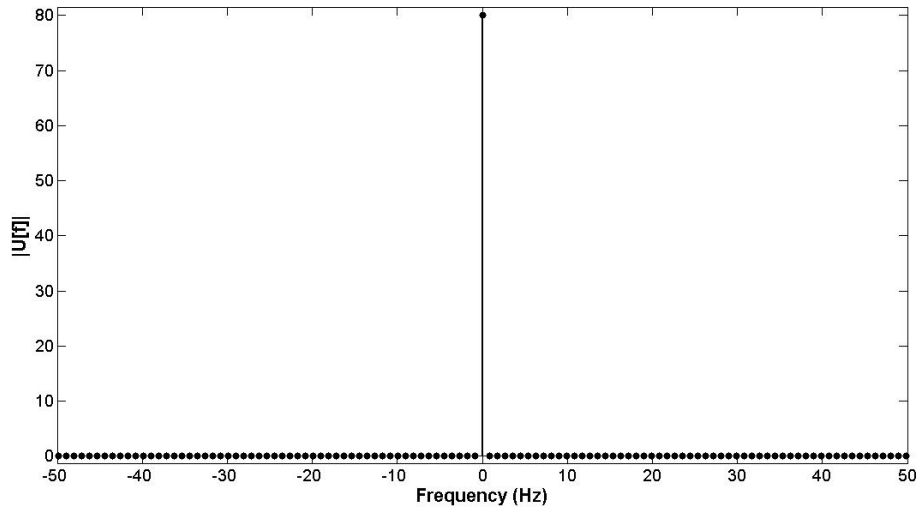


Figure 5.4.1: Amplitude of spectrum of constant velocity from equation (A.3.1)

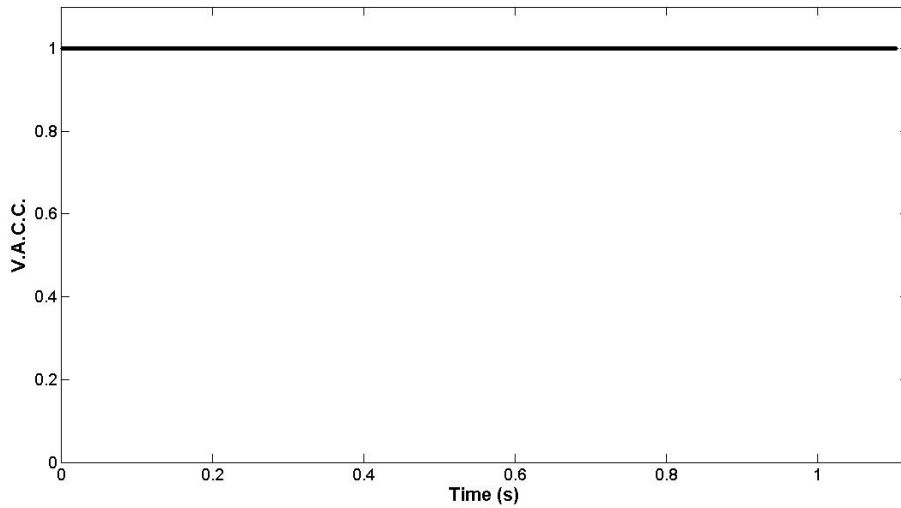


Figure 5.4.2: Velocity ACC for constant velocity from equation (5.4.3)

Spectrum of oscillating part of velocity contains a component at oscillation frequency and other components around it (Figures 5.4.3, 5.4.5). Correlation is going to zero around time difference of half of the oscillation period (Figures 5.4.4, 5.4.6).

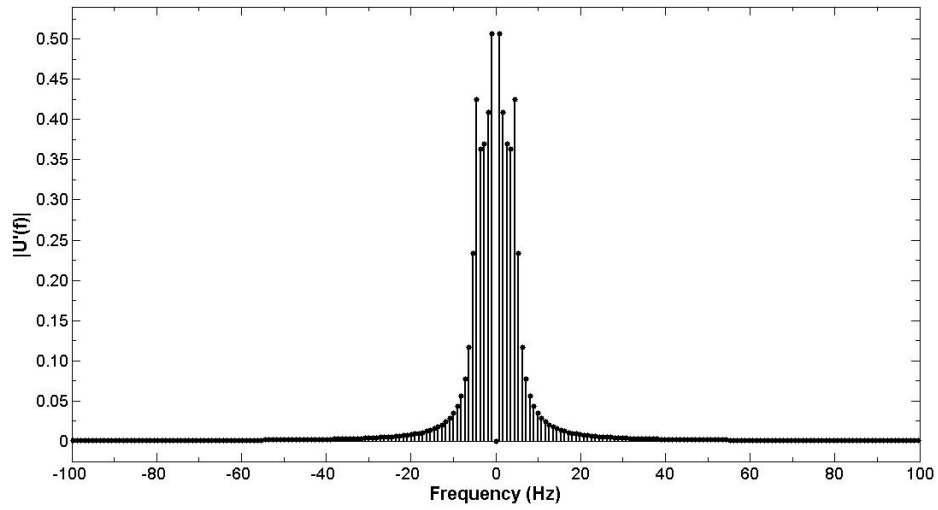


Figure 5.4.3: Amplitude of spectrum of fluctuating part of velocity for $A_f=10\%$ oscillation amplitude and $f_f=5\text{Hz}$ oscillation frequency from equation (A.3.1)

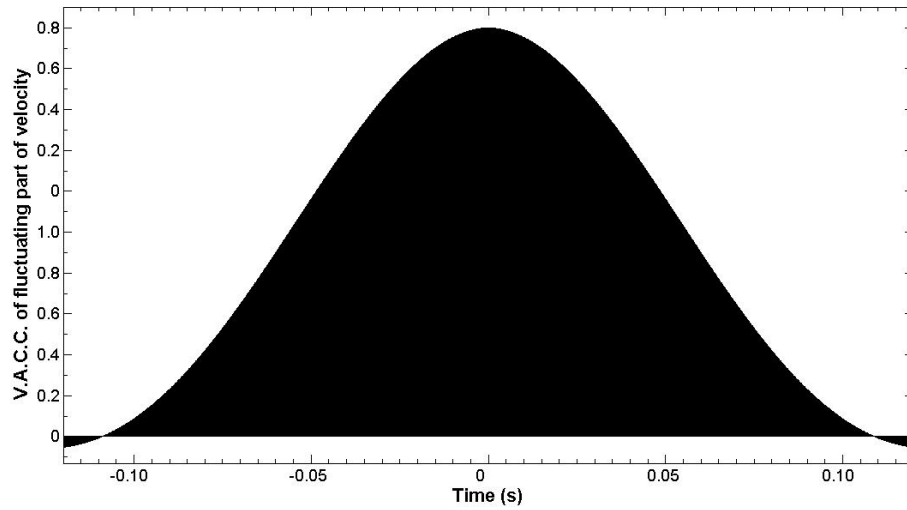


Figure 5.4.4: Velocity ACC of fluctuating part of velocity for $A_f=10\%$ oscillation amplitude and $f_f=5\text{Hz}$ oscillation frequency from equation (5.4.3)

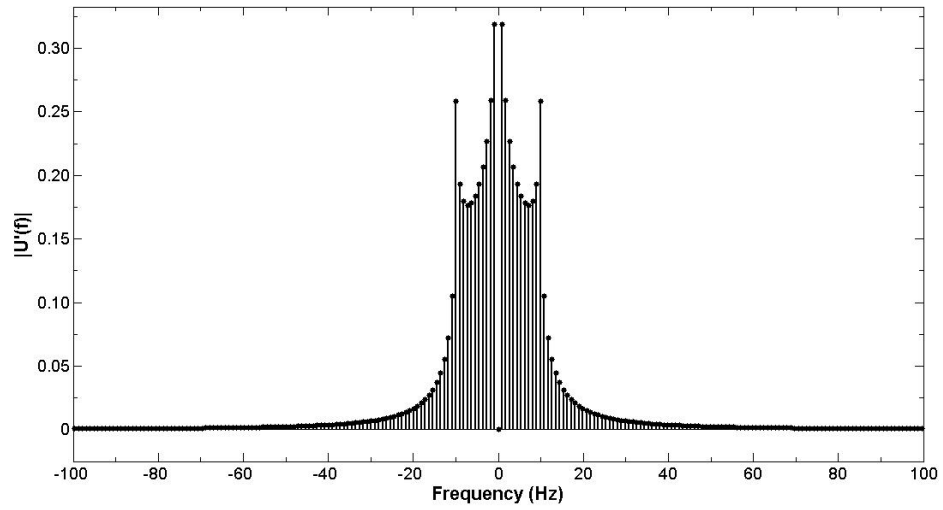


Figure 5.4.5: Amplitude of spectrum of fluctuating part of velocity for $A_f=10\%$ oscillation amplitude and $f_f=10\text{Hz}$ oscillation frequency from equation (A.3.1)

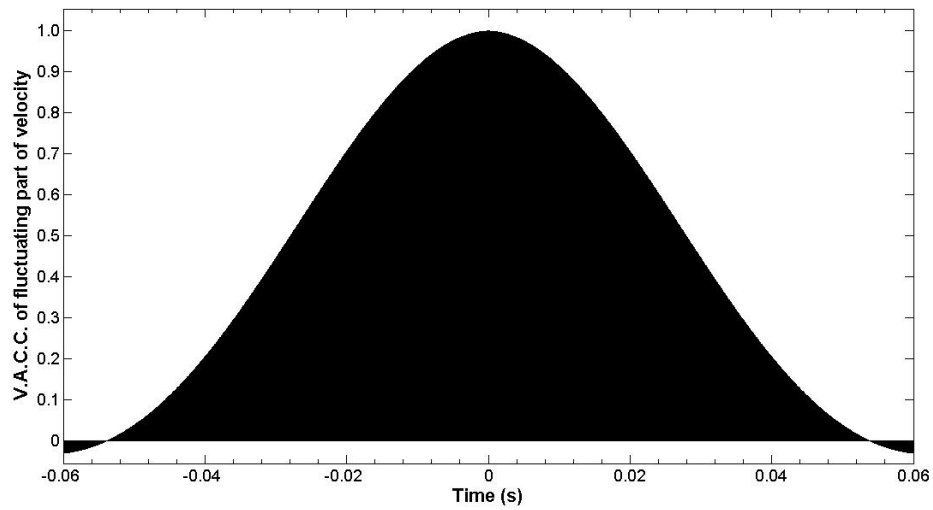


Figure 5.4.6: Velocity ACC of fluctuating part of velocity for $A_f=10\%$ oscillation amplitude and $f_f=10\text{Hz}$ oscillation frequency from equation (5.4.3)

5.5 Experimental Velocity ACC and Turbulence Measurements

5.5.1 Velocity ACC and Energy Spectrum of Turbulence

Velocity and I-Q signal measurements were performed at Reynold's number of 13148 and center of pipe (ID=46mm). Mean velocity along probe axis at this point (\bar{u}) is 116.32 mm/s and r.m.s. (root mean square of fluctuating part of velocity, u') along probe axis is 9.68mm/s. 4096 velocity values were measured. 128 pulses/velocity were used with $f_{prf}=1/T_{prf}=7246$ Hz, $N_c=4$, $f_o=4$ MHz, $c=1480$ m/s. 8000 I and 8000 Q signals were taken. Angle between probe and pipe was 70° . Then velocity ACC for fluctuating part of velocity (u') can be defined as,

$$R'_{u'}[\tau] = \frac{\overline{u'[n].u'[n+\tau]}}{\overline{u'[n].u'[n]}} \quad (5.5.1.1)$$

where n and τ are discrete times.

Time resolution of velocity ACC obtained from equation (5.4.3) by using I-Q signals is period of pulse sending (T_{prf}) while it is $128 \times T_{prf}$ for velocity ACC obtained from measured velocity values. Time resolution of velocity ACC obtained from measured velocities doesn't seem enough to capture real correlation (Figure 5.5.1.1) while it is much reasonable for the one obtained from equation (5.4.3) (Figure 5.5.1.2). These results are compatible with study of Garcia et al [63]. They defined a parameter F for turbulent flows which is the ratio of frequency of velocity sampling to frequency of large eddies present in the flow. They showed that the higher the ratio F , the better the description of turbulence is achieved from measurements. They said F should be bigger than 20 and shouldn't be less than 1.

$$F = \frac{f_{vel.samp.}}{f_{large\ eddy}} = \frac{f_{prf} / N}{v_c / D} \quad (5.5.1.2)$$

Where N is number of pulses to measure one velocity value, D is characteristic length which is pipe diameter, v_c is convective velocity. If we approximate v_c as

average velocity (\bar{v}), F value for velocity measurements with the specified parameters is 7.66. However F value for I-Q signal measurements is 980.05. This large increase of F value explains the improvement of velocity ACC while using I-Q signals directly through equation (5.4.3) rather than using measured velocity values.

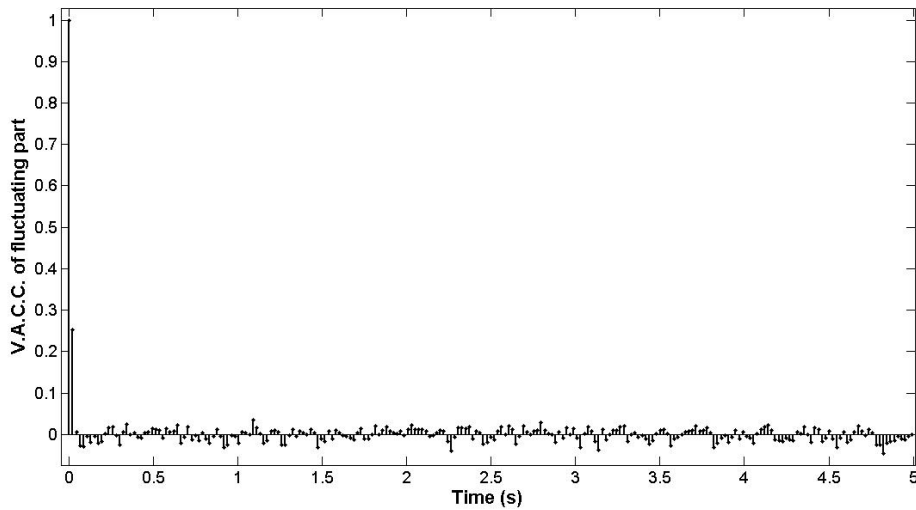


Figure 5.5.1.1: Velocity ACC of fluctuating part of measured velocities. Time resolution is 21.3 ms

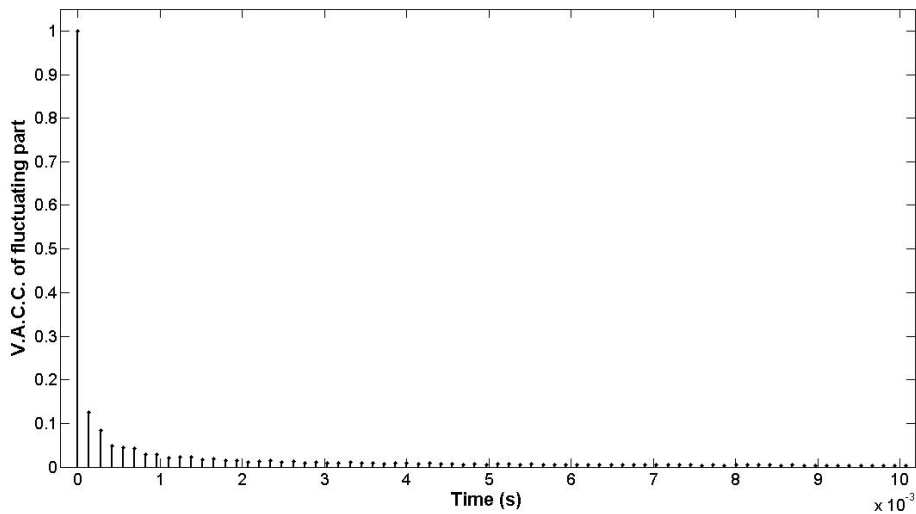


Figure 5.5.1.2: Velocity ACC of fluctuating part of velocity. This is obtained from measured I-Q signals by using equation (5.4.3). Time resolution is 0.138 ms

Moreover spatial resolution must be taken into account in UDV measurements. Our probe has a diameter of 5mm which is large compared to the pipe diameter 46mm. This means all I-Q signals were taken from a measurement volume of a cylinder with ~5 mm diameter and ~0.5 mm height. More accurate velocity ACCs can be obtained by using finer probes.

Energy spectrum of fluctuating part of velocity at pipe center was obtained which is simply the DFT of velocity ACC (Figure 5.5.1.3). Energy distribution over longitudinal turbulent length scales was obtained from energy spectrum by using longitudinal r.m.s. value. Energy cascade can be seen here (Figure 5.5.1.4). Energy scale is decreasing with decreasing eddy sizes (from integral to Kolmogorov length scales) or increasing frequencies.

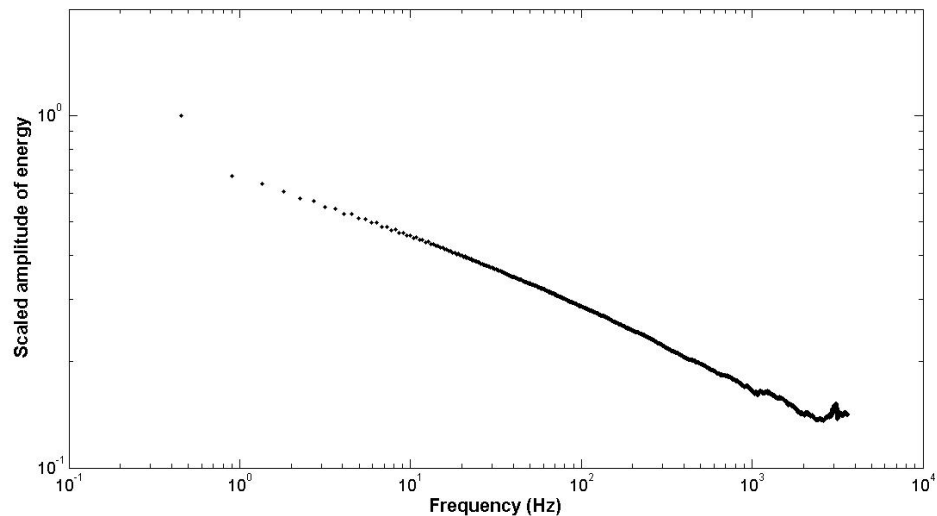


Figure 5.5.1.3: Energy spectrum of turbulence at pipe center by using velocity ACC from equation (5.4.3). Energy axis is scaled with maximum value. $N_{Re}=13148$

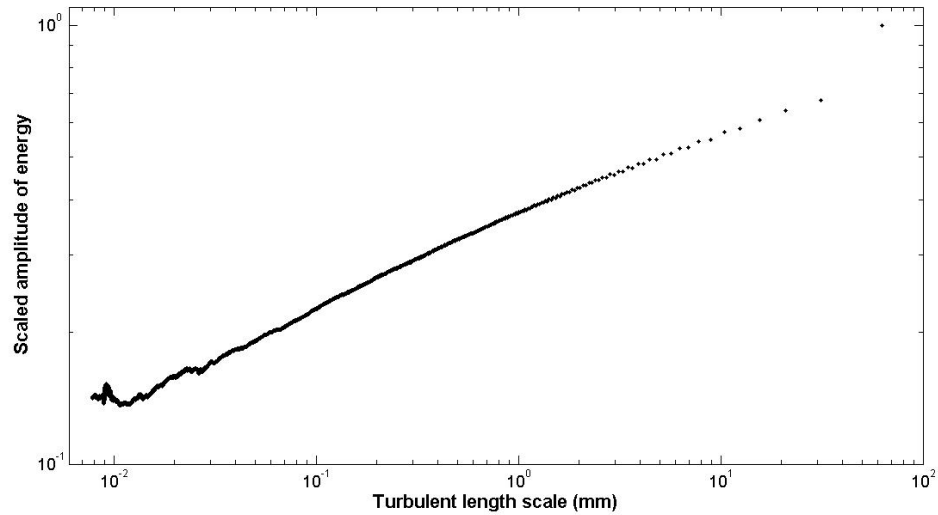


Figure 5.5.1.4: Energy distribution of turbulent length scales at pipe center. Energy axis is scaled with maximum value. $N_{Re}=13148$

5.5.2 Turbulence Parameters

If random variable u is statistically stationary and if number of velocity measurements and measurement period are large enough, we can use measured velocity values by means of UDV to obtain statistical properties of velocity. 4096 velocity measurements to obtain mean (\bar{v}) and r.m.s. (\tilde{u}) values were performed for each flow rate. 8000 I-Q signals were taken to obtain VACC through equation (5.4.3) for each flow rate. UDV measurement parameters are the same as mentioned in previous part. First measurements were carried out at the center of pipe for 11 different Reynolds numbers and then at a single Reynolds number, measurements were done for 6 different radial positions.

Changes of turbulence parameters in probe direction with Reynolds number and radial position in pipe are given below.

Turbulence parameters in probe direction for center of pipe

Centerline mean velocities are depicted in Figure 5.5.2.1 with respect to N_{Re} . In addition velocity fluctuation variation with N_{Re} is shown in Figure 5.5.2.2. High N_{Re} flow has fluctuations of lower fraction of local mean velocity. This is compatible with the study of Gad el Hak et al [53] in which they determined the axial turbulence intensity at pipe center as changing from 2.42% to 2.08% while N_{Re} is changing from 3506 to 7544. All length scales show an increasing type of trend with increasing Reynolds number (Figures 5.5.2.3., 5.5.2.4. and 5.5.2.6) indicating larger eddy sizes associated with higher flow rates at pipe center. Gad el Hak's LDV measurements for the center of 4mm ID pipe gave the same kind of increasing trends for integral and micro length scales [53]. Eddy diffusion coefficient is increasing with increasing Reynolds number (Figure 5.5.2.7) because of increasing strength of convective motion at pipe center. Energy dissipation rate is decreasing with increasing Reynolds number (Figure 5.5.2.5) because of decreasing turbulence intensity based on the mean velocity at pipe center (Figure 5.5.2.2). F value from equation (5.5.1.2) is changing between 14.36 and 4.01.

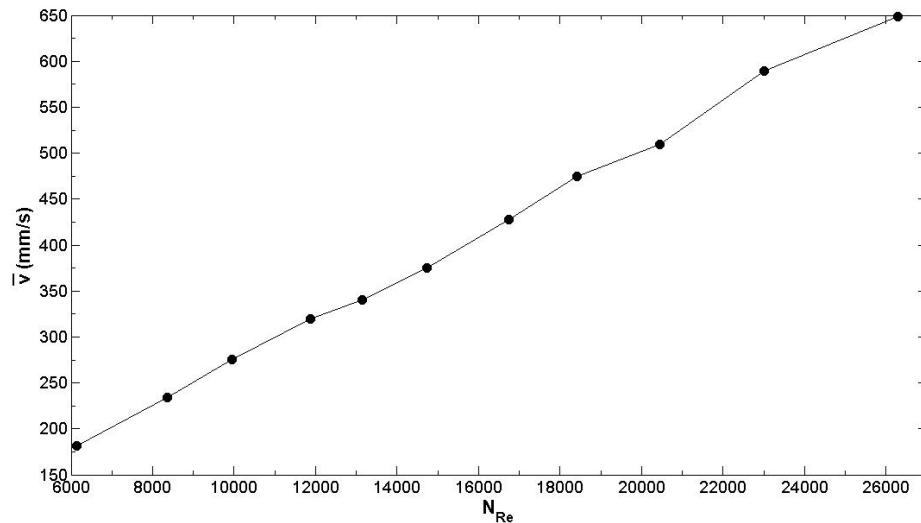


Figure 5.5.2.1: Mean longitudinal velocity at pipe center

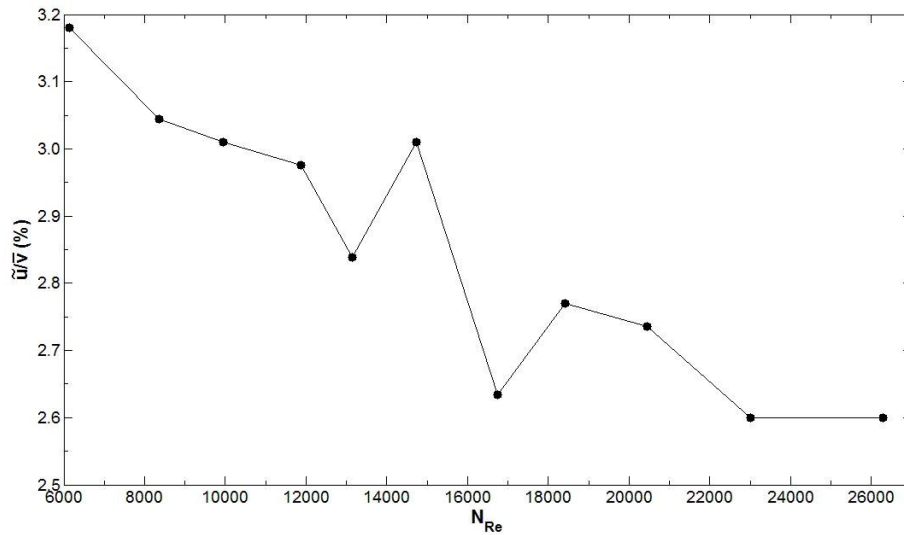


Figure 5.5.2.2: Amplitude of velocity fluctuations in probe direction as percentage of longitudinal mean velocity (turbulence intensity) at pipe center

Average value of turbulence intensity in probe direction (Figure 5.5.2.2) is 2.85. Axial and radial turbulent intensities are in nearly equal importance at pipe center [64]. Hence average percentage of turbulent intensity in the direction of probe which is installed with 70° angle on pipe will be 2.88 from study of Gad el Hak et al [53]. This intensity is average of several Reynolds number measurements from transition to 7544 and it is very close to our finding.

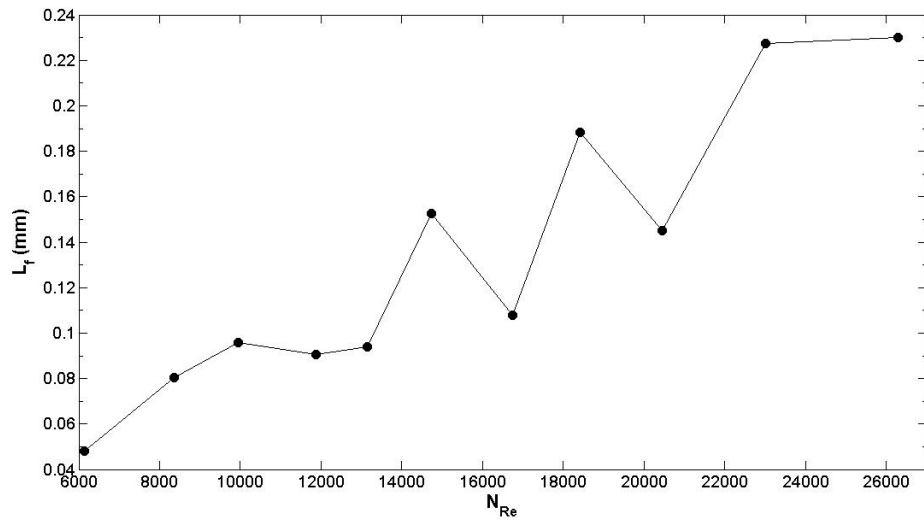


Figure 5.5.2.3: Eulerian integral length scale at pipe center from equation (3.1.5.8)

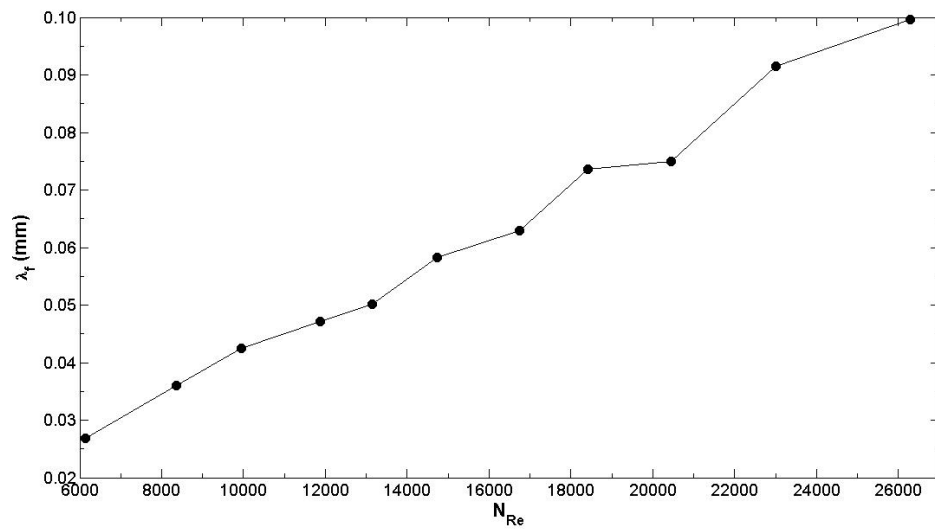


Figure 5.5.2.4: Eulerian micro length scale at pipe center from equation (3.1.5.6)

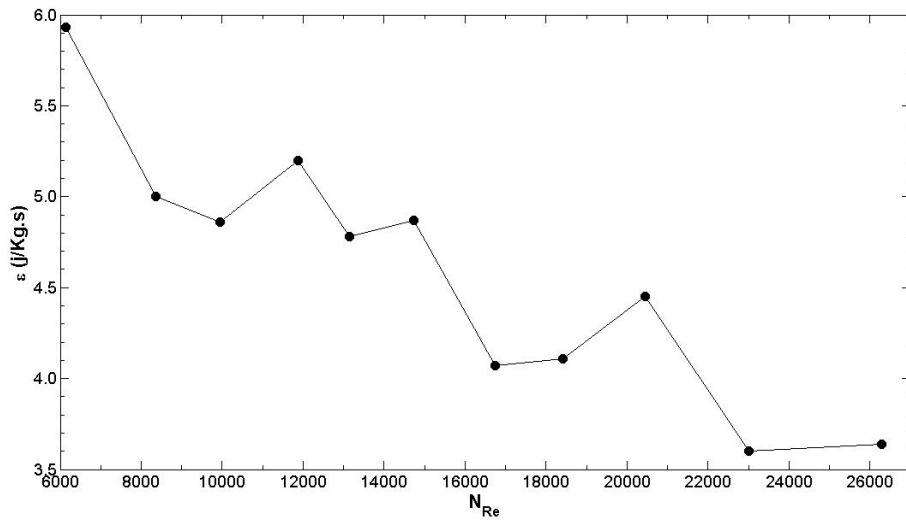


Figure 5.5.2.5: Rate of energy dissipation at pipe center from equation (3.1.5.9)

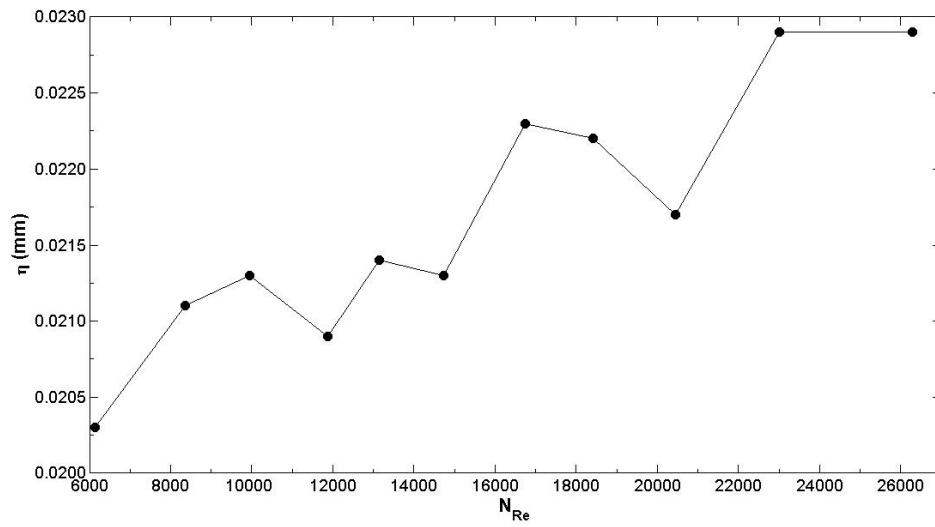


Figure 5.5.2.6: Kolmogorov length scale at pipe center from equation (3.1.7)

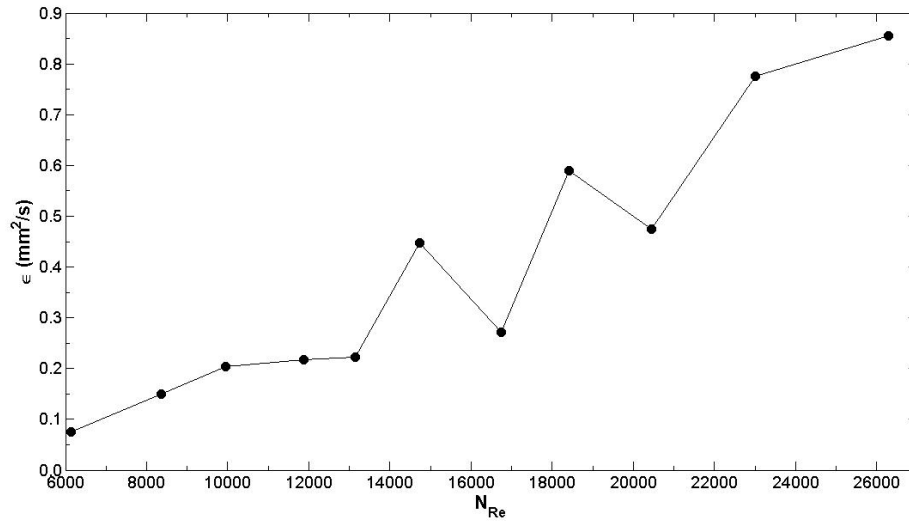


Figure 5.5.2.7: Eddy diffusion coefficient at pipe center from equation (3.1.5.8)

Turbulence parameters in probe direction for $N_{Re}=16733$

A sixth order polynomial with even powers was fitted to the measured average velocity data with no-slip boundary constraints (Figure 5.5.2.8) to obtain wall shear rate [28]. Wall shear rate from fitted polynomial is 126.25 s^{-1} and shear stress is 0.12625 Pa . Friction velocity $U_\tau = \sqrt{\tau_w / \rho}$ will be 0.01124 m/s . Blasius empirical relation of wall shear stress for turbulent pipe flow is [65],

$$\tau_w = \frac{1}{8} \lambda \cdot \rho \cdot v_{av}^2 \quad \text{where } \lambda = 0.316 / N_{Re}^{0.25} \quad (5.5.2.1)$$

v_{av} is average velocity in the pipe. τ_w from this equation is 0.4596 Pa and U_τ is 0.02144 m/s .

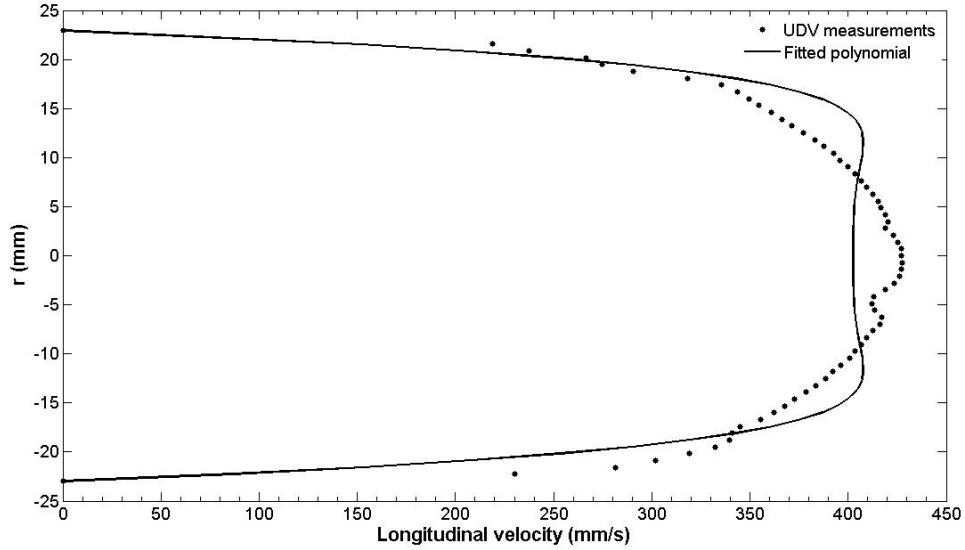


Figure 5.5.2.8: Longitudinal average velocity in pipe measured by UDV for $N_{Re}=16733$ and fitted constrained polynomial ($V=-4.367 \times 10^{-6} \cdot r^6 + 8.711 \times 10^{-4} \cdot r^4 + 402.71$)

r.m.s. measurements of Laufer [64] for radial and axial directions and their correlation were used to get r.m.s. values in $\theta=70^\circ$ probe direction through relation,

$$\frac{\tilde{u}}{U_\tau} = \sqrt{\cos^2 \theta \frac{\overline{v'^2}}{U_\tau^2} + \sin^2 \theta \frac{\overline{g'^2}}{U_\tau^2} + 2 \cos \theta \sin \theta \frac{\overline{v'g'}}{U_\tau^2}} \quad (5.5.2.2)$$

where v' is axial and g' is radial velocity fluctuations. As it is seen from Figure 5.5.2.9 measured r.m.s. distribution in probe direction is close and exhibiting the same behavior with data from Laufer's study. Far half measurements of pipe flow are giving better results in terms of velocity fluctuations as expected. This is because of near wall effects on UDV signals. Here the results of using theoretical friction velocity for normalization seem more reasonable and accurate. Since small decrease of fluctuation amplitudes with decreasing Reynolds number is expected. Near wall measurements of UDV is not accurate for the sizes of pipe and probe used.

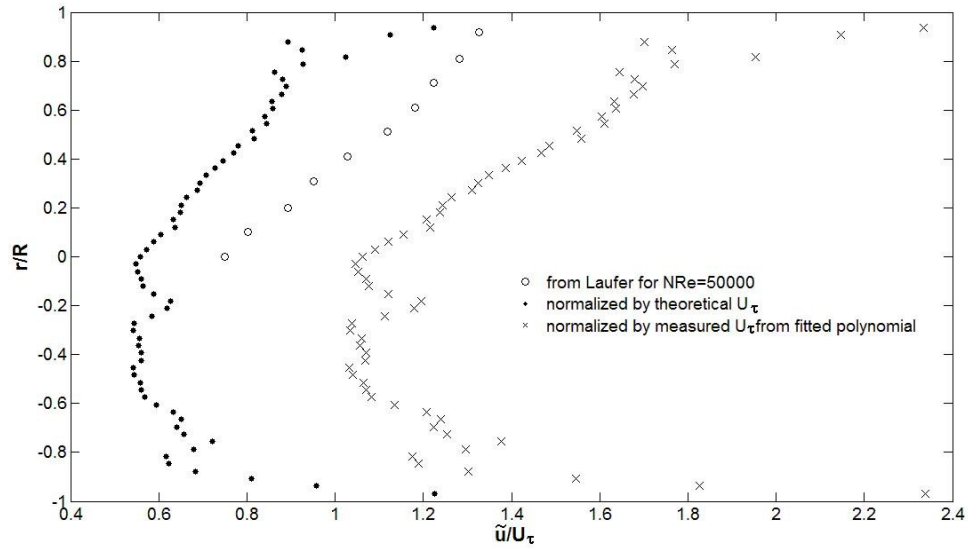


Figure 5.5.2.9: Normalized r.m.s. distribution in probe direction along diameter of pipe for $N_{Re}=16733$

Eddy diffusion coefficient increases from pipe center to wall (Figure 5.5.2.16) because of increasing turbulence intensity towards pipe wall (Figure 5.5.2.11). This is indicating that turbulent mixing is getting stronger towards pipe wall. It is evident that viscous effects are playing an important role in this phenomenon. Although integral and micro length scales (Figure 5.5.2.12 and 5.5.2.13) are not showing a systematic change while going away from center of pipe, Kolmogorov length scale is decreasing (Figure 5.5.2.15) because of increasing energy dissipation rate towards wall (Figure 5.5.2.14). Hence size of biggest eddies are not showing a systematic change from pipe center to one third of radius whereas size of smallest eddies are clearly decreasing towards pipe wall. This is braking turbulent kinetic energy coming from larger eddies in to smallest ones for complete viscous dissipation. F value for pipe center is 6.1.

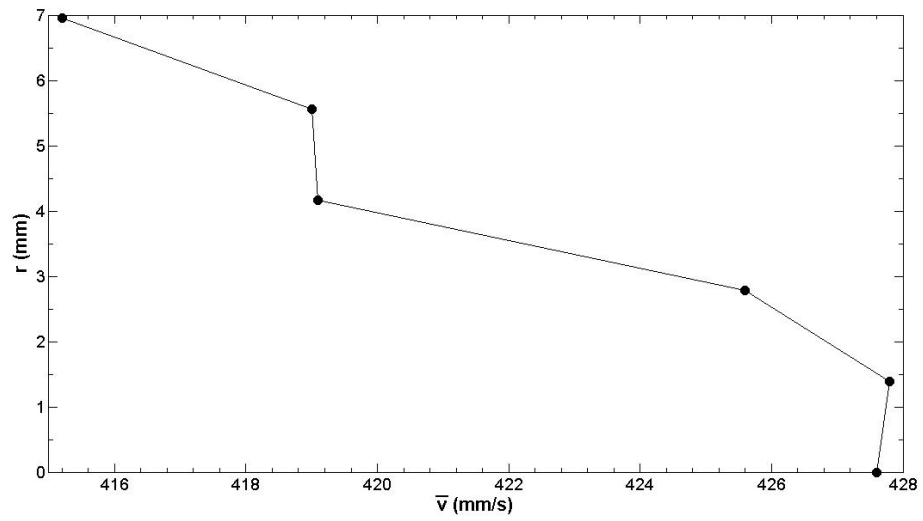


Figure 5.5.2.10: Mean longitudinal velocities at $N_{Re}=16733$

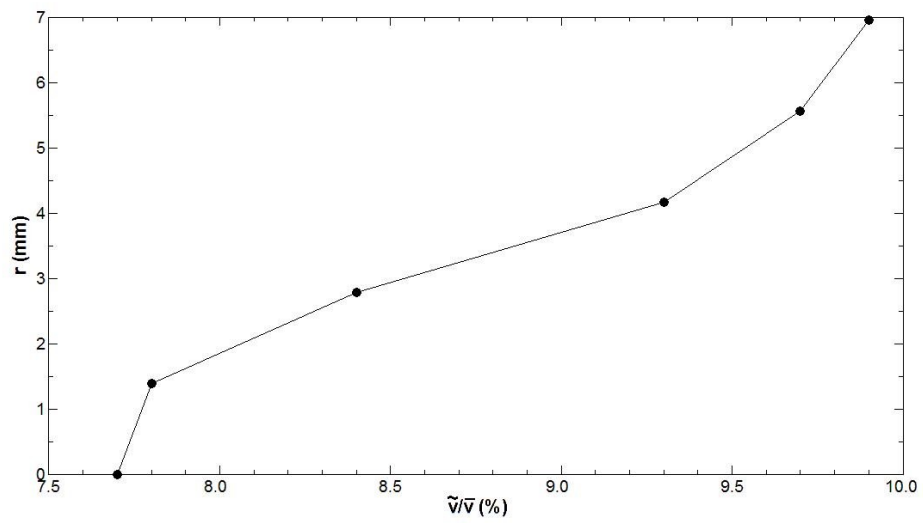


Figure 5.5.2.11: Amplitude of velocity fluctuations as percentage of mean velocity (turbulence intensity) at $N_{Re}=16733$

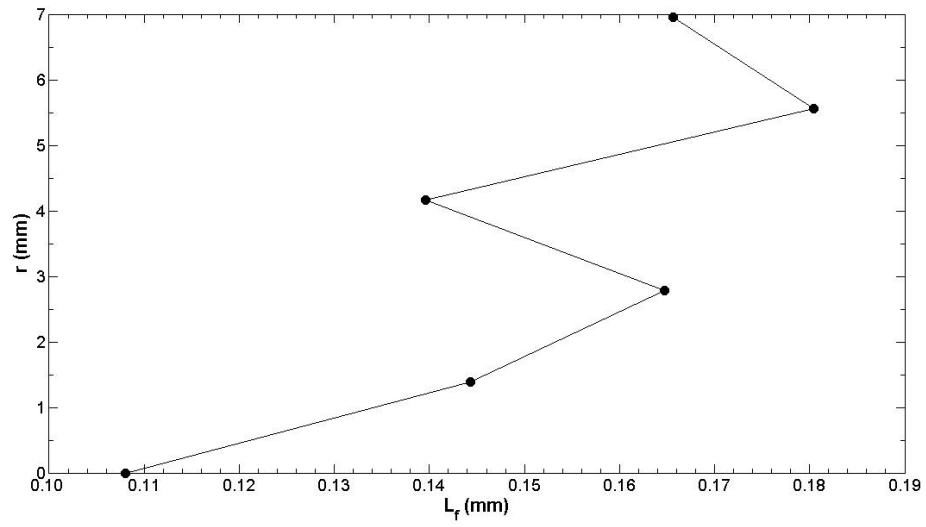


Figure 5.5.2.12: Eulerian integral length scale at $N_{Re}=16733$ from equation (3.1.5.8)

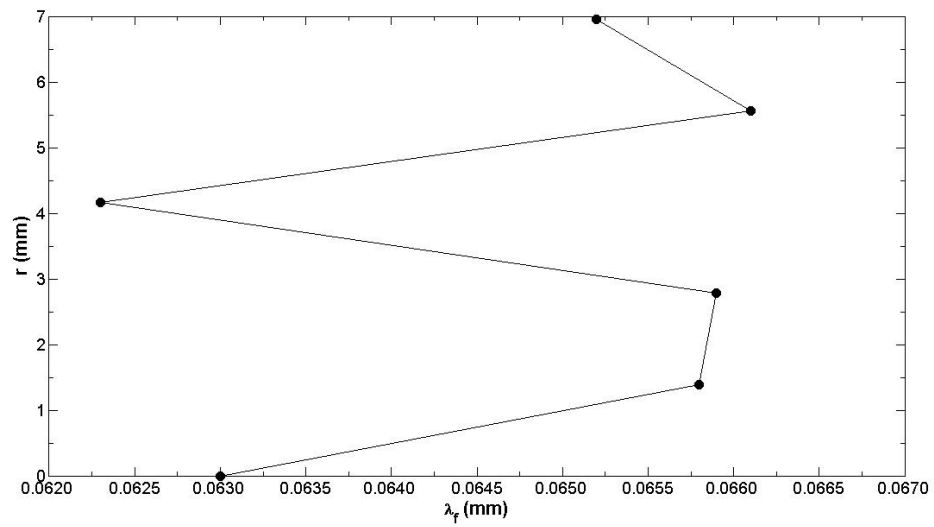


Figure 5.5.2.13: Eulerian micro length scale at $N_{Re}=16733$ from equation (3.1.5.6)

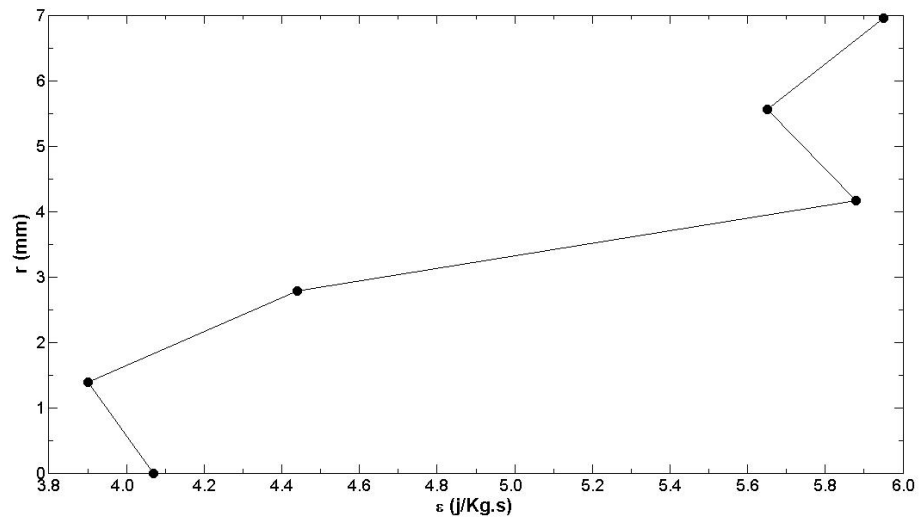


Figure 5.5.2.14: Rate of energy dissipation at $N_{Re}=16733$ from equation (3.1.5.9)

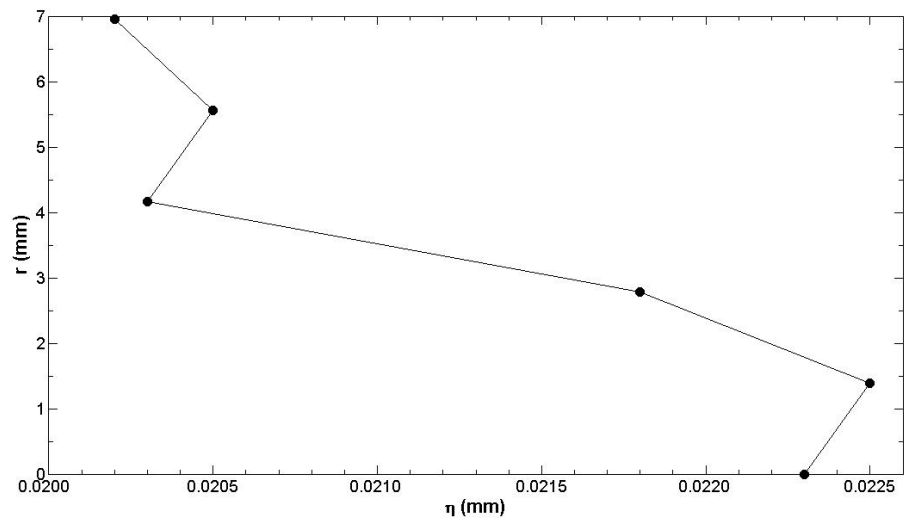


Figure 5.5.2.15: Kolmogorov length scale at $N_{Re}=16733$ from equation (3.1.7)

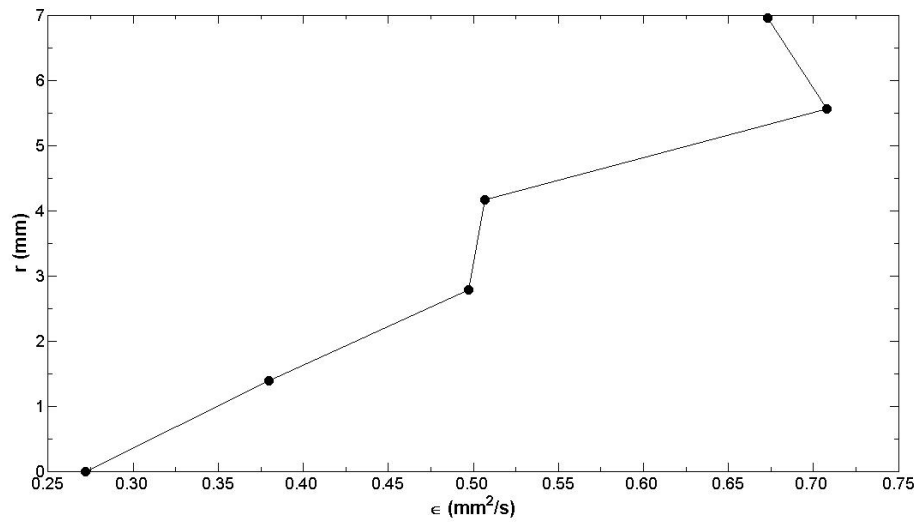


Figure 5.5.2.16: Eddy diffusion coefficient at $N_{Re}=16733$ from equation (3.1.5.8)

CHAPTER 6

OBTAINING GENERALIZED MAXWELL MODEL PARAMETERS FOR A LINEAR VISCOELASTIC FLUID BY UDV: A THEORETICAL APPROACH

In this part of the study viscoelastic behavior of a non-Newtonian fluid is investigated by UDV. A mathematical relation between rheological properties and UDV parameters is established. The fluid is assumed to be obeying a linear viscoelastic model which is an accurate approximation in the case of small strain in the fluid. In order to probe viscoelastic behavior of a fluid, flow should be time dependent, e.g. oscillating. This can be achieved by means of an oscillating piston assembly in a pipe (Figure 6.1).

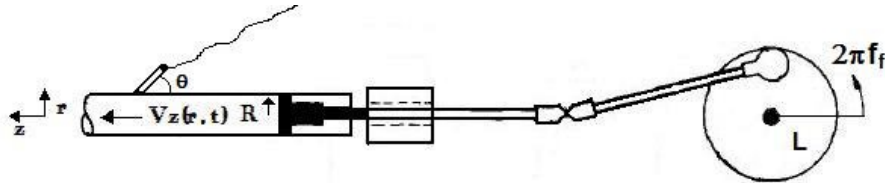


Figure 6.1: Oscillating piston system to drive an oscillating pipe flow. Angular velocity of disk ($2\pi f_f$) determines the frequency whereas radius of disk (L) determines the amplitude of flow oscillations.

Then oscillating pressure gradient in complex notation is,

$$-\frac{dP}{dz} = \text{Re}\{P^0 e^{j2\pi f_f t}\} \quad (6.1)$$

where f_f is flow oscillation frequency (Hz) and P^0 can be complex for a phase shift because oscillation can start from any phase point. $|P^0|$ must be taken as very small for the sake of linear viscoelasticity. We can postulate,

$$V_z(r, t) = \text{Re}\{V_z^o(r)e^{j2\pi f_r t}\}, V_r = 0, V_\theta = 0 \quad (6.2)$$

$$\tau_{rz}(r, t) = \text{Re}\{\tau_{rz}^o(r)e^{j2\pi f_r t}\} \quad (6.3)$$

where V_z^o and τ_{rz}^o are complex for a viscoelastic fluid since both velocity and shear stress are out of phase with pressure.

Next governing differential equations for a flowing fluid are considered. Here flow is assumed to be incompressible and uni-directional. End effects are neglected.

Equation of Continuity:

$$\underbrace{\frac{\partial \rho}{\partial t}}_0 + \frac{\partial(\rho V_z)}{\partial z} = 0 \Rightarrow \rho \frac{\partial V_z}{\partial z} = 0 \Rightarrow V_z \neq f(z) \quad (6.4)$$

(incompressible)

z-Component of Equation of Motion:

$$\rho \left(\frac{\partial V_z}{\partial t} + V_z \underbrace{\frac{\partial V_z}{\partial z}}_0 \right) = -\frac{\partial P}{\partial z} - \frac{1}{r} \frac{\partial}{\partial r} (r \cdot \tau_{rz}) + \rho \cdot \underbrace{\frac{g_z}{0}}_{\text{(gravity)}} \quad (6.5)$$

(from continuity)

Constitutive Equation:

$$\tau_{rz}(r, t) = - \int_{-\infty}^t G(t-t') \underbrace{\frac{\partial V_z(r, t')}{\partial r}}_{\dot{\gamma}_{rz}(r, t')} dt' \quad (6.6)$$

If we substitute equations (6.1), (6.2) and (6.3) into (6.5) and (6.6),

$$\begin{aligned} \rho \text{Re}\{V_z^o(r)j2\pi f_r e^{j2\pi f_r t}\} &= \text{Re}\{P^o e^{j2\pi f_r t}\} - \frac{1}{r} \frac{\partial}{\partial r} (r \cdot \text{Re}\{\tau_{rz}^o(r)e^{j2\pi f_r t}\}) \\ \text{Re}\{\rho V_z^o(r)j2\pi f_r e^{j2\pi f_r t}\} &= \text{Re}\{P^o e^{j2\pi f_r t}\} - \frac{1}{r} \frac{d}{dr} (r \cdot \tau_{rz}^o(r)) \\ \rho j2\pi f_r V_z^o(r) &= P^o - \frac{1}{r} \frac{d}{dr} (r \cdot \tau_{rz}^o(r)) \end{aligned} \quad (6.7)$$

and

$$\begin{aligned}
\operatorname{Re}\{\tau_{rz}^{\circ}(r) e^{j2\pi f_f t}\} &= -\int_{-\infty}^t G(t-t') \frac{\partial \operatorname{Re}\{V_z^{\circ}(r) e^{j2\pi f_f t'}\}}{\partial t'} dt' = \\
\operatorname{Re}\left\{-\frac{dV_z^{\circ}(r)}{dr} \int_0^{\infty} G(s) e^{-j2\pi f_f s} e^{j2\pi f_f t} ds\right\} \\
\tau_{rz}^{\circ}(r) &= -\frac{dV_z^{\circ}(r)}{dr} \underbrace{\int_0^{\infty} G(s) e^{-j2\pi f_f s} ds}_{\eta^*}
\end{aligned} \tag{6.8}$$

$G(s)$ is relaxation modulus and η^* is complex viscosity. If we combine (6.7) and (6.8),

$$\eta^* \frac{1}{r} \frac{d}{dr} \left(r \frac{dV_z^{\circ}(r)}{dr} \right) - \rho j 2\pi f_f V_z^{\circ}(r) = -P^{\circ} \tag{6.9}$$

This is a Bessel differential equation. Using the boundary conditions,

$$\begin{aligned}
\text{B.C.s } r=R, V_z^{\circ} &= 0 \\
r=0, V_z^{\circ} &\text{ is finite.}
\end{aligned}$$

solution gives,

$$V_z^{\circ}(r) = \frac{P^{\circ}}{j2\pi f_f \rho} \left(1 - \frac{J_0\left(\sqrt{-\frac{j2\pi f_f \rho}{\eta^*}} r\right)}{J_0\left(\sqrt{-\frac{j2\pi f_f \rho}{\eta^*}} R\right)} \right) \tag{6.10}$$

At the center of pipe ($r=0$),

$$\begin{aligned}
V_z^{\circ}(r=0) &= \frac{P^{\circ}}{j2\pi f_f \rho} \left(1 - \frac{1}{J_0\left(\sqrt{-\frac{j2\pi f_f \rho}{\eta^*}} R\right)} \right) \\
\Rightarrow V_z(r=0, t) &= \operatorname{Re}\left\{ \frac{P^{\circ}}{j2\pi f_f \rho} \left(1 - \frac{1}{J_0\left(\sqrt{-\frac{j2\pi f_f \rho}{\eta^*}} R\right)} \right) e^{j2\pi f_f t} \right\}
\end{aligned} \tag{6.11}$$

If infinite series representations of Bessel functions [60, pp.360] is employed up to the second term,

$$J_n(x) = x^n \sum_{m=0}^{\infty} \frac{(-1)^m x^{2m}}{2^{2m+n} m! \Gamma(m+n+1)}, \text{ where } \Gamma \text{ is gamma function}$$

$$\Rightarrow J_0\left(\sqrt{-\frac{j2\pi f_f \rho}{\eta^*}} R\right) \approx 1 - \frac{-\frac{j2\pi f_f \rho}{\eta^*} R^2}{4} = \frac{4\eta^* + j2\pi f_f \rho R^2}{4\eta^*} \quad (6.12)$$

The truncated series solution of the Bessel expression is an accurate approximation for small oscillation frequencies. For example for low density poly ethylene (LDPE) melt (complex viscosity from [56, pp.274], ρ at 150 °C is 780Kg/m³ [66, pp.94]) and for R=2.5cm, real part of error for this approximation is very close to zero while it is less than 0.2% for imaginary part of error up to oscillation frequency of $f_f=50$ Hz. This means the results of experiments even until 50 Hz are very useful without any significant error because of this series approximation.

With the approximated form of the Bessel function, the velocity at pipe center becomes,

$$\begin{aligned} \Rightarrow V_z(r=0, t) &= \text{Re}\left\{\frac{P^0}{j2\pi f_f \rho} \left(1 - \frac{4\eta^*}{4\eta^* + j2\pi f_f \rho R^2}\right) e^{j2\pi f_f t}\right\} \\ V_z(r=0, t) &= \text{Re}\left\{\frac{P^0 R^2}{4\eta^* + j2\pi f_f \rho R^2} e^{j2\pi f_f t}\right\} \end{aligned} \quad (6.13)$$

Using $\eta^* = \eta' - j\eta''$

$$V_z(r=0, t) = \text{Re}\left\{\frac{P^0 R^2 (4\eta' - j(2\pi f_f \rho R^2 - 4\eta''))}{16\eta'^2 + (2\pi f_f \rho R^2 - 4\eta'')^2} (\cos 2\pi f_f t + j \sin 2\pi f_f t)\right\} \quad (6.14)$$

If P^0 is real,

$$\begin{aligned} V_z(r=0, t) &= \frac{\overbrace{4P^0 R^2 \eta'}^{\eta_1} \cos(2\pi f_f t) + \overbrace{P^0 R^2 (2\pi f_f \rho R^2 - 4\eta'')}^{\eta_2} \sin(2\pi f_f t)}{\underbrace{16\eta'^2 + (2\pi f_f \rho R^2 - 4\eta'')^2}_{\eta_3}} \\ V_z(r=0, t) &= \frac{\eta_1 \cos(2\pi f_f t) + \eta_2 \sin(2\pi f_f t)}{\eta_3} \end{aligned} \quad (6.15)$$

where η_1 , η_2 and η_3 depend on material properties and f_f .

Next step is to use this velocity expression in the equation of sampled UDV signals from center of pipe (Eq. (4.2.1)). This equation was derived for one particle traveling in the measurement volume. This is a good approach if measurement volume is small enough and velocities of all particles within the volume are well correlated.

The reference time for this motion is starting time of measurement and if there is only axial velocity $V_z(t)$ at the measurement point,

$$d' = \int_0^t V_z(t) \cos \theta dt$$

where t in discrete form is,

$$t = \frac{d_o}{c} + (n-1)T_{\text{prf}} \Rightarrow d' = \int_0^{\frac{d_o}{c} + (n-1)T_{\text{prf}}} \frac{\eta_1 \cos(2\pi f_f t) + \eta_2 \sin(2\pi f_f t)}{\eta_3} \cos \theta dt$$

Then phase of the signal will be,

$$\text{Arg}\{s[n]\} = a_6 - a_2 \sin(a_4 + a_5(n-1)) + a_3 \cos(a_4 + a_5(n-1)) \quad (6.16)$$

$$\begin{aligned} \Rightarrow s[n] &= A_o e^{j(a_6 - a_2 \sin(a_4 + a_5(n-1)) + a_3 \cos(a_4 + a_5(n-1)))} = \\ &\underbrace{A_o \cos(a_6 - a_2 \sin(a_4 + a_5(n-1)) + a_3 \cos(a_4 + a_5(n-1)))}_{s_c[n]} + \\ &\underbrace{j A_o \sin(a_6 - a_2 \sin(a_4 + a_5(n-1)) + a_3 \cos(a_4 + a_5(n-1)))}_{s_i[n]} \end{aligned} \quad (6.17)$$

where $a_1 = \pi N_c$, $a_2 = \frac{4\pi f_o}{c} \frac{\eta_1 \cos \theta}{2\pi f_f \cdot \eta_3}$, $a_3 = \frac{4\pi f_o}{c} \frac{\eta_2 \cos \theta}{2\pi f_f \cdot \eta_3}$, $a_4 = 2\pi f_f \frac{d_o}{c}$,

$$a_5 = 2\pi f_f T_{\text{prf}}, a_6 = a_1 - a_3$$

We expect the ultrasound spectrum to be centered around zero frequency for long enough measurements ($T_{\text{prf}} \cdot N_{\text{prf}} \geq 1/f_f$) since there isn't net motion. Therefore we can use the amplitude of spectrum at zero frequency to determine the viscoelastic properties of fluid.

After evaluating the DFT of sampled signals in equation (6.17) (see Appendix A.4 for details), amplitude of US spectrum at zero frequency ($k=0$) is,

$$|S[k = 0]| = A_o N \left| J_o(a_2) J_o(a_3) + 2 \sum_{l=1}^{\infty} (-1)^l J_{2l}(a_2) J_{2l}(a_3) \right| \delta[k] \quad (6.18)$$

The second term makes equation quite complicated to solve. Fortunately we can neglect this term compared to the first term for small a_2 and a_3 values which means for small ratio of oscillation amplitude (P^o) to frequency (f_r) depending on the properties of fluid and some UDV parameters (see Figure 6.4).

$$\Rightarrow |S[k = 0]| = A_o N |J_o(a_2)| |J_o(a_3)| \delta[k] \quad (6.19)$$

Below are some graphical comparisons of numerically and analytically obtained spectrums from pipe center for UDV measurement parameters of: $A_o=1$, $N_c=4$, $f_o=4$ MHz, $c=1500$ m/s, $\theta=70^o$, $f_{prf}=7246$ Hz, $N_{pm}=7246$. Pipe radius is assumed as $R=0.025$ m and amplitude of oscillation of pressure gradient as 50000 Pa/m. LDPE melt at 150 o C ($\rho=780$ Kg/m 3) is taken as the viscoelastic fluid and generalized Maxwell model is used to obtain η' and η'' .

$$\eta' = \sum_m \frac{\eta_m}{1 + (\lambda_m 2\pi f_r)^2} \quad \eta'' = \sum_m \frac{\eta_m \lambda_m 2\pi f_r}{1 + (\lambda_m 2\pi f_r)^2} \quad (6.20)$$

Relaxation time (λ_m) and corresponding viscosity (η_m) data of LDPE for generalized Maxwell model is taken from literature [56, pp.274] (Table 6.1).

Table 6.1: Linear viscoelastic parameters in Generalized Maxwell Model for LDPE

m	λ_m (s)	η_m (Pa.s)
1	10^3	1.00×10^3
2	10^2	1.80×10^4
3	10^1	1.89×10^4
4	10^0	9.80×10^3
5	10^{-1}	2.67×10^3
6	10^{-2}	5.86×10^2
7	10^{-3}	9.48×10^1
8	10^{-4}	1.29×10^1

The analyzed velocity of LDPE with velocity change of a fictitious fluid and a Newtonian fluid are seen in Figure 6.2. Velocities are obtained from equation (6.15) and they are phase shifted for LDPE and fictitious viscoelastic fluid compared to the negative pressure gradient. It should be noted that phase of pressure oscillation is same with phase of negative pressure gradient. Phase shift of LDPE is more than that of fictitious viscoelastic fluid while there is not any phase shift for Newtonian fluid. This is because of faster relaxation spectrum of fictitious fluid (Figure 6.2.2) which gives more viscous but less elastic behavior to the fluid. Viscosity of Newtonian fluid was obtained from the limit value of real part (dynamic viscosity) of the complex viscosity while oscillation frequency goes to zero.

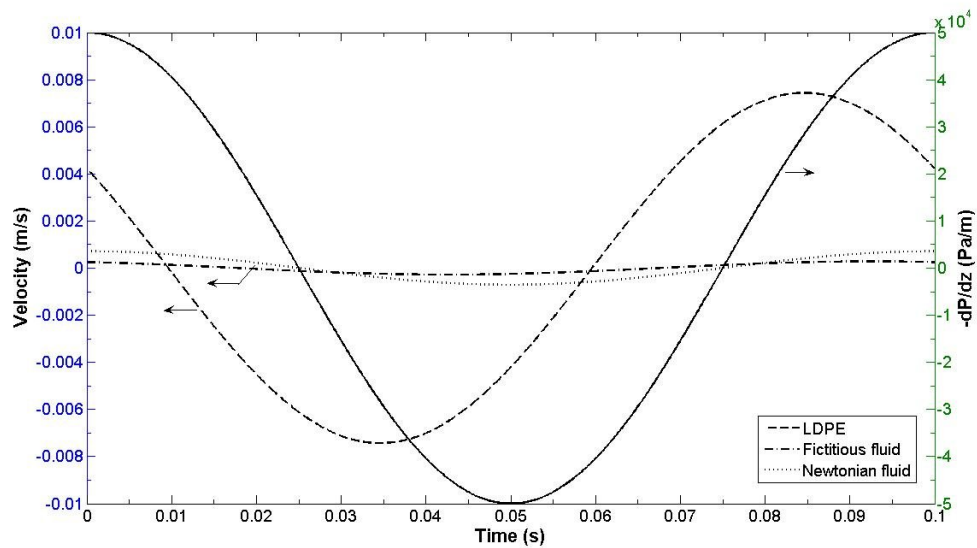


Figure 6.2: Phase shift of oscillating velocities with frequency of 10 Hz at the center of pipe compared to the negative pressure gradient (from Eq. (6.15)).

Both analytically (from Eq. (A.4.1)) and numerically obtained ultrasound spectrums are almost identical (Figure 6.3). Doppler frequency axis was converted to velocity through Doppler equation (Eq. (2.1.3)).

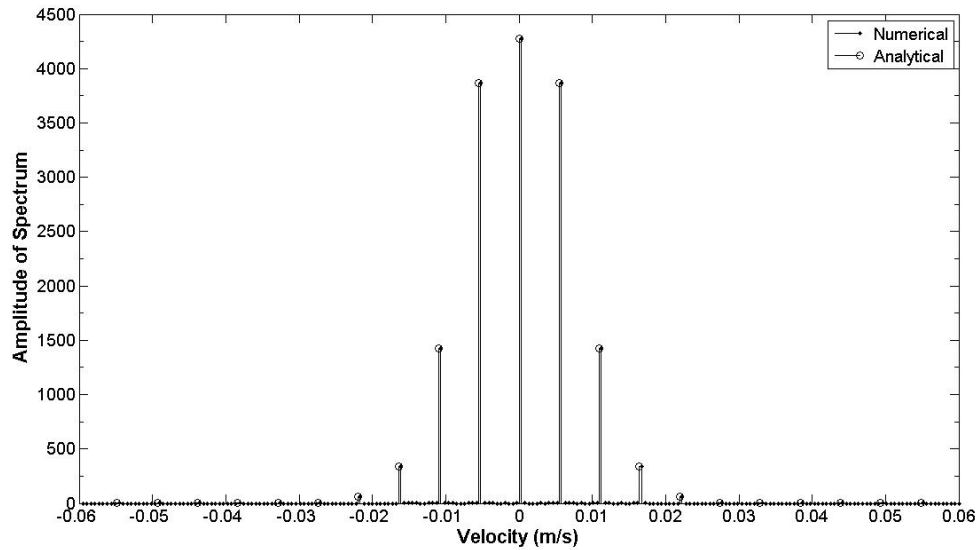


Figure 6.3: Numerically and analytically obtained amplitude of spectrum of ultrasonic signals taken from center of pipe for $f_f=10$ Hz oscillating flow ($P^o / f_f = 5000$).

The simplification on equation (6.18) by neglecting second term introduces considerable difference compared to numerical and whole analytical solutions especially at small flow oscillation frequencies under 5 Hz. This also depends on UDV measurement parameters, flow oscillation amplitude, pipe radius and fluid type through parameters a_2 and a_3 . Analytically and numerically obtained spectral amplitudes at zero frequency of the UDV spectrum seem compatible (Figure 6.4).

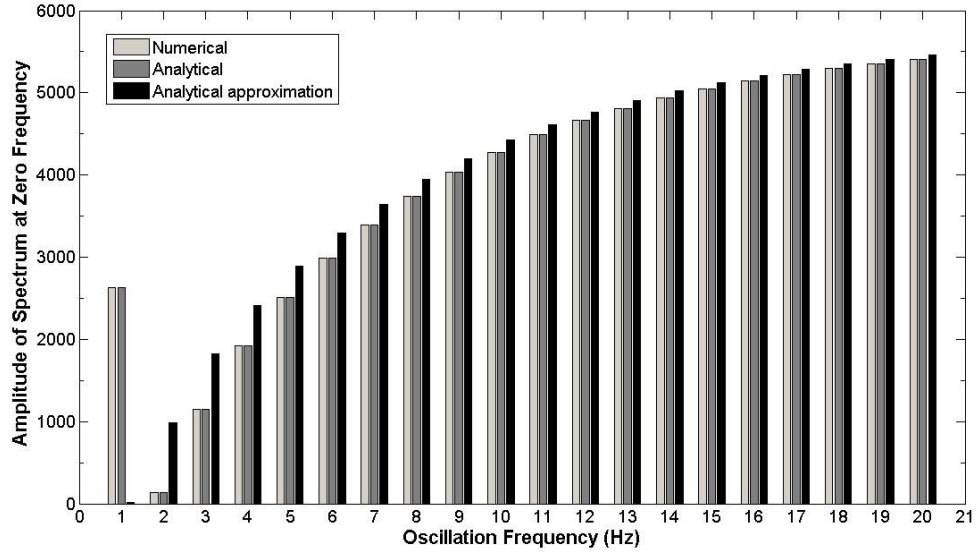


Figure 6.4: Numerically and analytically obtained amplitudes at center of UDV spectrum (zero frequency) corresponding to different flow oscillation frequencies.

6.1 Obtaining Generalized Maxwell Model Viscosities Using UDV Spectrum

Equation (6.19) can be used to get many viscosities corresponding to fluid relaxation times in Generalized Maxwell Model. This requires measurements at different flow oscillation frequencies and employing equation (6.19) for each frequency. But obtained set of equations is highly non-linear and requires some numerical solutions like non-linear least square minimization. If Generalized Maxwell Model is used to express η' and η'' , then a_2 and a_3 in equation (6.19) becomes,

$$a_2 = \frac{2f_0 \cos \theta \eta_1}{c.f_f \eta_3} = \frac{8f_0 \cos \theta . P^o R^2 \eta'}{16c.f_f \eta'^2 + c.f_f (\rho 2\pi f_f R^2 - 4\eta'')^2} = \frac{8f_0 \cos \theta . P^o R^2 \sum_{m=1}^M \frac{\eta_m}{1 + (\lambda_m 2\pi f_f)^2}}{16c.f_f \left(\sum_{m=1}^M \frac{\eta_m}{1 + (\lambda_m 2\pi f_f)^2} \right)^2 + c.f_f (\rho 2\pi f_f R^2 - 4 \left(\sum_{m=1}^M \frac{\eta_m \lambda_m 2\pi f_f}{1 + (\lambda_m 2\pi f_f)^2} \right))^2} \quad (6.1.1)$$

$$a_3 = \frac{2f_o \cos \theta \eta_2}{c.f_f \eta_3} = \frac{2f_o \cos \theta.P^o R^2 (\rho 2\pi f_f R^2 - 4\eta'')}{16c.f_f \eta'^2 + c.f_f (\rho 2\pi f_f R^2 - 4\eta'')^2} =$$

$$\frac{2f_o \cos \theta.P^o R^2 (\rho 2\pi f_f R^2 - 4(\sum_{m=1}^M \frac{\eta_m \lambda_m 2\pi f_f}{1 + (\lambda_m 2\pi f_f)^2}))}{16c.f_f (\sum_{m=1}^M \frac{\eta_m}{1 + (\lambda_m 2\pi f_f)^2})^2 + c.f_f (\rho 2\pi f_f R^2 - 4(\sum_{m=1}^M \frac{\eta_m \lambda_m 2\pi f_f}{1 + (\lambda_m 2\pi f_f)^2}))^2} \quad (6.1.2)$$

Here M is number of parameters in Generalized Maxwell Model. Therefore number of experimental measurements (i.e. equations) must be equal or greater than M. Equation (6.19) was tried to be solved in MATHEMATICA for model of 8 Maxwell elements. First $|S[k=0]|$ values for different oscillation frequencies were obtained by using 8 Generalized Maxwell Model parameters taken from literature (Table 6.1). ‘Nminimize’ command for non-linear least-square minimization was used. It was used to minimize following objective function (sum of squares),

$$\sum_{q=1}^{N_e} (|S_q| - A_o N |J_o(a_{2,q})| |J_o(a_{3,q})|)^2 \quad (6.1.3)$$

where N_e is number of oscillation frequencies that measurements have been done. Firstly 8 viscosity values (η_m $m=1,2,\dots,8$) were obtained by minimizing 8 equations for 8 different oscillation frequencies ($f_f=5,6,\dots,12$ Hz). Secondly 20 equations (for $f_f=5,6,\dots,24$ Hz) were used to obtain these 8 viscosity values corresponding to 8 different relaxation times. Both minimizations gave quite close results to real viscosity values and objective functions were obtained very close to zero.

For 8 equations:

$$|S_q| = \{2889.768, 3295.413, 3645.061, 3945.655, 4202.894, 4422.329, 4609.306, 4768.746\}$$

Objective function is 8.47546×10^{-18}

Viscosities as Pa.s are $\eta_1=106.473$, $\eta_2=19.194.9$, $\eta_3=17.586.7$, $\eta_4=9.814.04$, $\eta_5=2.669.99$, $\eta_6=586$, $\eta_7=94.7997$, $\eta_8=12.9005$

For 20 equations:

$|S_q| = \{2889.768, 3295.413, 3645.061, 3945.655, 4202.894, 4422.329, 4609.306, 4768.746, 4905.003, 5021.822, 5122.368, 5209.280, 5284.748, 5350.583, 5408.279, 5459.071, 5503.984, 5543.867, 5579.429, 5611.261\}$

Objective function is 2.14935×10^{-14}

Viscosities as Pa.s are $\eta_1 = 375\ 619$, $\eta_2 = 54\ 186.9$, $\eta_3 = 10\ 694.1$, $\eta_4 = 9\ 884.84$, $\eta_5 = 2\ 669.93$, $\eta_6 = 586$, $\eta_7 = 94.7998$, $\eta_8 = 12.9003$

This implies that the non-linear equation (6.19) can be solved numerically after getting enough number of UDV measurements to obtain viscosities of Generalized Maxwell Model. After getting parameters of Maxwell elements one can easily obtain relaxation spectrum for viscoelastic fluid of interest. As it is seen viscosity values corresponding to longer relaxation times ($\lambda_m \gg 1s$) are not close to the real values. This may be related with measurement period of UDV which is 1s in our analysis.

6.2 Effects of Material Type and Oscillation Frequency on Spectrum

5300 is critical value for P° / f_r for defined measurement and material parameters of LDPE. When it gets bigger than this value, side bands around zero frequency become stronger than zero frequency amplitude (Figure 6.2.1).

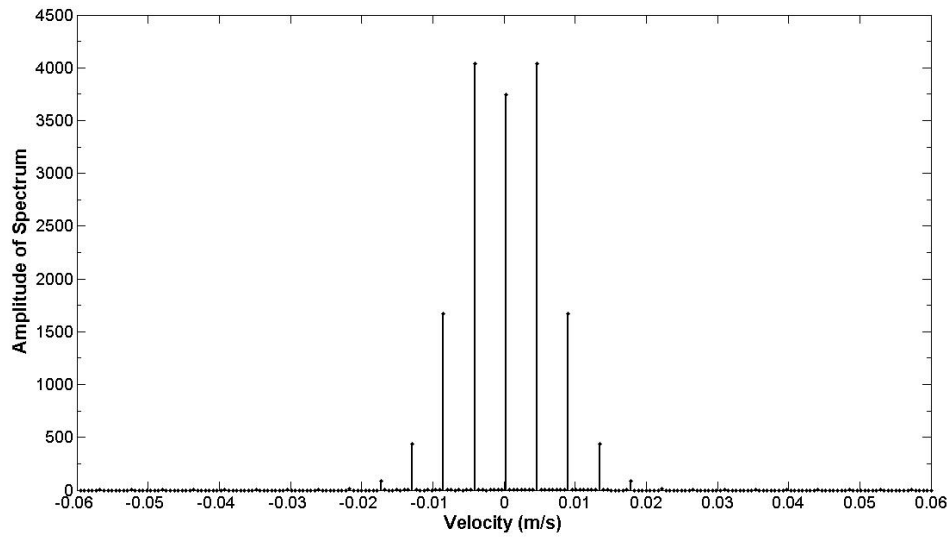


Figure 6.2.1: Numerically obtained amplitude of spectrum of ultrasonic signals taken from center of pipe for flow oscillating at 8 Hz ($P^o / f_f = 6250$).

Relaxation spectrums of LDPE and a fictitious viscoelastic fluid are seen at Figure 6.2.2. Spectrum of fictitious fluid is dominant at small relaxation times compared to the spectrum of LDPE which means relaxation dynamics of fictitious fluid is faster than LDPE. Therefore fictitious fluid has a more viscous but less elastic structure compared to the LDPE.

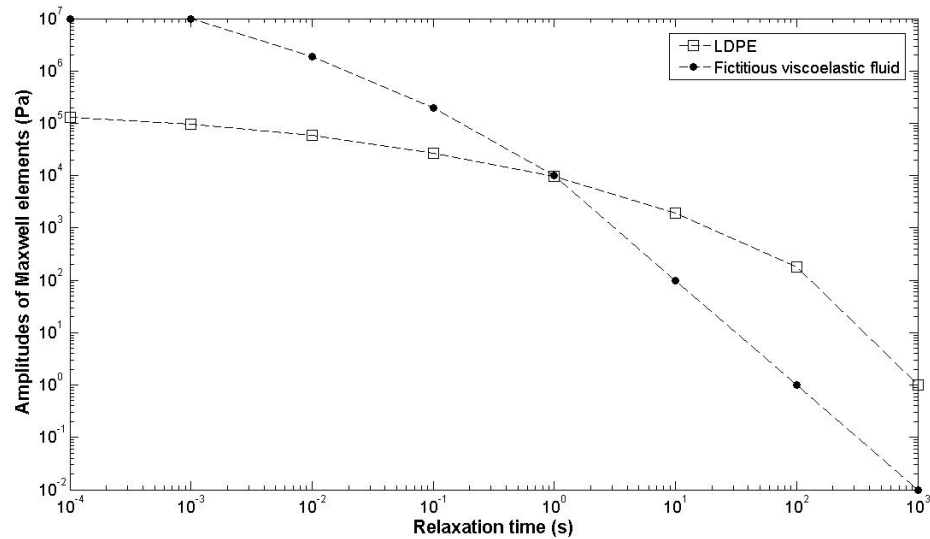


Figure 6.2.2: Analyzed two different discrete relaxation spectrums of Generalized Maxwell Model for two different fluids.

As it is seen from velocity changes in Figure 6.2.3, for the same oscillation frequency, amplitude of velocity oscillations for fictitious viscoelastic fluid is less than that of LDPE because of much faster stress relaxation. Oscillation amplitude for Newtonian fluid is close to the fast relaxing fictitious fluid since it has an immediate relaxation mechanism which decreases stress and hence acceleration of fluid. For LDPE increasing of oscillation frequency from 10 Hz to 20 Hz is increasing the oscillation amplitude. But there is not a significant change for fictitious viscoelastic fluid in the case of this frequency change. This may be because of these oscillation frequency or time scales are very fast for LDPE which doesn't have a complete relaxation time for such fast changing loadings. For faster oscillations (20 Hz) material has less time to be relaxed which causes increase on oscillation amplitude. On the contrary for fictitious viscoelastic fluid these oscillations (time scales of 0.1 sec. and 0.05 sec.) are not faster than relaxation speed of material. Therefore this frequency change of oscillation doesn't create an important amplitude change on velocity oscillations. We can say that material's relaxation dynamics is fast enough so that it can't be altered by such a change on flow dynamics.

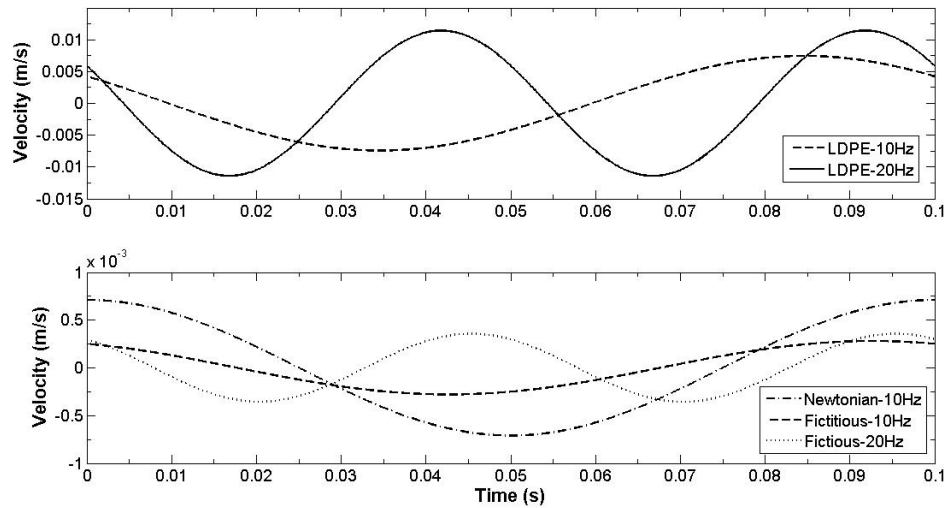


Figure 6.2.3: Oscillating velocities at pipe center for three different fluids and two different oscillation frequencies (from Eq. (6.15)).

Numerically obtained US spectrum amplitudes from center of pipe for flow of three different fluids and two oscillation frequencies are seen in Figure 6.2.4. Zero frequency component of US spectrum is highest and it stands for average velocity which is obviously zero in our oscillating flow case. Side components appear at the positive and negative multiples of flow oscillation frequency. It is easy to see that increasing amplitude of flow oscillation (for LDPE) decreases the frequency component of UDV at center of spectrum and spreads the energy around center which is caused from increasing variance of velocity at measurement point. It can be said that variance of US spectrum for viscoelastic fluid with longer relaxation times (more elastic LDPE) is higher than variance of US spectrum for viscoelastic fluid with shorter relaxation times (more viscous fictitious fluid). US spectrum of a viscoelastic fluid goes to the spectrum of a Newtonian fluid when elastic properties of fluid disappear.

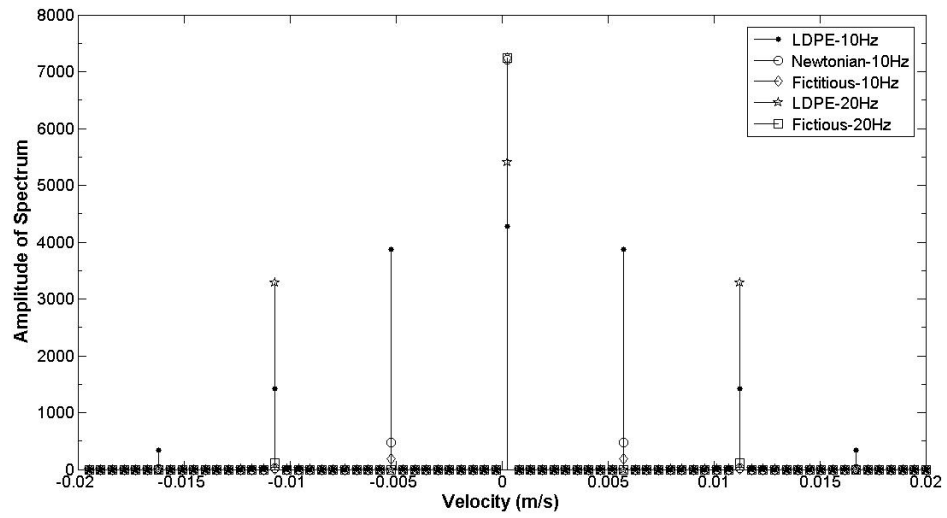


Figure 6.2.4: Numerically obtained Ultrasound Doppler spectrums from center of pipe for three different fluids and two different oscillation frequencies

CHAPTER 7

CONCLUSIONS

Mathematical relations which show effect of some complex flows on UDV signals were obtained in this study. Analysis was started from single frequency oscillating flows. Analytical results revealed that ratio of oscillation amplitude to frequency is a critical parameter which has a critical value according to frequency and speed of sound. Critical value for dimensionless a_4 parameter is determined as nearly 1.45. Average velocity profiles determined by UDV technique don't seem reliable if this critical value is exceeded. Beyond this limit ghost profiles appear around mean velocity profile which eventually gets stronger than mean velocity values. Speed of sound c comes across as a limiting factor of time resolution. Numerical results also confirmed analytical results in this part of the study.

In the second part statistical properties of a random velocity were related to the properties of back sampled US signals. This kind of analysis is particularly useful to investigate turbulent flows and to obtain turbulent parameters with a few seconds measurement. Probability density function (PDF) of velocity is one important statistical property which was related to spectrum of US signals. Both PDF values obtained from velocity measurements and US spectrum compared well with each other. Results have indicated that PDF of random velocity creates the distribution pattern of US spectrum. Velocity auto-correlation function (ACF) which is another statistically important parameter was obtained from both measured velocity values and raw in-phase and quadrature (I-Q) parts of signals by using derived analytical relation. Time and spatial resolution of UDV measurements were limiting factors for rapidly changing flows. Time resolution (0.138 ms) of ACF obtained from I-Q signals was several times higher compared to the one (21.3 ms) obtained from velocity measurements. This improved velocity ACF was used to calculate some

turbulent parameters for different Reynolds Numbers and radial positions in a pipe. Local average velocity based intensity of pipe turbulence was obtained as decreasing at pipe center with increasing N_{Re} , while it was increasing towards pipe wall at a fixed N_{Re} . Eddy diffusion coefficient was increasing both with increasing N_{Re} and increasing radial position within the pipe. Measured turbulence intensities along radial direction have given a good compatibility with literature values. Results indicated UDV as a valuable technique to measure turbulent parameters in very short times. Size of probe compared to the size of flow geometry is very important to catch spatial changes correctly.

In the last part of study linear viscoelastic material properties were related to US spectrum theoretically. This study just stayed in theoretical bases because of experimental difficulties of maintaining flow of a polymeric viscoelastic material. Dynamic oscillation experiment of a viscoelastic fluid was analyzed. US spectrum obtained from oscillating flow of such a fluid was derived in terms of complex material functions. Complex material functions were expressed by Generalized Maxwell Model and zero frequency components in spectrum were used to get viscosities corresponding to relaxation times. Although obtained relation between Generalized Maxwell Model viscosities and UDV spectrum is highly non-linear and complicated, it has been showed that such non-linear least square problems can be solved by means of modern computer programs like Mathematica. UDV technique was proposed as a useful tool to get relaxation spectrum of a viscoelastic material after conducting some experimental measurements.

As a result UDV is a promising technique for process monitoring in a quick and non-invasive way. Technique has lived many improvements especially for the last two decades but still has some limitations to be solved. Time and spatial resolutions are two of them. Using a complementary measurement technique (LDV, PTV) might be necessary as some authors suggest. More detailed theoretical analysis is required to understand US signals after interacting with complex flow media. In spite of many simplifications that were made in our analysis, results are encouraging and useful for future detailed analysis.

REFERENCES

1. J. Peter Clark, 'Everything flows', Food Technology, Vol.60, No.11, pp.68-71, Nov. 2006
2. J. Wiklund, M. Johansson, J. Shaik, P. Fischer, E. Windhab, M. Stading, A.M. Hermansson, 'In-line ultrasound based rheometry of industrial and model suspensions flowing through pipes', 3rd International Symposium on Ultrasonic Doppler Methods for Fluid Mechanics and Fluid Engineering (ISUD), EPFL, Lausanne, Switzerland, September 9-11, 2002
3. K.H.Henneke, A.Melling, Z.Wang, F.Durst, B.Kunkel, K.Bachmann, 'Assesment of spatial and temporal velocity profiles distal of normally functioning Björk-Shiley prosthesis by the Doppler method', International J. of Cardiology, Vol.37, pp.381-387, 1992
4. J.A.Jensen, 'Algorithms for estimating blood velocities using ultrasound', Ultrasonics, Vol.38, pp.358-362, 2000
5. J. Udesen, M. B. Nielsen, K. R.Nielsen and J.A.Jensen, 'Blood vector velocity estimation using an autocorrelation approach: In vivo Investigation', IEEE Ultrasonics Symposium 2005, pp.162-165, 2005
6. Y.Takeda, 'Development of an ultrasound velocity profile monitor', Nuclear Engineering and Design, Vol.126, pp.277-284, 1991
7. L.C.Lynnworth, Y.Liu, 'Ultrasonic flowmeters:Half-century progress report, 1955-2005', Ultrasonics, Vol.44, pp.1371-1378, 2006
8. S.Eckert, G.Gerbeth, 'Velocity measurements in liquid sodium by means of Ultrasound Doppler Velocimetry', Experiments in Fluids, Vol.32, pp.542-546, 2002
9. Daniel Brito, Henri Claude Nataf, Philippe Cardin, Julien Aubert, Jean Paul Masson, 'Ultrasonic Doppler velocimetry in liquid gallium', Experiments in Fluids, Vol.31, pp.653-663, 2001

10. Hiroshige Kikura, Masanori Aritomi, Yasushi Takeda, 'Velocity measurement on Taylor-Couette flow of a magnetic fluid with small aspect ratio', *Journal of Magnetism and Magnetic Materials*, Vol. 289, pp.342-345, 2005
11. N.Doğan, M.J.McCarthy, R.L.Powell, 'Measurement of polymer melt rheology using ultrasonics-based in-line rheometry', *Measurement Science and Technology*, Vol.16, pp.1684-1690, 2005
12. Boris Ouriev, Erich Windhab, 'Novel ultrasound based time averaged flow mapping method for die entry visualization in flow of highly concentrated shear thinning and shear thickening suspensions', *Measurement Science and Technology*, Vol.14, pp.140-147, 2003
13. Tiefeng Wang, Jinfu Wang, Fei Ren, Yong Jin, 'Application of Doppler ultrasound velocimetry in multiphase flow', *Chemical Engineering Journal*, Vol.92, pp.111-122, 2003
14. Hideo Nakamura, Masaya Kondo, Yutaka Kukita, 'Simultaneous measurement of liquid velocity and interface profiles of horizontal duct wavy flow by ultrasonic velocity profile meter', *Nuclear Engineering and Design*, Vol.184, pp.339-348, 1998
15. C.Manes, D.Pokrajac, I.McEwan, V.Nikora, L.Campbell, 'Application of UVP within porous beds', *J. Of Hydraulic Engineering*, Vol.132, No.9, pp.983-986, 2006
16. U.Lemmin, T.Rolland, 'Acoustic velocity profiler for laboratory and field studies', *Journal of Hydraulic Engineering*, Vol.123, No.12, pp.1089-1098, 1997
17. M.Teufel, D.Trimis, A.Lohmuller, Y.Takeda, F.Durst, 'Determination of velocity profiles in oscillating pipe flows by using laser Doppler velocimetry and ultrasonic measuring devices', *Flow Meas.Instrum.*, Vol.3, No.2, pp.95-101,1992
18. Perviz Sayan, Joachim Ulrich, 'The effect of particle size and suspension density on the measurement of ultrasonic velocity in aqueous solutions', *Chemical Engineering and Processing*, Vol.41, pp.281-287, 2002
19. S.Franchini, A.Sanz-Andres, A.Cuerva, 'Measurement of velocity in rotational flows using ultrasonic anemometry: the flowmeter', *Exp. Fluids*, Vol.42, pp.903-911, 2007
20. Christos P. Markou, David N. Ku, 'Accuracy of velocity and shear rate measurements using pulsed Doppler ultrasound: A comparison of signal analysis techniques', *Ultrasound in Med. & Biol.*, Vol.17, No.8, pp.803-814, 1991

21. Patricia Ern, Jose Eduardo Wesfreid, 'Flow between time periodically co-rotating cylinders' *J. Fluid Mech.*, Vol.397, pp.73-98, 1999
22. G. Cloutier, D. Chen, L.G. Durand, 'Performance of time-frequency representation techniques to measure blood flow turbulence with pulsed-wave Doppler ultrasound', *Ultrasound in Med. & Biol.*, Vol.27, No.4, pp. 535–550, 2001
23. Yasuhiro Ozaki, Tatsuya Kawaguchi, Yasushi Takeda, Koichi Hishida, Masanobu Maeda, 'High time resolution ultrasonic velocity profiler', *Experimental Thermal and Fluid Science*, Vol.26, pp.253-258, 2002
24. G.K.Aldis, R.S.Thompson, 'Calculation of Doppler spectral power density functions', *IEEE Transactions on Biomedical Engineering*, Vol.39, No 10, pp.1022-1031, 1992
25. S. He and J. D. Jackson, 'A study of turbulence under conditions of transient flow in a pipe', *J. Fluid Mech.*, Vol.408, pp.1-38, 2000
26. Lu Wang, Kathryn L. McCarthy, Michael J. McCarthy, 'Effect of temperature gradient on ultrasonic Doppler velocimetry measurement during pipe flow', *Food Research International*, Vol.37, pp.633-642, 2004
27. Johan Wiklund, Imam Shahram, Mats Stading, 'Methodology for in-line rheology by ultrasound Doppler velocity profiling and pressure difference techniques', *Chemical Engineering Science*, Vol.62, pp.4277-4293, 2007
28. Volkan Köseli, Şerife Zeybek, Yusuf Uludağ, 'Online Viscosity Measurement of Complex Solutions Using Ultrasound Doppler Velocimetry', *Turk J. Chem.*, Vol.30 , pp.297-305, 2006
29. K. W. Ferrara, B. G. Zagar, J. B. Sokil-Melgar, R. H. Silverman, I. M. Aslanidis, 'Estimation of Blood Velocity with High Frequency Ultrasound', *IEEE Transactions On Ultrasonics, Ferroelectrics, And Frequency Control*, Vol.43, No.1, pp.149-157, 1996
30. D.Censor, V.L.Newhouse, T.Vontz, H.V.Ortega, 'Theory of ultrasound Doppler spectra velocimetry for arbitrary beam and flow configurations', *IEEE Transactions on Biomedical Eng.* Vol.35 , No.9, pp.740-751,1988
31. G.Alfonsi, 'Analysis of streamwise velocity fluctuations in turbulent pipe flow with the use of an ultrasonic Doppler flowmeter', *Flow Turbulence and Combustion*, Vol.67, pp.137-142, 2001

32. P. Petitjeans, J.E.Wesfreid, J.C.Attiach, 'Vortex stretching in a laminar boundary layer flow', *Experiments in Fluids*, Vol.22, pp.351-353, 1997
33. B.Brunoe, B.W.Karney, M.Mecarelli, M.Ferrante, 'Velocity profiles and unsteady pipe friction in transient flow', *J. Of Water Resources Planning and Management*, Vol.126, No 4, pp.236-244, 2000
34. C.Shen, U.Lemmin, 'Intensity fluctuations of ultrasonic scattering in a highly turbulent flow', *Ultrasonics*, Vol.37, pp.603-613, 2000
35. T. Niederdrank, 'Correlations of back scattered ultrasound from scattering suspensions in turbulent flow', *Ultrasonics*, Vol.33, No.3, pp.239-242, 1995
36. U.Kidmose, L.Pedersen, M.Nielsen, 'Ultrasonics in evaluating rheological properties of dough from different wheat varieties and during ageing', *J. of Texture Studies*, Vol.32, pp.321-334, 2001
37. B.Ouriev, 'Investigation of the wall slip effect in highly concentrated disperse systems by means of non-invasive UVP-PD method in the pressure driven shear flow', *Colloid Journal*, Vol.64, No.6 pp.740-745, 2002
38. J.Stepisnik, P.T.Callaghan, 'Low-frequency velocity correlation spectrum of fluid in a porous media by modulated gradient spin echo', *Magnetic Resonance Imaging*, Vol.19, pp.469-472, 2001
39. P.T.Callaghan, J.Stepisnik, 'Frequency-domain analysis of spin motion using modulated-gradient NMR', *Journal of Magnetic Resonance Series A*, Vol.117, pp.118-122, 1995
40. K. K. Shung, Y. W. Yuan, D. Y. Fei, J.M. Tarbell, 'Effect of flow disturbance on ultrasonic backscatter from blood', *J. Acoustic Soc. Am.*, Vol.75(4), pp.1265-1272, 1984
41. V. Hans, G.Poppen, E. Von Lavante, S. Perpeet, 'Vortex shedding flow-meters and ultrasound detection: signal processing and influence of bluff body geometry', *Flow Measurement and Instrumentation*, Vol.9, pp.79-82, 1998
42. DOP 2000 Ultrasonic Doppler Velocimeter User Manual, Signal Processing-Switzerland, 2002
43. Yasushi Takeda, 'Velocity profile measurement by ultrasonic Doppler method', *Experimental Thermal and Fluid Science*, Vol.10, pp.444-453, 1995

44. Met-Flow SA, 'The Ultrasonic Velocity Profiler', <http://www.met-flow.com>, October 2008
45. Signal Processing SA, 'Ultrasonic Doppler Velocimeters', <http://www.signal-processing.com>, June 2009
46. Discrete time signal processing, 2nd Ed., Alan. V. Oppenheim, Ronald W. Schaffer, John R. Buck, Prentice Hall, 1999
47. Turbulence, 2nd Ed., J. O. Hinze, McGraw-Hill, 1975
48. A First Course in Turbulence, H.Tennekes, J.L. Lumley, MIT Press, 1972
49. Turbulence Modeling for CFD, David. C. Wilcox, DCW Industries Inc., 1993
50. Theory and Problems of Probability, Random Variables and Random Processes, Hwei Hsu, McGraw-Hill, 1997
51. Probability, Random Variables and Stochastic Processes, 3rd Ed., Athanasios Papoulis, McGraw-Hill, 1991
52. Environmental Fluid Mechanics, Hillel Rubin, Joseph F. Atkinson, Marcel Dekker Inc, 2001
53. Mohamed Gad-El Hak, J. B. Morton, Howard Kutchai, 'Turbulent flow of red cells in dilute suspensions, Effect on kinetics of O₂ uptake ', Biophysical Journal, Vol.18, pp.289-300, 1977
54. U. Lemmin, 'Dynamics of horizontal turbulent mixing in a near shore zone of Lake Geneva', Limnol. Oceanogr., Vol.34(2), pp.420-434, 1989
55. Environmental Fluid Mechanics: Theories and Applications, Philip Roberts, Donald Webster
56. Dynamics of Polymeric Liquids Volume 1: Fluid Mechanics, 2nd Ed., R. Byron Bird, Robert C. Armstrong, Ole Hassager, John Wiley & Sons, 1987
57. Polymer Engineering Science and Viscoelasticity: An introduction, Hal F. Brinson, L. Catherine Brinson, Springer, 2008
58. Introduction to Polymer Viscoelasticity, 3rd Ed., Montgomery T. Shaw, William J. MacKnight, John Wiley & Sons, 2005
59. Viscoelastic Properties of Polymers, 3rd Ed., John D. Ferry, John Wiley & Sons, 1980

60. Handbook of Mathematical Functions with Formulas, Graphs, and Mathematical Tables, Milton Abramowitz and Irene A. Stegun, Dover, 1964
61. Fundamentals of Fluid Mechanics, 5th Ed., B.R. Munson, D.F. Young and T.H. Okiishi, John Wiley, 2006
62. Introduction to Methods of Applied Mathematics or Advanced Mathematical Methods for Scientists and Engineers, Sean Mauch, Mauch Publishing Comp., 2003
63. C. M. Garcia, M. I. Cantero, Y. Nino, M. H. Garcia, 'Turbulence Measurements with Acoustic Doppler Velocimeters', Journal of Hydraulic Engineering, Vol.131(12), pp.1062-1073, 2005
64. J. Laufer, 'The Structure of Turbulence in Fully Developed Pipe Flow', National Advisory Committee for Aeronautics, Report 1174, 1953
65. Boundary Layer Theory, 7th Ed., H. Schlichting, McGraw-Hill, 1979
66. Physical Properties of Polymers Handbook, 2nd Ed., James E. Mark, Springer, 2007
67. Digital Signal Processing Handbook, Vijay K. Madisetti, Douglas B. Williams, CRC, 1999

APPENDIX A

MATHEMATICAL DERIVATIONS

A.1 DFT of Sampled US Signals for Measurement Volume of Oscillating Velocity Flow

If sampled signal is expressed in terms of cosine and sine components,

$$s[n] = s_c[n] + js_s[n] = A_o \cos(a_7 - a_3(n-1) + a_4 \cos(a_5 + a_6(n-1))) \\ + jA_o \sin(a_7 - a_3(n-1) + a_4 \cos(a_5 + a_6(n-1)))$$

$$\text{from } \cos(x + y) = \cos x \cdot \cos y - \sin x \cdot \sin y \text{ and} \\ \sin(x + y) = \sin x \cdot \cos y + \cos x \cdot \sin y$$

$$s_c[n] = A_o \cos(a_7 - a_3(n-1) + a_4 \cos(a_5 + a_6(n-1))) \\ = A_o \{ \cos(a_7 - a_3(n-1)) \cos(a_4 \cos(a_5 + a_6(n-1))) \\ - \sin(a_7 - a_3(n-1)) \sin(a_4 \cos(a_5 + a_6(n-1))) \} \\ s_s[n] = A_o \sin(a_7 - a_3(n-1) + a_4 \cos(a_5 + a_6(n-1))) \\ = A_o \{ \sin(a_7 - a_3(n-1)) \cos(a_4 \cos(a_5 + a_6(n-1))) \\ + \cos(a_7 - a_3(n-1)) \sin(a_4 \cos(a_5 + a_6(n-1))) \}$$

If n is replaced by m and then m-1 is substituted by n, cosine (real) and sine (imaginary) parts of the signal become,

$$s_c[n+1] = A_o \{ \cos(a_7 - a_3.n) \cos(a_4 \cos(a_5 + a_6.n)) \\ - \sin(a_7 - a_3.n) \sin(a_4 \cos(a_5 + a_6.n)) \} \\ s_s[n+1] = A_o \{ \sin(a_7 - a_3.n) \cos(a_4 \cos(a_5 + a_6.n)) \\ + \cos(a_7 - a_3.n) \sin(a_4 \cos(a_5 + a_6.n)) \}$$

It should be noted that m is changing between 1 and N_{prn} (total number of pulses) while n is between 0 and $N_{prn}-1$ (like a discrete time signal). Discrete Fourier transform (DFT) of the sampled periodic signal is:

$$\begin{aligned}
\text{D.F.T.}\{s[n+1]\} &= \text{D.F.T.}\{s_c[n+1]\} + j\text{D.F.T.}\{s_s[n+1]\} \\
s_c[n+1] &= A_o \underbrace{\{\cos(a_7 - a_3.n)\}}_{f_{1c}[n]} \underbrace{\cos(a_4 \cos(a_5 + a_6.n))}_{f_{2c}[n]} \\
&\quad - \underbrace{\sin(a_7 - a_3.n)}_{f_{3c}[n]} \underbrace{\sin(a_4 \cos(a_5 + a_6.n))}_{f_{4c}[n]} \\
\Rightarrow \text{D.F.T.}\{s_c[n+1]\} &= A_o \{\text{D.F.T.}\{f_{1c}[n].f_{2c}[n]\} - \text{D.F.T.}\{f_{3c}[n].f_{4c}[n]\}\} \\
&= A_o \left\{ \frac{1}{N_{\text{prn}}} \text{D.F.T.}\{f_{1c}[n]\} * \text{D.F.T.}\{f_{2c}[n]\} - \frac{1}{N_{\text{prn}}} \text{D.F.T.}\{f_{3c}[n]\} * \text{D.F.T.}\{f_{4c}[n]\} \right\}
\end{aligned}$$

where * is convolution sum. By using reference [60, pp.361]

$$A_c[k] = \text{D.F.T.}\{f_{1c}[n]\} = \frac{N_{\text{prn}}}{2} [e^{ja_7} \cdot \delta[k + \frac{N_{\text{prn}}a_3}{2\pi}] + e^{-ja_7} \cdot \delta[k - \frac{N_{\text{prn}}a_3}{2\pi}]]$$

$$B_c[k] = \text{D.F.T.}\{f_{2c}[n]\}$$

$$= N_{\text{prn}} \left\{ J_0(a_4) \cdot \delta[k] + \sum_{l=1}^{\infty} (-1)^l J_{2l}(a_4) (e^{j2la_5} \delta[k - \frac{2la_6 N_{\text{prn}}}{2\pi}] + e^{-j2la_5} \delta[k + \frac{2la_6 N_{\text{prn}}}{2\pi}]) \right\}$$

$$C_c[k] = \text{D.F.T.}\{f_{3c}[n]\} = \frac{N_{\text{prn}}}{2} [e^{j(a_7 + \frac{3\pi}{2})} \cdot \delta[k + \frac{N_{\text{prn}}a_3}{2\pi}] - e^{j(\frac{3\pi}{2} - a_7)} \cdot \delta[k - \frac{N_{\text{prn}}a_3}{2\pi}]]$$

$$D_c[k] = \text{D.F.T.}\{f_{4c}[n]\}$$

$$= N_{\text{prn}} \left\{ \sum_{l=0}^{\infty} (-1)^l J_{2l+1}(a_4) (e^{j(2l+1)a_5} \delta[k - \frac{(2l+1)a_6 N_{\text{prn}}}{2\pi}] + e^{-j(2l+1)a_5} \delta[k + \frac{(2l+1)a_6 N_{\text{prn}}}{2\pi}]) \right\}$$

DFT of cosine part after evaluating the convolutions is,

$$\begin{aligned}
\text{D.F.T.}\{s_c[n+1]\} &= \frac{A_o}{N_{\text{prn}}} \{A_c[k] * B_c[k] - C_c[k] * D_c[k]\} \\
&= \frac{A_o N_{\text{prn}}}{2} \left\{ J_0(a_4) \cdot e^{ja_7} \delta[k + \frac{N_{\text{prn}}a_3}{2\pi}] + J_0(a_4) \cdot e^{-ja_7} \delta[k - \frac{N_{\text{prn}}a_3}{2\pi}] \right. \\
&\quad + e^{ja_7} \sum_{l=1}^{\infty} (-1)^l J_{2l}(a_4) (e^{j2la_5} \delta[k + \frac{(N_{\text{prn}}a_3 - 2la_6 N_{\text{prn}})}{2\pi}] + e^{-j2la_5} \delta[k + \frac{(N_{\text{prn}}a_3 + 2la_6 N_{\text{prn}})}{2\pi}]) \\
&\quad \left. + e^{-ja_7} \sum_{l=1}^{\infty} (-1)^l J_{2l}(a_4) (e^{j2la_5} \delta[k - \frac{(N_{\text{prn}}a_3 + 2la_6 N_{\text{prn}})}{2\pi}] + e^{-j2la_5} \delta[k + \frac{(2la_6 N_{\text{prn}} - N_{\text{prn}}a_3)}{2\pi}]) \right\}
\end{aligned}$$

$$\begin{aligned}
& -e^{j(a_7 + \frac{3\pi}{2})} \sum_{l=0}^{\infty} (-1)^l J_{2l+1}(a_4) \cdot (e^{j(2l+1)a_5} \delta[k + \frac{(N_{\text{prn}} a_3 - (2l+1)a_6 N_{\text{prn}})}{2\pi}] \\
& + e^{-j(2l+1)a_5} \delta[k + \frac{(N_{\text{prn}} a_3 + (2l+1)a_6 N_{\text{prn}})}{2\pi}]) \\
& + e^{j(\frac{3\pi}{2} - a_7)} \sum_{l=0}^{\infty} (-1)^l J_{2l+1}(a_4) \cdot (e^{j(2l+1)a_5} \delta[k - \frac{(N_{\text{prn}} a_3 + (2l+1)a_6 N_{\text{prn}})}{2\pi}] \\
& + e^{-j(2l+1)a_5} \delta[k - \frac{(N_{\text{prn}} a_3 - (2l+1)a_6 N_{\text{prn}})}{2\pi}]) \}.
\end{aligned}$$

Similarly for the sine component of complex signal,

$$\begin{aligned}
s_s[n+1] &= A_o \{ \underbrace{\sin(a_7 - a_3 \cdot n)}_{f_{1s}[n]} \underbrace{\cos(a_4 \cos(a_5 + a_6 \cdot n))}_{f_{2s}[n]} \\
& + \underbrace{\cos(a_7 - a_3 \cdot n)}_{f_{3s}[n]} \underbrace{\sin(a_4 \cos(a_5 + a_6 \cdot n))}_{f_{4s}[n]} \} \\
& \Rightarrow \text{D.F.T.} \{s_s[n+1]\} = A_o \{ \text{D.F.T.} \{f_{1s}[n]\} \cdot f_{2s}[n] + \text{D.F.T.} \{f_{3s}[n]\} \cdot f_{4s}[n] \} \\
& = A_o \{ \frac{1}{N_{\text{prn}}} \text{D.F.T.} \{f_{1s}[n]\} * \text{D.F.T.} \{f_{2s}[n]\} + \frac{1}{N_{\text{prn}}} \text{D.F.T.} \{f_{3s}[n]\} * \text{D.F.T.} \{f_{4s}[n]\} \}
\end{aligned}$$

By using reference **[60, pp.361]**

$$A_s[k] = \text{D.F.T.} \{f_{1s}[n]\} = \frac{N_{\text{prn}}}{2} [e^{j(a_7 + \frac{3\pi}{2})} \cdot \delta[k + \frac{N_{\text{prn}} a_3}{2\pi}] - e^{-j(a_7 - \frac{3\pi}{2})} \cdot \delta[k - \frac{N_{\text{prn}} a_3}{2\pi}]]$$

$$\begin{aligned}
B_s[k] &= \text{D.F.T.} \{f_{2s}[n]\} \\
&= N_{\text{prn}} \{ J_0(a_4) \cdot \delta[k] + \sum_{l=1}^{\infty} (-1)^l J_{2l}(a_4) (e^{j2la_5} \delta[k - \frac{2l a_6 N_{\text{prn}}}{2\pi}] + e^{-j2la_5} \delta[k + \frac{2l a_6 N_{\text{prn}}}{2\pi}]) \}
\end{aligned}$$

$$C_c[k] = \text{D.F.T.} \{f_{3s}[n]\} = \frac{N_{\text{prn}}}{2} [e^{ja_7} \delta[k + \frac{N_{\text{prn}} a_3}{2\pi}] + e^{-ja_7} \delta[k - \frac{N_{\text{prn}} a_3}{2\pi}]]$$

$$\begin{aligned}
D_s[k] &= \text{D.F.T.} \{f_{4s}[n]\} \\
&= N_{\text{prn}} \{ \sum_{l=0}^{\infty} (-1)^l J_{2l+1}(a_4) (e^{j(2l+1)a_5} \delta[k - \frac{(2l+1)a_6 N_{\text{prn}}}{2\pi}] + e^{-j(2l+1)a_5} \delta[k + \frac{(2l+1)a_6 N_{\text{prn}}}{2\pi}]) \}
\end{aligned}$$

DFT of sine part after evaluating the convolutions becomes,

$$\begin{aligned}
\Rightarrow \text{D.F.T. } \{s_s[n+1]\} &= \frac{A_o}{N_{\text{prn}}} \{A_s[k] * B_c[k] + C_s[k] * D_s[k]\} \\
&= \frac{A_o N_{\text{prn}}}{2} \{J_o(a_4) \cdot e^{j(a_7 + \frac{3\pi}{2})} \delta[k + \frac{N_{\text{prn}} a_3}{2\pi}] - J_o(a_4) \cdot e^{-j(a_7 - \frac{3\pi}{2})} \delta[k - \frac{N_{\text{prn}} a_3}{2\pi}] \\
&+ e^{j(a_7 + \frac{3\pi}{2})} \sum_{l=1}^{\infty} (-1)^l J_{2l}(a_4) (e^{j2la_5} \delta[k + \frac{(N_{\text{prn}} a_3 - 2l a_6 N_{\text{prn}})}{2\pi}] + e^{-j2la_5} \delta[k + \frac{(N_{\text{prn}} a_3 + 2l a_6 N_{\text{prn}})}{2\pi}]) \\
&- e^{-j(a_7 - \frac{3\pi}{2})} \sum_{l=1}^{\infty} (-1)^l J_{2l}(a_4) (e^{j2la_5} \delta[k - \frac{(N_{\text{prn}} a_3 + 2l a_6 N_{\text{prn}})}{2\pi}] + e^{-j2la_5} \delta[k + \frac{(2l a_6 N_{\text{prn}} - N_{\text{prn}} a_3)}{2\pi}]) \\
&+ e^{ja_7} \sum_{l=0}^{\infty} (-1)^l J_{2l+1}(a_4) \cdot (e^{j(2l+1)a_5} \delta[k + \frac{(N_{\text{prn}} a_3 - (2l+1)a_6 N_{\text{prn}})}{2\pi}] \\
&+ e^{-j(2l+1)a_5} \delta[k + \frac{(N_{\text{prn}} a_3 + (2l+1)a_6 N_{\text{prn}})}{2\pi}]) \\
&+ e^{-ja_7} \sum_{l=0}^{\infty} (-1)^l J_{2l+1}(a_4) \cdot (e^{j(2l+1)a_5} \delta[k - \frac{(N_{\text{prn}} a_3 + (2l+1)a_6 N_{\text{prn}})}{2\pi}] \\
&+ e^{-j(2l+1)a_5} \delta[k - \frac{(N_{\text{prn}} a_3 - (2l+1)a_6 N_{\text{prn}})}{2\pi}]) \}.
\end{aligned}$$

If cosine and sine parts are combined,

$$\begin{aligned}
\text{D.F.T. } \{s[n+1]\} &= \text{D.F.T. } \{s_c[n+1]\} + \overset{(e^{\frac{j\pi}{2}})}{j} \text{D.F.T. } \{s_s[n+1]\} \\
&= A_o N_{\text{prn}} J_o(a_4) \cdot e^{ja_7} \delta[k + \frac{N_{\text{prn}} a_3}{2\pi}] \\
&+ A_o N_{\text{prn}} e^{ja_7} \sum_{l=1}^{\infty} (-1)^l J_{2l}(a_4) (e^{j2la_5} \delta[k + \frac{(N_{\text{prn}} a_3 - 2l a_6 N_{\text{prn}})}{2\pi}] + \\
&e^{-j2la_5} \delta[k + \frac{(N_{\text{prn}} a_3 + 2l a_6 N_{\text{prn}})}{2\pi}]) \\
&+ A_o N_{\text{prn}} e^{j(a_7 + \frac{\pi}{2})} \sum_{l=0}^{\infty} (-1)^l J_{2l+1}(a_4) \cdot (e^{j(2l+1)a_5} \delta[k + \frac{(N_{\text{prn}} a_3 - (2l+1)a_6 N_{\text{prn}})}{2\pi}] + \\
&e^{-j(2l+1)a_5} \delta[k + \frac{(N_{\text{prn}} a_3 + (2l+1)a_6 N_{\text{prn}})}{2\pi}])
\end{aligned}$$

$$\begin{aligned}
& \text{since } S[k] = \text{D.F.T. } \{s[n]\} = \text{D.F.T. } \{s[n+1]\} \cdot e^{-j\left(\frac{2\pi}{N_{\text{prn}}}\right)k.1} \\
\Rightarrow S[k] &= A_o N_{\text{prn}} J_o(a_4) \cdot e^{j(a_7+a_3)} \delta\left[k + \frac{N_{\text{prn}} a_3}{2\pi}\right] \\
&+ A_o N_{\text{prn}} e^{ja_7} \sum_{l=1}^{\infty} (-1)^l J_{2l}(a_4) (e^{j(2l(a_5-a_6)+a_3)}) \delta\left[k + \frac{N_{\text{prn}}(a_3 - 2la_6)}{2\pi}\right] \\
&+ e^{-j(2l(a_5-a_6)-a_3)} \delta\left[k + \frac{N_{\text{prn}}(a_3 + 2la_6)}{2\pi}\right] \\
&+ A_o N_{\text{prn}} e^{j\left(a_7 + \frac{\pi}{2}\right)} \sum_{l=0}^{\infty} (-1)^l J_{2l+1}(a_4) (e^{j((2l+1)(a_5-a_6)+a_3)}) \delta\left[k + \frac{N_{\text{prn}}(a_3 - (2l+1)a_6)}{2\pi}\right] \\
&+ e^{-j((2l+1)(a_5-a_6)-a_3)} \delta\left[k + \frac{N_{\text{prn}}(a_3 + (2l+1)a_6)}{2\pi}\right]
\end{aligned}$$

A.2 Auto-Correlation Function in Terms of Energy Spectrum

$$\begin{aligned}
R_s[\tau] &= \frac{1}{N_{\text{prn}}} \sum_{n=0}^{N_{\text{prn}}-1} (s[n] \cdot s^*[n+\tau]) = \\
&\frac{1}{N_{\text{prn}}} \sum_{n=0}^{N_{\text{prn}}-1} \left(\frac{1}{N_{\text{prn}}} \sum_{k'=0}^{N_{\text{prn}}-1} S[-k'] \cdot e^{j\frac{2\pi}{N_{\text{prn}}}(-k').n} \right) \left(\frac{1}{N_{\text{prn}}} \sum_{k=0}^{N_{\text{prn}}-1} S^*[-k] \cdot e^{-j\frac{2\pi}{N_{\text{prn}}}(-k).(n+\tau)} \right) \\
&= \frac{1}{N_{\text{prn}}^3} \sum_{k'=0}^{N_{\text{prn}}-1} S[-k'] \sum_{k=0}^{N_{\text{prn}}-1} S^*[-k] \cdot e^{j\frac{2\pi}{N_{\text{prn}}}k.\tau} \underbrace{\sum_{n=0}^{N_{\text{prn}}-1} e^{-j\frac{2\pi}{N_{\text{prn}}}k'.n} e^{j\frac{2\pi}{N_{\text{prn}}}k.n}}_{N_{\text{prn}} \delta[k'-k]} \\
&= \frac{1}{N_{\text{prn}}^2} \sum_{k=0}^{N_{\text{prn}}-1} S[-k] \cdot S^*[-k] \cdot e^{j\frac{2\pi}{N_{\text{prn}}}k.\tau} = \frac{1}{N_{\text{prn}}} \sum_{k=0}^{N_{\text{prn}}-1} \frac{|S[-k]|^2}{N_{\text{prn}}} \cdot e^{j\frac{2\pi}{N_{\text{prn}}}k.\tau} \\
&= \frac{1}{N_{\text{prn}}} \sum_{k=0}^{N_{\text{prn}}-1} E[-k] \cdot e^{j\frac{2\pi}{N_{\text{prn}}}k.\tau}
\end{aligned}$$

A.3 Velocity Auto-Correlation Function (ACF)

$$\phi[n] = \gamma_1 - \gamma_2 u.n + \gamma_4 u$$

If DFT of both sides is taken,

$$\begin{aligned} \text{D.F.T.}\{\phi[n]\} &= \text{D.F.T.}\{\gamma_1\} - \text{D.F.T.}\{\gamma_2 u[n]\} + \text{D.F.T.}\{\gamma_4 u\} \\ \text{D.F.T.}\{\text{Tan}^{-1}\left(\frac{Q}{I}\right)\} &= \gamma_1 N_{\text{prm}} \delta[k] - \gamma_2 \frac{N_{\text{prm}}}{2\pi} j \frac{\partial U[k]}{\partial k} + \gamma_4 U[k] \end{aligned}$$

where $U[k]$ is discrete spectrum of $u[n]$.

$$\Rightarrow -j \frac{N_{\text{prm}} \gamma_2}{2\pi} \frac{\partial U[k]}{\partial k} + \gamma_4 U[k] + \gamma_1 N_{\text{prm}} \delta[k] = \text{D.F.T.}\left\{\text{Tan}^{-1}\left(\frac{Q}{I}\right)\right\}$$

since $U[k]$ is only function of k ,

$$\begin{aligned} -j \underbrace{\frac{N_{\text{prm}} \gamma_2}{2\pi}}_{\phi_1} \frac{dU[k]}{dk} + \underbrace{\gamma_4}_{\phi_2} U[k] + \underbrace{\gamma_1 N_{\text{prm}}}_{\phi_3} \delta[k] &= \underbrace{\text{D.F.T.}\left\{\text{Tan}^{-1}\left(\frac{Q}{I}\right)\right\}}_{\phi_4} \\ \phi_1 \frac{dU[k]}{dk} + \phi_2 U[k] + \phi_3 \delta[k] &= \phi_4 \end{aligned}$$

This is inhomogeneous 1st order ODE. ϕ_4 parameter can be obtained from sampled and demodulated I-Q Doppler signals. If we solve this differential equation [62, pp.792],

$$U[k] = \frac{1}{\phi_1} e^{-\frac{\phi_2}{\phi_1} k} \int_0^k (\phi_4 - \phi_3 \delta[k]) e^{\frac{\phi_2}{\phi_1} k} dk + U[0] \delta[k] e^{-\frac{\phi_2}{\phi_1} k}$$

$U[k]$ is spectrum of velocity and it can be used to find $U[0]$ as follows,

$$\begin{aligned} U[k] &= \sum_{n=0}^{N_{\text{prm}}-1} u[n] e^{-j \frac{2\pi}{N_{\text{prm}}} k \cdot n} \quad \text{when } k = 0 \\ U[0] &= \sum_{n=0}^{N_{\text{prm}}-1} u[n] \Rightarrow \bar{u} = \frac{U[0]}{N_{\text{prm}}} \Rightarrow U[0] = \bar{u} \cdot N_{\text{prm}} \end{aligned}$$

N_{prm} is number of emitted signals or number of velocity values affecting these signals and \bar{u} is average velocity.

$$\begin{aligned} U[k] &= \frac{1}{\phi_1} e^{-\frac{\phi_2}{\phi_1} k} \int_0^k (\phi_4 - \phi_3 \delta[k]) e^{\frac{\phi_2}{\phi_1} k} dk + N_{\text{prm}} \bar{u} \delta[k] e^{-\frac{\phi_2}{\phi_1} k} \\ U[k] &= N_{\text{prm}} \bar{u} \delta[k] + \frac{j \cdot 2\pi}{N_{\text{prm}} \gamma_2} e^{-\frac{j \cdot 2\pi \cdot \gamma_4}{N_{\text{prm}} \cdot \gamma_2} k} \int_0^k \overbrace{\left(\text{DFT}\left\{\text{Tan}^{-1}\left(\frac{Q}{I}\right)\right\} - \gamma_1 N_{\text{prm}} \delta[k]\right)}^{\phi_4} e^{\frac{j \cdot 2\pi \cdot \gamma_4}{N_{\text{prm}} \cdot \gamma_2} k} dk \quad (\text{A.3.1}) \end{aligned}$$

where

$$\begin{aligned}\gamma_1 &= \pi N_c \\ \gamma_2 &= \frac{4\pi f_o T_{prf}}{c} \\ \gamma_4 &= \frac{4\pi f_o T_{prf}}{c} - \frac{4\pi f_o d_{o,i}}{c^2} = \frac{4\pi f_o (c T_{prf} - d_{o,i})}{c^2}\end{aligned}$$

First term in equation (A.3.1) corresponds to the spectral component coming from mean part of velocity and second term for randomly fluctuating part of velocity. Auto-correlation function of discrete velocity function $u[n]$ can be written in terms of energy spectrum and amplitude of spectrum of $u[n]$ as follows,

$$\begin{aligned}R_u[\tau] &= \text{D.F.T.}^{-1} \{S_u[k]\} = \frac{1}{N_{prn}} \sum_{k=0}^{N_{prn}-1} \left\{ \lim_{N_{prn} \rightarrow \infty} \frac{1}{N_{prn}} |U[k]|^2 \right\} e^{j \frac{2\pi}{N_{prn}} k \cdot \tau} \\ R_u[\tau] &= \text{D.F.T.}^{-1} \left\{ \lim_{N_{prn} \rightarrow \infty} \frac{1}{N_{prn}} \left| N_{prn} \bar{u} \delta[k] + \frac{j \cdot 2\pi}{N_{prn} \gamma_2} e^{-\frac{j \cdot 2\pi \cdot \gamma_4}{N_{prn} \cdot \gamma_2} k} \int_0^k (\phi_4 - \gamma_1 N_{prn} \delta[k]) e^{\frac{j \cdot 2\pi \cdot \gamma_4}{N_{prn} \cdot \gamma_2} k} dk \right|^2 \right\}\end{aligned}$$

A.4 DFT of Sampled US Signals for Measurement Volume of Viscoelastic Fluid Flow

Sampled US signals are,

$$\begin{aligned}s[n] &= A_o e^{j(a_6 - a_2 \sin(a_4 + a_5(n-1)) + a_3 \cos(a_4 + a_5(n-1)))} = \\ &= \underbrace{A_o \cos(a_6 - a_2 \sin(a_4 + a_5(n-1)) + a_3 \cos(a_4 + a_5(n-1)))}_{s_c[n]} + \\ &+ \underbrace{j A_o \sin(a_6 - a_2 \sin(a_4 + a_5(n-1)) + a_3 \cos(a_4 + a_5(n-1)))}_{s_s[n]}\end{aligned}$$

where $a_1 = \pi N_c$, $a_2 = \frac{4\pi f_o}{c} \frac{\eta_1 \cos \theta}{2\pi f_f \cdot \eta_3}$, $a_3 = \frac{4\pi f_o}{c} \frac{\eta_2 \cos \theta}{2\pi f_f \cdot \eta_3}$, $a_4 = 2\pi f_f \frac{d_o}{c}$,

$$a_5 = 2\pi f_f T_{prf}, \quad a_6 = a_1 - a_3$$

After using following trigonometric identities,

$$\cos(x + y) = \cos x \cos y - \sin x \sin y$$

$$\sin(x + y) = \sin x \cos y + \cos x \sin y$$

DFT of $s[n]$ can be obtained from DFT of cosine (in phase) and sine (quadrature) parts. After using following identities [60] and convolutions,

$$\cos(z \sin \theta) = J_0(z) + 2 \sum_{k=1}^{\infty} J_{2k}(z) \cos(2k\theta)$$

$$\sin(z \sin \theta) = 2 \sum_{k=0}^{\infty} J_{2k+1}(z) \sin((2k+1)\theta)$$

spectrum of shifted signal $s[n+1]$ will be,

$$\begin{aligned} \text{DFT}\{s[n+1]\} &= \text{DFT}\{s_c[n+1]\} + j \text{DFT}\{s_s[n+1]\} \\ &= A_0 N (C_1 + j C_2) \{ J_0(a_2) J_0(a_3) \delta[k] + J_0(a_2) \sum_{l=1}^{\infty} (-1)^l J_{2l}(a_3) e^{j2l a_4} \delta[k - \frac{2la_5 N}{2\pi}] \\ &\quad + J_0(a_2) \sum_{l=1}^{\infty} (-1)^l J_{2l}(a_3) e^{-j2l a_4} \delta[k + \frac{2la_5 N}{2\pi}] + J_0(a_3) \sum_{l=1}^{\infty} J_{2l}(a_2) e^{j2l a_4} \delta[k - \frac{2la_5 N}{2\pi}] \\ &\quad + \sum_{l=1, l'=1}^{\infty} (-1)^{l'} J_{2l}(a_2) J_{2l'}(a_3) e^{j2(1+l') a_4} \delta[k - \frac{2(1+l') a_5 N}{2\pi}] \\ &\quad + \sum_{l=1, l'=1}^{\infty} (-1)^{l'} J_{2l}(a_2) J_{2l'}(a_3) e^{j2(1-l') a_4} \delta[k + \frac{2(1-l') a_5 N}{2\pi}] \\ &\quad + J_0(a_3) \sum_{l=1}^{\infty} J_{2l}(a_2) e^{-j2l a_4} \delta[k + \frac{2la_5 N}{2\pi}] + \sum_{l=1, l'=1}^{\infty} (-1)^{l'} J_{2l}(a_2) J_{2l'}(a_3) e^{j2(1-l') a_4} \delta[k + \frac{2(1-l') a_5 N}{2\pi}] \\ &\quad + \sum_{l=1, l'=1}^{\infty} (-1)^{l'} J_{2l}(a_2) J_{2l'}(a_3) e^{-j2(1+l') a_4} \delta[k + \frac{2(1+l') a_5 N}{2\pi}] \\ &\quad - J_0(a_3) \sum_{l=0}^{\infty} J_{2l+1}(a_2) e^{j(2l+1) a_4} \delta[k - \frac{(2l+1) a_5 N}{2\pi}] \\ &\quad - \sum_{l=0, l'=1}^{\infty} (-1)^{l'} J_{2l+1}(a_2) J_{2l'}(a_3) e^{j(2l+2l'+1) a_4} \delta[k - \frac{(2l+2l'+1) a_5 N}{2\pi}] \\ &\quad - \sum_{l=0, l'=1}^{\infty} (-1)^{l'} J_{2l+1}(a_2) J_{2l'}(a_3) e^{j(2l-2l'+1) a_4} \delta[k + \frac{(2l-2l'+1) a_5 N}{2\pi}] \\ &\quad + J_0(a_3) \sum_{l=0}^{\infty} J_{2l+1}(a_2) e^{-j(2l+1) a_4} \delta[k + \frac{(2l+1) a_5 N}{2\pi}] \\ &\quad + \sum_{l=0, l'=1}^{\infty} (-1)^{l'} J_{2l+1}(a_2) J_{2l'}(a_3) e^{j(2l'-2l-1) a_4} \delta[k + \frac{(2l-2l'+1) a_5 N}{2\pi}] \end{aligned}$$

$$\begin{aligned}
& + \sum_{l=0, l'=1}^{\infty} (-1)^{l'} J_{2l+1}(a_2) J_{2l'}(a_3) e^{-j(2l+2l'+1)a_4} \delta\left[k + \frac{(2l+2l'+1)a_5 N}{2\pi}\right] \} \\
& - A_0 N (C_2 - jC_1) \left\{ J_0(a_2) \sum_{l'=0}^{\infty} (-1)^{l'} J_{2l'+1}(a_3) e^{j(2l'+1)a_4} \delta\left[k - \frac{(2l'+1)a_5 N}{2\pi}\right] \right. \\
& + J_0(a_2) \sum_{l'=0}^{\infty} (-1)^{l'} J_{2l'+1}(a_3) e^{-j(2l'+1)a_4} \delta\left[k + \frac{(2l'+1)a_5 N}{2\pi}\right] \\
& + \sum_{l=1, l'=0}^{\infty} (-1)^{l'} J_{2l}(a_2) J_{2l'+1}(a_3) e^{j(2l+2l'+1)a_4} \delta\left[k - \frac{(2l+2l'+1)a_5 N}{2\pi}\right] \\
& + \sum_{l=1, l'=0}^{\infty} (-1)^{l'} J_{2l}(a_2) J_{2l'+1}(a_3) e^{j(2l-2l'-1)a_4} \delta\left[k + \frac{(2l'-2l+1)a_5 N}{2\pi}\right] \\
& + \sum_{l=1, l'=0}^{\infty} (-1)^{l'} J_{2l}(a_2) J_{2l'+1}(a_3) e^{j(2l'-2l+1)a_4} \delta\left[k + \frac{(2l-2l'-1)a_5 N}{2\pi}\right] \\
& \left. + \sum_{l=1, l'=0}^{\infty} (-1)^{l'} J_{2l}(a_2) J_{2l'+1}(a_3) e^{-j(2l+2l'+1)a_4} \delta\left[k + \frac{(2l+2l'+1)a_5 N}{2\pi}\right] \right\} \\
& + A_0 N (C_2 - jC_1) \left\{ \sum_{l=0, l'=0}^{\infty} (-1)^{l'} J_{2l+1}(a_2) J_{2l'+1}(a_3) e^{j(2l+2l'+2)a_4} \delta\left[k - \frac{(2l+2l'+2)a_5 N}{2\pi}\right] \right. \\
& + \sum_{l=0, l'=0}^{\infty} (-1)^{l'} J_{2l+1}(a_2) J_{2l'+1}(a_3) e^{j(2l-2l')a_4} \delta\left[k + \frac{(2l'-2l)a_5 N}{2\pi}\right] \} \\
& - A_0 N (C_2 - jC_1) \left\{ \sum_{l=0, l'=0}^{\infty} (-1)^{l'} J_{2l+1}(a_2) J_{2l'+1}(a_3) e^{j(2l'-2l)a_4} \delta\left[k + \frac{(2l-2l')a_5 N}{2\pi}\right] \right. \\
& \left. + \sum_{l=0, l'=0}^{\infty} (-1)^{l'} J_{2l+1}(a_2) J_{2l'+1}(a_3) e^{-j(2l+2l'+2)a_4} \delta\left[k + \frac{(2l+2l'+2)a_5 N}{2\pi}\right] \right\}
\end{aligned}$$

where $C_1 = \cos(a_6)$, $C_2 = \sin(a_6)$

Actual spectrum is phase shifted form of the given spectrum above since,

$$S[k] = \text{DFT}\{s[n]\} = \text{DFT}\{s[n+1]\} \cdot e^{-j\frac{2\pi}{N}k.1} \quad (\text{A.4.1})$$

Zero frequency component of the US spectrum and its amplitude become,

$$\begin{aligned}
 S[k=0] &= \text{DFT}\{s[n+1]\}\Big|_{k=0} \cdot e^{-j\frac{2\pi}{N}0} \\
 &= A_o N (C_1 + jC_2) \{J_o(a_2)J_o(a_3)\delta[k] + 2\sum_{l=1}^{\infty} (-1)^l J_{2l}(a_2)J_{2l}(a_3)\delta[k]\} \\
 &\quad + A_o N (C_2 - jC_1) \{ \sum_{l=0}^{\infty} (-1)^l J_{2l+1}(a_2)J_{2l+1}(a_3)\delta[k] \} \\
 &\quad - A_o N (C_2 - jC_1) \{ \sum_{l=0}^{\infty} (-1)^l J_{2l+1}(a_2)J_{2l+1}(a_3)\delta[k] \} \\
 \Rightarrow |S[k=0]| &= A_o N \underbrace{\sqrt{C_1^2 + C_2^2}}_1 \left| J_o(a_2)J_o(a_3) + 2\sum_{l=1}^{\infty} (-1)^l J_{2l}(a_2)J_{2l}(a_3) \right| \delta[k] \\
 |S[k=0]| &= A_o N \left| J_o(a_2)J_o(a_3) + 2\sum_{l=1}^{\infty} (-1)^l J_{2l}(a_2)J_{2l}(a_3) \right| \delta[k]
 \end{aligned}$$

APPENDIX B

SIGNAL PROCESSING TABLES

Table B.1: Properties of DFT

<i>Periodic sequence (period N)</i>	<i>DFT (period N)</i>
$x[n]$	$X[k]$
$x_1[n], x_2[n]$	$X_1[k], X_2[k]$
$a.x_1[n] + b.x_2[n]$	$a.X_1[k] + b.X_2[k]$ (linearity)
$X[n]$	$N.x[-k]$ (duality)
$x[n-m]$	$e^{-j(2\pi/N)km} X[k]$ (time shift)
$e^{j(2\pi/N)\ell n} x[n]$	$X[k - \ell]$ (frequency shift)
$\sum_{m=0}^{N-1} x_1[m]x_2[n-m]$ (periodic convolution)	$X_1[k].X_2[k]$
$x_1[n].x_2[n]$	$\frac{1}{N} \sum_{\ell=0}^{N-1} X_1[\ell]X_2[k-\ell]$ (periodic convolution)
$x^*[n]$	$X^* [-k]$
$x^*[-n]$	$X^* [k]$
$x[n]$ (if real)	$X[k]=X^*[-k]$ (symmetry property)

Table B.2: Some DFT pairs [67]

<i>Discrete sequence</i>	<i>DFT</i>
$x[n]$	$X[k]$
$x[n-n_0]$	$X[k] e^{-jk\omega_0 n_0}$

Table B.2 Continued

$x[a.n]$	$\frac{1}{ a } X\left(\frac{k}{a}\right)$
$X[n]$	$N.x[-k]$
$n.x[n]$	$\frac{N}{2\pi} j \frac{\partial X[k]}{\partial k}$
N	$\frac{N^2}{2\pi} j \frac{d \delta[k]}{dk}$
$\frac{d^m x[n]}{dn^m}$	$(j k w_o)^m X[k]$
$\delta[n]$	1
$\delta[n-n_o]$	$e^{-jk w_o n_o}$
1	$N.\delta[k]$
$a^n u[n] \quad (a < 1)$	$\frac{1}{1 - a.e^{-jk w_o}}$
$\text{rect}\left[\frac{n}{T}\right] = \begin{cases} 1 & -T/2 \leq n \leq T/2 \\ 0 & \text{else} \end{cases}$	$T \frac{\sin[kw_o T / 2]}{kw_o T / 2} = T.\text{sinc}[kw_o T / 2]$
$\text{sinc}[B.n / 2]$	$\frac{N}{B} \text{rect}\left[\frac{k w_o}{B}\right]$
$e^{j w_o n}$	$N \delta\left[k - \frac{w_o N}{2\pi}\right]$
$\cos[w_o n]$	$\frac{N}{2} \left(\delta\left[k - \frac{w_o N}{2\pi}\right] + \delta\left[k + \frac{w_o N}{2\pi}\right]\right)$
$\sin[w_o n]$	$\frac{N}{2j} \left(\delta\left[k - \frac{w_o N}{2\pi}\right] - \delta\left[k + \frac{w_o N}{2\pi}\right]\right)$

Table B.3: Some useful relations in signal processing

<i>Relation</i>	<i>Explanation</i>
$\cos(x) = \frac{e^{jx} + e^{-jx}}{2}$	Cosine part of a complex exponential
$\sin(x) = \frac{e^{jx} - e^{-jx}}{2j}$	Sine part of a complex exponential
$\cos(x) + j\sin(x) = e^{jx}$	Euler identity
$E = \sum_{n=0}^{N-1} x[n] ^2 = \frac{1}{N} \sum_{k=0}^{N-1} X[k] ^2$	Parseval's relation: total energies in time and frequency domain are equal.
$P = \frac{1}{N} \sum_{n=0}^{N-1} x[n] ^2 = \frac{1}{N} \sum_{k=0}^{N-1} \frac{ X[k] ^2}{N}$	Power in time and frequency domains.
$X_x[k] = \lim_{N \rightarrow \infty} \frac{1}{N} X[k] ^2$	Energy spectrum of $x[n]$ in terms of amplitude of spectrum of $x[n]$
$X_x[k] = \text{DFT}\{R_x[\tau]\}$	Energy spectrum in terms of ACF of $x[n]$

CURRICULUM VITAE

PERSONAL INFORMATION

Surname, Name : Köseli, Volkan
Nationality : Turkish (T.C.)
Date and Place of Birth : 4 July 1978 , Ankara
Marital Status : Married
Email : vkoseli@yahoo.com

EDUCATION

Degree	Institution	Year of Graduation
M.Sc.	Hacettepe University, Chemical Engineering	2002
B.Sc.	Hacettepe University, Chemical Engineering	2000
High School	Kazan High School, Ankara	1995

WORK EXPERIENCE

Year	Place	Enrollment
2003 - present	METU, Department of Chemical Engineering	Research Assistant
2008 - 2009	University of California, Davis	Visiting Scholar
2000 - 2003	Hacettepe University, Department of Chemical Engineering	Research Assistant

FOREIGN LANGUAGES

Advanced English

INTERNATIONAL SYMPOSIUMS

5th International Symposium on Ultrasonic Doppler Methods for Fluid Mechanics and Fluid Engineering (ISUD), 12-14 September 2006, Swiss Federal Institute of Technology (ETHZ), Zürich, Switzerland

PUBLICATIONS

1. Sevil Dinçer, Volkan Köseli, Hande Kesim, Zakir M.O. Rzaev, Erhan Pişkin, 'Radical copolymerization of N-isopropylacrylamide with anhydrides of maleic and citraconic acids', *European Polymer Journal*, Vol.38, pp.2143-2152, 2002
2. Volkan Köseli, Zakir M.O. Rzaev, Erhan Pişkin, 'Bioengineering Fuctional Copolymers. III. Synthesis of Biocompatible Poly[(N-isopropylacrylamide - co-maleic anhydride)-g-poly(ethylene oxide)]/Poly(ethylene imine) Macrocomplexes and Their Thermostabilization Effect on the Activity of the Enzyme Penicillin G Acylase' , *Journal of Polymer Science: Part A: Polymer Chemistry*, Vol.41, 1580-1593, 2003
3. Volkan Köseli, Şerife Zeybek, Yusuf Uludağ, 'Online Viscosity Measurement of Complex Solutions Using Ultrasound Doppler Velocimetry', *Turk J. Chem.*, Vol.30 , pp.297-305, 2006